Intracardiac Echocardiography for Transvenous Lead Extractions: Evaluating its Utility in a Vascular Phantom Model

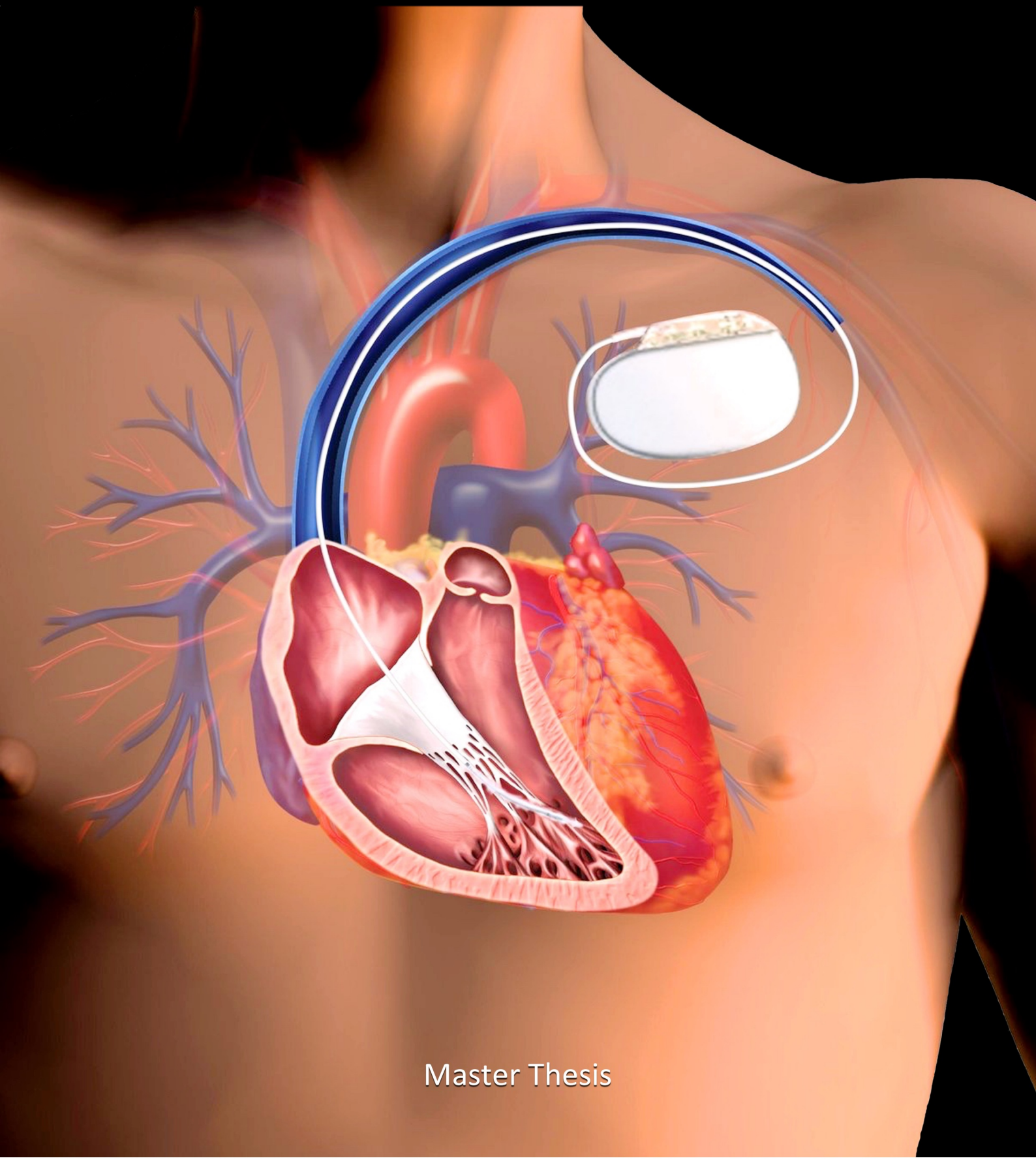

Master Thesis

TU Delft
J. Dankelman

Lynn-Jade Jong
February 2019

PHILIPS
B.H.W. Hendriks

Intracardiac Echocardiography for Transvenous Lead Extractions: Evaluating its Utility in a Vascular Phantom Model

MASTER THESIS

By

Lynn-Jade Jong

to obtain the degree of Master of Science in Biomedical Engineering

at the Delft University of Technology,

to be defended on February 20, 2019

Student number: 4585836
Project duration: July 1, 2018 – December 31, 2018
Supervisors: Prof. Dr. B.H.W. Hendriks, TU Delft/Philips Research
Prof. Dr. J. Dankelman, TU Delft

Delft University of Technology and Philips Research

The cover image is acquired from [1].

PREFACE

Whilst starting my studies in Biomedical Engineering about five and a half years ago, I was driven by the thoughts to engage technology with medicine. Innovations in the field of medical technology were enabling clinicians to better diagnose and treat diseases, and from my perspective back then I imagined myself contributing to these innovations. However, acquired experience during both my bachelors and masters showed this purpose to be more challenging than expected. I reasoned that a comprehensive understanding of both fields is of paramount importance, not only to translate a clinical problem into a technical illustration but also to propose a solution that can be appropriately translated back. This latter often seemed to be the bottleneck because a solution could work in the eyes of an engineer, but how to convince the physician of its utility? Eager to set the first steps to this purpose before completion of my masters at TU Delft, and to gently gain a better understanding of both fields and its current problems encountered, I decided to perform my graduation project for Philips Research, In-Body Systems in Eindhoven.

This latter appeared to be a good choice for me. The six months that I spent at In-Body Systems, I have really enjoyed the time working on my project. This was not solely because this project exactly exposed the necessity for proper collaboration between academy, industry and clinical centres but also demonstrated the great diversity of the work of a biomedical engineer and the further possibilities one can accomplish. Besides, this time has definitely not been successful without the support of people that surrounded me throughout the entire project from both Philips Research and TU Delft.

First, my supervisors Benno Hendriks and Jenny Dankelman, I appreciate the manner in which you guided me through my thesis, in which you provided me with valuable feedback and simultaneously gave me the possibility to explore the field of research. Second, my daily supervisors from Philips Research Charles Sio and Gerald Lucassen, and the other colleagues Martin Pekař and Pepijn Wortelboer involved in the lead extraction project. Thank you for supporting me on regular basis and providing me with different valuable perspectives, advices and feedback. Furthermore, I also would like to thank the researchers from the MISIT lab for their expertise and interests in my project and Arjan van Dijke, for his assistance in the lab. On top of that, I want to thank the clinicians and researchers from the Erasmus MC hospital for giving me the opportunity to attend several lead extraction procedures.

Last but not least, special thanks to my parents John and Jacintha, my family and my boyfriend Sebastiaan, who have always supported me.

Lynn-Jade Jong
The Hague, January 2019

ABSTRACT

Transvenous lead extractions (TLEs) are minimally invasive procedures in which pacing or implantable cardioverter defibrillator leads are extracted under guidance of 2D X-ray fluoroscopy. Despite the fact that fluoroscopy is currently the gold standard for TLEs, it has several limitations in terms of visualization of anatomical structures, areas of high risk and complications. Since TLEs carry a small but distinct risk of major complications including laceration of the Superior Vena Cava (SVC), bleeding and death, this study aimed to evaluate the utility of intracardiac echocardiography (ICE) to overcome current problems of fluoroscopy and to reduce major complications during TLEs. Hereby the presented work first had the objective of designing and constructing a tissue-mimicking vascular phantom model with realistic geometry and echogenicity to simulate a real-life lead extraction environment suitable for ultrasound imaging and second, of evaluating the utility of ICE for different visualization planes of the lead-tissue interface whilst using the phantom model.

In order to accomplish this, different mould prototypes were designed and constructed with additive manufacturing in order to enable polyvinyl alcohol (PVA) pouring of the phantom. Following several iteration steps of the prototypes, an ultrasound compatible PVA phantom model of the SVC and approximate innominate veins with realistic geometry could be constructed according a developed methodology, adopted and modified from previous protocols. Subsequently, its suitability to serve as a real-life lead extraction environment in terms of echogenicity was assessed by comparison of its results with findings from previous conducted clinical studies. Ultimately, both the constructed phantom and a porcine model were used to evaluate the performance of ICE in three experiments whereby several visualization planes of the lead-tissue interface were examined.

The results of this study demonstrate that a side-looking phased-array ICE catheter could image different structures of the lead-tissue interface including the vessel wall of the SVC, area of scar tissue, free-floating and adherent cardiac leads as well as the advancement of an extraction sheath over the lead. It was found that the structures could be clearly distinguished from each other in terms of echogenicity. The scar tissue along the lead-tissue interface was visualized as an echo dense signal, characterized by a linear echogenic shadow, and equivalent to prior clinical observations. From the results, it also appeared that a parallel view and cross-sectional view outside the SVC gave more insight into lead binding sites and their location with respect to the vessel wall than a conventional parallel view inside the SVC.

It can be concluded that it is feasible to design and construct a vascular phantom model with realistic geometry and echogenicity, adequate for the simulation of a real-life lead extraction environment and to evaluate the utility of ICE for TLEs. This study has demonstrated that ICE is a valuable tool to visualize and assess the lead-tissue interface, which is crucial to avoid major complications during TLEs. Thus, implementation of ICE imaging into TLEs has the potential to add to a more effective and safer procedure.

CONTENTS

LIST OF FIGURES

LIST OF TABLES

LIST OF ACRONYMS

BMF	Blood-Mimicking Fluid
BMI	Body Mass Index
CIED	Cardiovascular Electronic Implantable Device
CNR	Contrast-to-Noise Ratio
CRT	Cardiac Resynchronization Therapy
CT	Computed Tomography
FOV	Field of View
FT	Freeze Thaw
IBS	In-Body Systems
ICD	Implantable Cardioverter-Defibrillator
ICE	Intracardiac Echocardiography
IVC	Inferior Vena Cava
MRI	Magnetic Resonance Imaging
PLA	Polylactic Acid
PVA	Polyvinyl Alcohol
RA	Right Atrium
RV	Right Ventricle
STL	Stereolithography
SVC	Superior Vena Cava
TEE	Transesophageal Echocardiography
TLE	Transvenous Lead Extraction
TTE	Transthoracic Echocardiography
US	Ultrasound

A Vascular Ultrasound Phantom for simulation of a Transvenous Lead Extraction environment

Lynn-Jade S. Jong[a], Benno H.W. Hendriks[a,b], Jenny Dankelman[a]

[a] BioMechanical Engineering Department, Delft University of Technology, 2628 CD Delft, The Netherlands
[b] Philips Research, Department of In-Body Systems, 5656 AE Eindhoven, The Netherlands

Abstract — Transvenous lead extractions (TLEs) are complex and risky procedures with a small but distinct rate of reported major complications and mortality. This study describes the design and construction of a vascular ultrasound (US) phantom to simulate a TLE environment and to evaluate the utility of US modalities for TLE procedures to reduce major complications. A tissue mimicking phantom model of a human junction of the superior vena cava and innominate veins was developed and tailored to reported geometry from literature. This phantom model was constructed from a designed and 3D printed mould and consisted of tissue mimicking materials polyvinyl alcohol and calciumcarbonate. To evaluate the performance of this phantom, its ability to discriminate different structures of the lead-tissue interface (vessel wall, scar tissue and cardiac lead) in terms of echogenicity was examined on 2D intracardiac echocardiography images for two different views. The results demonstrated a clear distinction of these structures and visualization of the lead-tissue interface for both views. The echo dense signals of the scar tissue along the lead-tissue interface, characterized by a linear echogenic shadow, were consistent with observations from prior clinical studies. Therefore, this vascular US phantom was considered suitable in terms of geometry and echogenicity to simulate a TLE environment and to evaluate US modalities for TLEs.

Keywords **— Transvenous Lead Extraction, Medical Phantom, Ultrasound, Intracardiac Echocardiography, Polyvinyl Alcohol**

I. Introduction

Transvenous lead extractions (TLEs) are minimally invasive procedures in which pacing or implantable cardioverter defibrillator leads are extracted under guidance of 2D fluoroscopy. The demand for TLE procedures has grown considerably to an annual extraction rate of about 24.000 patients worldwide [1] which is due to an increased number of cardiovascular electronic implantable device infections and other indications (e.g. lead fracture or failure) [2, 3]. Furthermore, advancement of tools and extraction techniques as well as the growth of clinical experience over time positively influenced the outcome of TLE and promoted further adoption on global scale [1, 4]. Despite these clinical and technological advances, TLE remains a complex and risky procedure with a small but distinct rate of reported major complications and mortality; these reported values vary even widely across studies, with major complications from 0.4% to 3.4% and mortality rates of 0% to 1.9% [4-8].

Of these major complications, which primarily comprise life-threatening vascular tears, it is estimated that two-thirds occur in the superior vena cava (SVC) [3]. Operators mostly fear injury to the SVC because of the corresponding mortality, exceeding the 50%, even when there is rapid detection and subsequent surgical intervention [2, 9, 10]. This is because the SVC has a relatively thin vessel wall and unfavourable position, near the right pleura and pericardium. Given the bending shape characteristics of the SVC, the lead rarely takes a straight course through this part [11]. Particularly, in case of development of endovascular scar tissue that may encapsulate the lead body at several places, difficulty and risk of extraction are increased [1]. Thus, when attempting to liberate the lead from surrounding tissue, a perforation can be easily induced with possibly fatal consequences (e.g. bleeding into the chest and/or pericardium) [2].

Given that fluoroscopy is limited in the ability to visualize anatomical structures, areas of high risk and complications properly [11-13], several ultrasound (US) modalities have been introduced to overcome current limitations of fluoroscopy and to reduce major complications during TLEs [2, 12, 14-16]. One of these modalities is phased—array intracardiac echocardiography (ICE) of which its utility has been recently evaluated in two small clinical studies [2, 14]. Although ICE appears to be a promising technique to assess the lead-tissue interface (i.e. the lead binding sites) and to identify procedural complications [2, 12-14] more studies are necessary to test and evaluate its possibilities for TLEs more comprehensively. As it is not always feasible to perform standardized and repetitive tests in patients, alternatives are required such as animal models or medical phantoms, which serve as substitute for human tissue.

Although porcine hearts closely resemble human hearts [17], their use is not a matter of course due to practical and ethical reasons. In addition, proper evaluation of US modalities for TLEs, necessitates a real-life lead extraction environment with intravascular lead binding sites. Since porcine hearts are not naturally 'diseased', it is challenging to obtain such realistic patient scenarios. As alternative to animal models, tissue-mimicking phantoms are widely adopted to mimic human soft tissue and allow technology testing in a patient-safe and environment-friendly manner [18-21].

Particularly, so called 'home made' phantoms are more affordable and accessible than commercial available phantoms [19] and allow to be tailored to a lead extraction environment. Hereby some important considerations are the phantom's vascular geometry and echogenicity (i.e. the ability to produce US echoes) as well as the feasibility of creating a lumen with endovascular scar tissue (for introduction of a cardiac lead), necessary to provide an appropriate simulation model for TLEs. However, to the author's knowledge, no phantoms have been previously developed to simulate a TLE environment, neither commercially nor in academic setting. Therefore, the present paper describes the design and construction of a vascular phantom model to simulate a real-life TLE environment, and suitable for US imaging to evaluate the utility of US modalities for TLE procedures.

II. Materials and Methods

A. Mould design and construction

In order to allow construction of the vascular phantom model, first a mould was developed which was made in design software Solidworks (Dassault Systèmes, France) and constructed with additive manufacturing using 3D printing software (Cura, Ultimaker, Netherlands). This mould, presented in **Fig. 1**, consisted of a thermoplastic polylactic acid material with 11 cm in length, 9 cm in width and 3.5 cm in depth. Its inner shape, a vascular tree, represents a human junction of the SVC and innominate veins. This junction was chosen for the reason that it is considered most complex and critical to induce a vascular tear during a TLE procedure [2, 3, 11].

Fig. 1A explains the structures of the vascular tree. It consists of a fixed inner tube, which is the first part of the SVC. The second part of the SVC can be connected to the fixed inner tube through attachment points and contains an open space with 3 mm thickness, intended for endovascular scar tissue. Besides the open space for scar tissue, another open space of 2 mm distance is left to create a vessel wall. The other tubular parts, which represent the left and right innominate vein, can be connected to the second part of the SVC. To induce a gradual transition in terms of diameter from the SVC towards the right innominate vein (**Fig. 1**B), an upper part has been constructed which adopts the desired geometry and simultaneously allows maintenance of the 2 mm thin vessel wall.

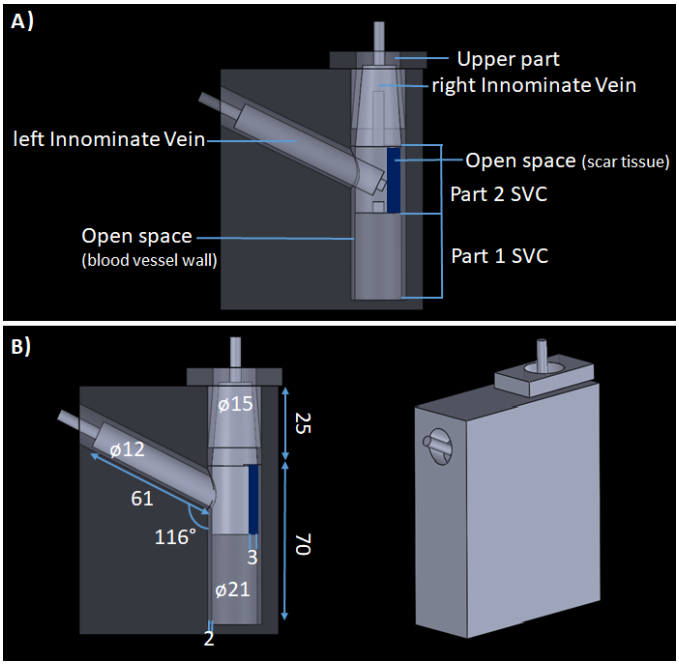

Fig. 1. Design of the vascular tree mould. A) Indication of its inner structures. B) Left: Geometry (i.e. length, inner diameter, thickness in mm) of the vascular tree. Right: Mould with two openings for pouring. The small outer tubular structures allow for easy extraction of the inner structures after phantom construction.

B. Phantom construction

Polyvinyl alcohol (PVA) was chosen as tissue-mimicking material for the phantom. This widely adopted hydrogel [20-24] is a chemically synthesized polymer, which is suitable for US imaging and equivalent to various types of soft tissue in terms of acoustic properties [20, 25]. It allows precise modelling of its mechanical properties when subjected to a number of freeze thaw (FT) cycles, and construction of multiple heterogeneous layer structures useful to create endovascular scar tissue. On top of that, it has a long-term durability when keeping from dehydration and bacterial growth [24, 26, 27].

Preparation of the PVA gel was performed according a developed protocol, which was primarily adopted and modified from a methodology described by T. de Jong et al. 2017 [28]. PVA powder (Selvol PVOH 165, Sekisui Chemical Group NJ, USA) with a high degree of hydrolysis (99%+) was selected to obtain strong hydrogen bond formations, thus for optimal crosslinking in the sample when subjected to FT cycles. A 7 wt% PVA to water was used to create the phantom since this was the maximum recommended soluble concentration [28, 29]. On top of that, a small amount of 0.1 wt% acoustic scatterer, made of powdered silicon dioxide glass spheres (Silica gel 60, KGaA, Darmstadt, Germany), was added to enhance the acoustic reflectance of the phantom. The PVA gel and acoustic scatterers were added to water. Once the particles were well dispersed, they were magnetically stirred at an initial speed of 400 rpm using a hot plate magnetic stirrer with temperature controller. The mixture was heated to a temperature of 93°C and hold for 30 minutes. Then, the

solution was removed from the hotplate in order to cool to room temperature.

Whilst the previous described PVA gel mixture, which served as basis to create the vessel wall of the phantom, allowed to cool down, another mixture was prepared with the intention to create scar tissue. Hereby, the used composition material consisted of powdered calcium carbonate $CaCO_3$ (500 g Calciumcarbonat, Original Rügener Schlämmkreide, Germany), which was chosen because of its the ability to increase material density with creation of specific internal structures, often resulting in a higher texture strength and desired to mimic scar tissue [30]. A concentration of 50 wt% $CaCO_3$ was added to a mixture of 7 wt% PVA and 0.5 wt% acoustic scatterer. Subsequently, the entirety was added to water followed by repetition of the aforementioned preparation cycle.

To construct the vascular phantom, the scar tissue, comprising the $CaCO_3$ gel mixture, first required to be manufactured. This was performed by pouring of the $CaCO_3$ mixture into the open space of a tubular mould (similar to the second part of the SVC, illustrated in **Fig. 1**A), which was closed at the side and bottom. After pouring, the tubular mould with $CaCO_3$ mixture was placed in a temperature controllable freezer set at -19 °C and underwent a number of 2 FT cycles, of which one cycle included 16 hours of freezing and 8 hours of thawing at room temperature. Following subjection of 2 FT cycles, the constructed scar tissue was positioned in the mould, within the open space of the second part of the SVC that was attached to the fixed inner tube (see **Fig. 1**A). Then, after connection of the tubular structures (i.e. left and right innominate vein, upper part) to the second part of the SVC, the PVA gel mixture was poured in the mould through the two openings located at the top and side (**Fig. 1**B). Subsequently, the mould was placed in a freezer and underwent a number of 2 FT cycles under similar circumstance as aforementioned. This means that the FT cycle was repeated twice to create the vessel wall and four times to create the endovascular scar tissue.

C. ICE imaging

To evaluate the performance of the vascular phantom as simulation model for TLEs and testing model for US imaging, we investigated whether the phantom could discriminate different structures of the lead-tissue interface (i.e. vessel wall, scar tissue and cardiac lead) in terms of echogenicity. Therefore, the phantom was anatomically positioned in a circular glass beaker, filled with water. The SVC of the phantom was attached to a holder through metal wires and clips. Subsequently, a 2 mm thin pacing lead was inserted into the left innominate vein and through the scar tissue at the inner wall of the SVC (**Fig. 1**). A 9-Fr phased-array Viewflex ICE catheter (Viewflex, St Jude Medical, St Paul, MN, USA) was used to image the phantom at a frequency of 6.25 MHz. This catheter was coupled to a catheter interface module (St. Jude Medical, Inc., St. Paul, MN, USA) which was connected to a CX50 US system (Philips Medical Systems, Andover, MA, USA). The SVC of the phantom was taken as field of view since this area consisted of a vessel wall and lead binding sites (i.e. lead in scar tissue). Subsequently, two views of the ICE catheter were examined, namely a longitudinal view both outside and inside the SVC. To image the latter, the ICE catheter was introduced into the entry of the right innominate vein to approach the SVC.

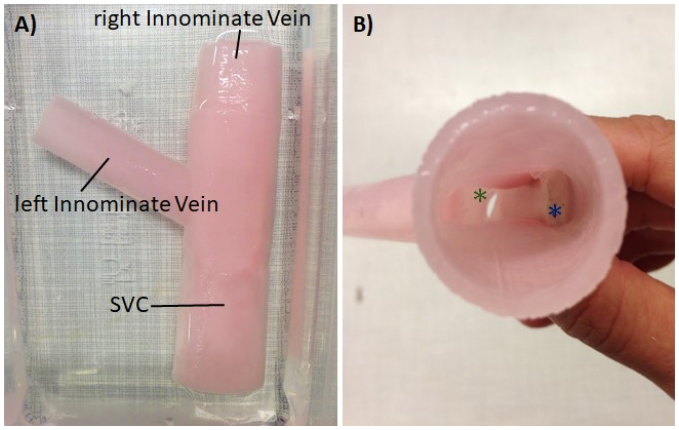

Fig. 2. Construction of the vascular phantom model. A) Description of the phantom. B) The SVC with calcified scar tissue (blue asterisk) at its inner wall. Green asterisk: Stenosis between the SVC and right innominate vein. Notice that for an appropriate anatomy interpretation the entire phantom should be horizontally rotated by an angle of 180°.

III. RESULTS

A. Vascular phantom

A vascular phantom model, presented in **Fig. 2**, was constructed to mimic a human junction of the SVC and innominate veins in terms of geometry (see **Fig. 1**B) [31-37]. The left innominate vein is sharply angulated with respect to the SVC whereas the right innominate vein directly descends into the SVC (**Fig. 2**A). The constructed endovascular scar tissue at the inner wall of the SVC (**Fig. 2**B) is calcified and has a thickness of 3 mm, this latter is equivalent to human scar thicknesses [1]. The stenosis between the SVC and right innominate vein was due to inflow of PVA gel to the attachment points of the tubular structures during pouring and can be easily avoided by proper sealing of the edges (e.g. with Vaseline) prior to pouring.

B. ICE findings

Fig. 3A and B shows the ICE images with the two views of the SVC of the phantom. The lead-tissue interface is clearly visible for both views, whereby the lead is visualized as linear and echo dense. A longitudinal view of the ICE catheter outside the SVC (**Fig. 3**A) shows the vessel wall proximate to the ICE transducer with an echo-dense signal of the scar tissue. The area beyond the scar tissue is characterized by a linear echogenic shadow, which is also observable in a longitudinal view of the ICE catheter inside the SVC (**Fig. 3**B), As a result, the vessel wall located at the distal end of the image plane, has completely disappeared in both views. In the longitudinal view

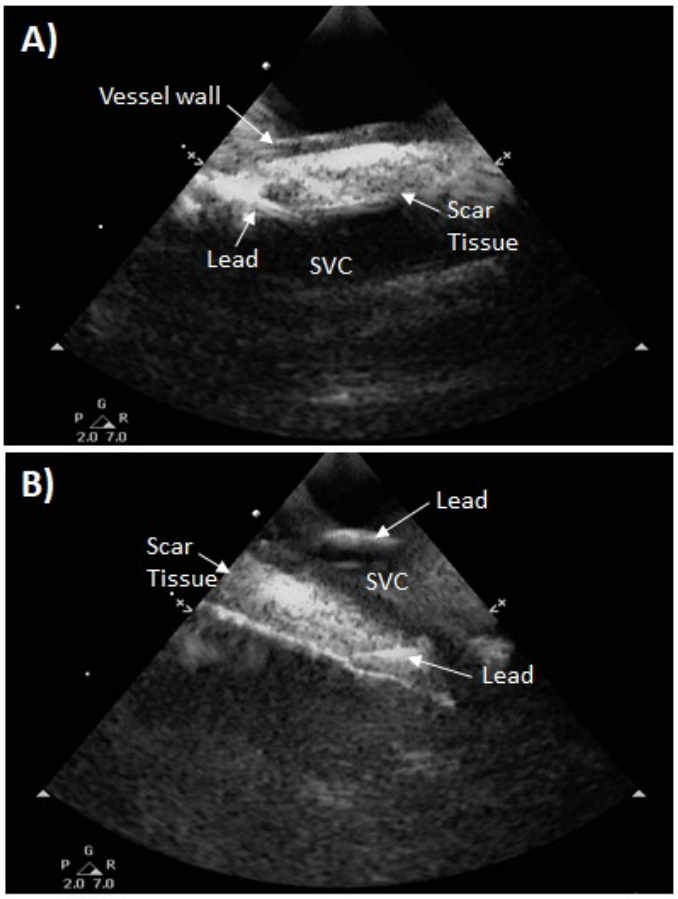

Fig. 3. 2D ICE images of the SVC of the vascular phantom with its lead-tissue interface. A) Longitudinal view of the ICE catheter outside the SVC. B) Longitudinal view of the ICE catheter inside the SVC.

inside the SVC, the lead is visualized twice, both as free-floating and adhered to scar tissue. This is because the lead body was solely encapsulated at a few sites. Consequently, both its free-floating and adhered part were in the image plane of the ICE transducer.

IV. Discussion

To the author's knowledge, this is the first study that has introduced a methodology to design and construct a 'home made' vascular phantom model for simulation of a TLE environment and suitable for US imaging to evaluate the utility of US modalities for TLE procedures. The study has demonstrated that evaluation of US modalities (i.e. ICE) for TLEs can be also performed on a tissue-mimicking PVA phantom as alternative to animals or patients. This has the advantage of saving costs and ethical issues on animal experiments and possibly even early clinical evaluations in the longer term but may also accelerate pre-clinical and clinical research on this topic.

It was shown that the phantom could be clearly visualized on ICE and allowed for discrimination, in terms of echogenicity, of its vessel wall, endovascular scar tissue and a pacing lead. On top of that, the echo dense signals of the scar tissue along the lead-tissue interface, characterized by a linear echogenic shadow, were consistent with observations from prior clinical studies [12, 14].

Whilst the objective was to evaluate the phantom's performance on 2D ICE, this study has simultaneously demonstrated that a phased-array ICE catheter can be used to visualize and assess the lead-tissue interface, which is important to predict the difficulty and risk of extraction [14]. Although the examined visualization planes both presented the lead-tissue interface, it was found that a longitudinal view outside the SVC was more valuable due to its ability to visualize the vessel wall. This is because the location of the vessel wall with respect to the lead binding sites is crucial information for the operator to determine whether the extraction sheath should be repositioned to disrupt lead adhesions without inducing vascular tears. Nevertheless, the longitudinal view outside the SVC was solely feasible because of its application in an experimental set-up but currently does not seem anatomically possible, as opposed to a longitudinal view inside the SVC.

The present study has proposed a vascular phantom model for testing of US modalities to reduce adverse effects during TLE procedures. However, this medical phantom might also be utilized for training of physicians that perform TLEs. Given that a TLE is an invasive procedure, in which most serious adverse effects occur with the operator's early experience and little regular practice, it demands highly trained and experienced operators to consistently deliver safe and effective care [38-40]. Unfortunately, currently there is a lack of means to provide the training, practice and repetition necessary to acquire the desired technical expertise. Only few sites are available where practitioners could gain adequate clinical experience, and watching an instructional video demonstration or observing how another operator performs the extraction is not sufficient [3, 40]. As this could be problematic, alternative solutions are required, such as phantom models that serve as training tool. Particularly, with the current phantom it would be interesting to examine whether it is able to produce similar extraction forces such as those perceived in realistic patient scenarios, to acquire tactile skills as additive to the skills acquired from visual learning (ICE could also aid in this process by simultaneously providing visual feedback). This is because tactile skills are hard to teach, while excessive pulling and primarily pushing forces are a main malefactor of complications, such as SVC tears [41]. Thus, this phantom model might be potentially utilized to provide adequate training and acquisition of these skills by offering realistic situations in an environment free of risk.

A. Study Limitations

Although the vascular junction of the phantom was tailored to reported geometry from literature [31-37], this study is limited to a phantom with a wall thickness of 2 mm rather than a desired thickness of 1 mm [42]. This thickness was chosen to minimize the risk of vessel rupturing during extraction of the phantom from the mould. Since the goal is to strive towards

human veins, the mould should be optimized with a geometry that allows manufacturing of a 1 mm thin vessel wall. Hereby, it should be examined whether the optimized mould still allows for complete phantom construction and extraction.

To acquire the ICE images of the phantom, the measurements were solely conducted in water. This was because the phantom showed an anechoic signal on ICE, both in blood-mimicking fluid and in porcine whole blood. We assume this is due to little difference in acoustic impedance between the phantom material and the medium in which it was measured (i.e. blood mimicking fluid, porcine blood). Regarding this, a study of Fromageau et al. 2007 [21] has demonstrated that within PVA samples the structure's main density and speed of sound have a logarithmic increasing relationship when the number of FT cycles increases. Since the acoustic impedance is the product of the structure's main density and speed of sound [43], a recommendation for future research would be to increase the number of FT cycles of the phantom. This is to examine whether a higher main density and speed of sound would also increase the difference in acoustic impedance between the phantom material and medium, and subsequently the echo signal of the phantom. Besides this, the acoustic impedance of the phantom material and medium should be measured to verify the assumption.

Although the results of this study appear to be promising and the PVA phantom closely mimics a human junction of the SVC and innominate in terms of geometry and echogenicity, the phantom should ideally include highly lifelike mechanical, optical, mobile and acoustic properties to realistically simulate a TLE and to provide an adequate testing environment for US modalities. As the latter primarily requires matching acoustic properties, a suggestion for future research would be to measure and compare the phantom's acoustic impedance and speed of sound with a 'diseased' human SVC (i.e. with endovascular scar tissue).

The phantom model, described within this study, represented a feared high risk area which is essential to evaluate US modalities properly for TLEs. However, the reader should keep in mind that these modalities should be evaluated on their performance to visualize the lead-tissue interface such that, complications can be avoided or otherwise been detected fast enough to intervene on time. Hence, for future research it is recommended to extend this phantom model to an entire heart, so that complications (e.g. inducing a SVC perforation with an extraction sheath and a consequent hemothorax/inducing a myocardial perforation with an inserting lead and a consequent pericardial effusion) can be simulated with the purpose of examining whether or not the US modality is able to detect these complications.

V. Conclusion

We have demonstrated the feasibility of producing a vascular PVA phantom model for simulation of a TLE environment and suitable for US imaging to test US modalities for use during TLEs. We conclude that the phantom is suitable to mimic a 'diseased' human junction of the SVC and innominate veins in terms of geometry and echogenicity. Hence, this model may potentially serve as a patient-safe testing environment for US modalities to reduce major complications during TLEs.

VI. Acknowledgements

We want to thank Charles Sio, Gerald Lucassen, Martin Pekař and Pepijn Wortelboer from Philips Research for their collaboration. We also want to thank Arjan van Dijke from Delft University of Technology for his assistance in the laboratory.

VII. References

1. Maytin, M., R. John, and L.M. Epstein, *Device pocket scar predicts transvenous lead extraction difficulty.* J Innov Card Rhythm Manage, 2015. **6**: p. 2173-2177.
2. Schaller, R.D., M.M. Sadek, and J.M. Cooper, *Simultaneous lead traction from above and below: A novel technique to reduce the risk of superior vena cava injury during transvenous lead extraction.* Heart Rhythm, 2018.
3. Kusumoto, F.M., et al., *2017 HRS expert consensus statement on cardiovascular implantable electronic device lead management and extraction.* Heart Rhythm, 2017. **14**(12): p. e503-e551.
4. Wazni, O., et al., *Lead extraction in the contemporary setting: the LExICon study: an observational retrospective study of consecutive laser lead extractions.* J Am Coll Cardiol, 2010. **55**(6): p. 579-86.
5. Oestreich, B.A., et al., *Use of Transesophageal Echocardiography to Improve the Safety of Transvenous Lead Extraction.* JACC Clin Electrophysiol, 2015. **1**(5): p. 442-448.
6. Endo, Y., et al., *Clinical utility of intraprocedural transesophageal echocardiography during transvenous lead extraction.* Journal of the American Society of Echocardiography, 2008. **21**(7): p. 861-867.
7. ROUX, J.F., et al., *Laser lead extraction: predictors of success and complications.* Pacing and clinical electrophysiology, 2007. **30**(2): p. 214-220.
8. Jones IV, S.O., et al., *Large, single-center, single-operator experience with transvenous lead extraction: outcomes and changing indications.* Heart Rhythm, 2008. **5**(4): p. 520-525.
9. Hauser, R.G., et al., *Deaths and cardiovascular injuries due to device-assisted implantable cardioverter–defibrillator and pacemaker lead extraction.* Europace, 2009. **12**(3): p. 395-401.
10. Lou, X., et al., *Successful stent implantation for superior vena cava injury during transvenous lead extraction.* HeartRhythm Case Rep, 2015. **1**(6): p. 394-396.
11. Topaz, O., *Lasers in cardiovascular interventions*. 2015: Springer.
12. Bongiorni, M.G., et al., *Intracardiac echocardiography in patients with pacing and defibrillating leads: a feasibility study.* Echocardiography, 2008. **25**(6): p. 632-638.
13. Bartel, T., et al., *Why is intracardiac echocardiography helpful? Benefits, costs, and how to learn.* Eur Heart J, 2014. **35**(2): p. 69-76.
14. Sadek, M.M., et al., *Utility of intracardiac echocardiography during transvenous lead extraction.* Heart Rhythm, 2017. **14**(12): p. 1779-1785.
15. Hilberath, J.N., et al., *Rescue transoesophageal echocardiography for refractory haemodynamic instability during transvenous lead extraction.* European Heart Journal–Cardiovascular Imaging, 2014. **15**(8): p. 926-932.
16. Regoli, F., et al., *Clinical utility of routine use of continuous transesophageal echocardiography monitoring during transvenous lead extraction procedure.* Heart Rhythm, 2015. **12**(2): p. 313-20.
17. Lelovas, P.P., N.G. Kostomitsopoulos, and T.T. Xanthos, *A comparative anatomic and physiologic overview of the porcine heart.* Journal of the American Association for Laboratory Animal Science, 2014. **53**(5): p. 432-438.

18. Chmarra, M.K., et al., *Multimodal phantom of liver tissue.* PLoS One, 2013. **8**(5): p. e64180.
19. Culjat, M.O., et al., *A review of tissue substitutes for ultrasound imaging.* Ultrasound Med Biol, 2010. **36**(6): p. 861-73.
20. Surry, K., et al., *Poly (vinyl alcohol) cryogel phantoms for use in ultrasound and MR imaging.* Physics in Medicine & Biology, 2004. **49**(24): p. 5529.
21. Fromageau, J., et al., *Estimation of polyvinyl alcohol cryogel mechanical properties with four ultrasound elastography methods and comparison with gold standard testings.* IEEE transactions on ultrasonics, ferroelectrics, and frequency control, 2007. **54**(3).
22. Nadkarni, S.K., et al., *A pulsating coronary vessel phantom for two- and three-dimensional intravascular ultrasound studies.* Ultrasound in medicine & biology, 2003. **29**(4): p. 621-628.
23. Wan, W., et al., *Optimizing the tensile properties of polyvinyl alcohol hydrogel for the construction of a bioprosthetic heart valve stent.* Journal of Biomedical Materials Research: An Official Journal of The Society for Biomaterials, The Japanese Society for Biomaterials, and The Australian Society for Biomaterials and the Korean Society for Biomaterials, 2002. **63**(6): p. 854-861.
24. Chu, K.C. and B.K. Rutt, *Polyvinyl alcohol cryogel: An ideal phantom material for MR studies of arterial flow and elasticity.* Magnetic Resonance in Medicine, 1997. **37**(2): p. 314-319.
25. Ceh, D., T.M. Peters, and E.C. Chen. *Acoustic characterization of polyvinyl chloride and self-healing silicone as phantom materials*. in *Medical Imaging 2015: Physics of Medical Imaging*. 2015. International Society for Optics and Photonics.
26. Pogue, B.W. and M.S. Patterson, *Review of tissue simulating phantoms for optical spectroscopy, imaging and dosimetry.* J Biomed Opt, 2006. **11**(4): p. 041102.
27. Li, W., B. Belmont, and A. Shih, *Design and manufacture of polyvinyl chloride (PVC) tissue mimicking material for needle insertion.* Procedia Manufacturing, 2015. **1**: p. 866-878.
28. de Jong, T.L., et al., *PVA matches human liver in needle-tissue interaction.* J Mech Behav Biomed Mater, 2017. **69**: p. 223-228.
29. Sekisui. *Solution preparation guidelines - Selvol polyvinyl alcohol*. 2018 4 December 2018]; Available from: https://www.sekisui-sc.com/wp-content/uploads/SelvolPVOH_SolutionPreparationGuidelines_EN.pdf.
30. Yusof, N.S.M., et al., *Ultrasound imaging characterization on tissue mimicking materials for cardiac tissue phantom: Texture analysis perspective.* Malaysian Journal of Fundamental and Applied Sciences, 2017. **13**(4-2): p. 501-508.
31. Sonavane, S.K., et al., *Comprehensive imaging review of the superior vena cava.* Radiographics, 2015. **35**(7): p. 1873-1892.
32. Mahlon, M.A. and H.-C. Yoon, *CT angiography of the superior vena cava: normative values and implications for central venous catheter position.* Journal of Vascular and Interventional Radiology, 2007. **18**(9): p. 1106-1110.
33. Mozes, G. and P. Gloviczki, *Venous embryology and anatomy*, in *The Vein Book*. 2007, Elsevier. p. 15-25.
34. Gibson, F. and A. Bodenham, *Misplaced central venous catheters: applied anatomy and practical management.* Br J Anaesth, 2013. **110**(3): p. 333-46.
35. McMurdo, K., et al., *Normal and occluded mediastinal veins: MR imaging.* Radiology, 1986. **159**(1): p. 33-38.
36. Salik, E., A. Daftary, and M.G. Tal, *Three-dimensional anatomy of the left central veins: implications for dialysis catheter placement.* Journal of Vascular and Interventional Radiology, 2007. **18**(3): p. 361-364.
37. AbuRahma, A., *Noninvasive Vascular Diagnosis: A Practical Textbook for Clinicians*, ed. F. Edition. 2017: Springer Science & Business Media.
38. Byrd, C.L., et al., *Clinical study of the laser sheath for lead extraction: the total experience in the United States.* Pacing and Clinical Electrophysiology, 2002. **25**(5): p. 804-808.
39. van Erven, L., J.M. Morgan, and C. Scientific Initiatives, *Attitude towards redundant leads and the practice of lead extractions: a European survey.* Europace, 2010. **12**(2): p. 275-6.
40. Wilkoff, B.L., et al., *Transvenous lead extraction: Heart Rhythm Society expert consensus on facilities, training, indications, and patient management: this document was endorsed by the American Heart Association (AHA).* Heart Rhythm, 2009. **6**(7): p. 1085-104.
41. Maytin, M., T.P. Daily, and R.G. Carillo, *Virtual reality lead extraction as a method for training new physicians: a pilot study.* Pacing Clin Electrophysiol, 2015. **38**(3): p. 319-25.
42. SCI. *Scientific Computing and Imaging Institute - Arterial System Lecture Block 10 Bioengineering 6000 CV Physiology*. 2019 2 January 2019]; Available from: http://www.sci.utah.edu/~macleod/bioen/be6000/notes/L10-arteries-veins.pdf.
43. Secrest, S., *Basic Principles of Ultrasonography.* VETERINARY TECHNICIAN, 2006. **27**(12): p. 756.

1

INTRODUCTION

1.1. BACKGROUND

Transvenous lead extractions (TLEs) are minimally invasive procedures in which pacing or implantable cardioverter defibrillator (ICD) leads are extracted under guidance of 2D X-ray fluoroscopy. The demand for TLE procedures has grown considerably to an annual extraction rate of about 24.000 patients worldwide [2] which is due to an increased number of cardiovascular electronic implantable device (CIED) infections and other indications such as lead fracture or failure [3, 4]. Furthermore, advancement of tools and extraction techniques as well as the growth of clinical experience over time positively influenced the outcome of TLE and promoted further adoption on global scale [2, 5]. Despite these clinical and technological advances, TLE remains a complex and risky procedure with a small but distinct rate of reported major complications and mortality; these reported values vary even widely across studies, with major complications from 0.4% to 3.4% and mortality rates of 0% to 1.9% [5-9]. Of these major complications, which primarily comprise life-threatening vascular tears, it is estimated that two-thirds occur in the superior vena cava (SVC) [4]. Operators mostly fear injury to the SVC because of the corresponding mortality, exceeding the 50%, even when there is rapid detection and subsequent surgical intervention [3, 10, 11]. This can be explained by the fact that the SVC has a relatively thin vessel wall and unfavourable position, near the right pleura and pericardium. Given the bending shape characteristics of the SVC, the lead rarely takes a straight course through this part. Thus, when attempting to liberate the lead from surrounding tissue with an extraction sheath, a perforation can be easily induced with possibly fatal consequences such as bleeding into the chest and/or pericardium [3]. Although development of powered extraction sheaths (e.g. lasers and rotational cutting sheaths), yielded improved success rates of TLE, it has not reduced the rate of SVC injury [3, 5, 10, 12, 13], which might be a principal impediment to perform this procedure.

1.2. PROBLEM DESCRIPTION

As aforementioned, TLE's are currently guided under 2D X-ray fluoroscopy, which is considered the standard of reference for this procedure as well as for other cardiovascular interventions. From a previous performed literature study and additional conversations with electrophysiologists in the field [14], it became clear that although fluoroscopy can be performed relatively easy [15] and visualizes the vascular system with subsequent advancement of the extraction sheath, it has several limitations regarding visualization of anatomical structures. First, it is unable to visualize the venous and myocardial wall although it is essential to determine whether the extraction sheath still follows a proper intravascular course. Second, it does not detect high-risk areas during sheath advancement such as vessel tortuosity, myocardial invagination or the presence of endovascular scar tissue. The latter is due to the foreign body response to intravascular leads and develops over time in pacemaker patients (this will be described in section 2.3.1 of Chapter 2) [2]. Third, potential major complications (e.g. hemothorax, vegetation embolization) cannot be detected early with fluoroscopy [16-18].

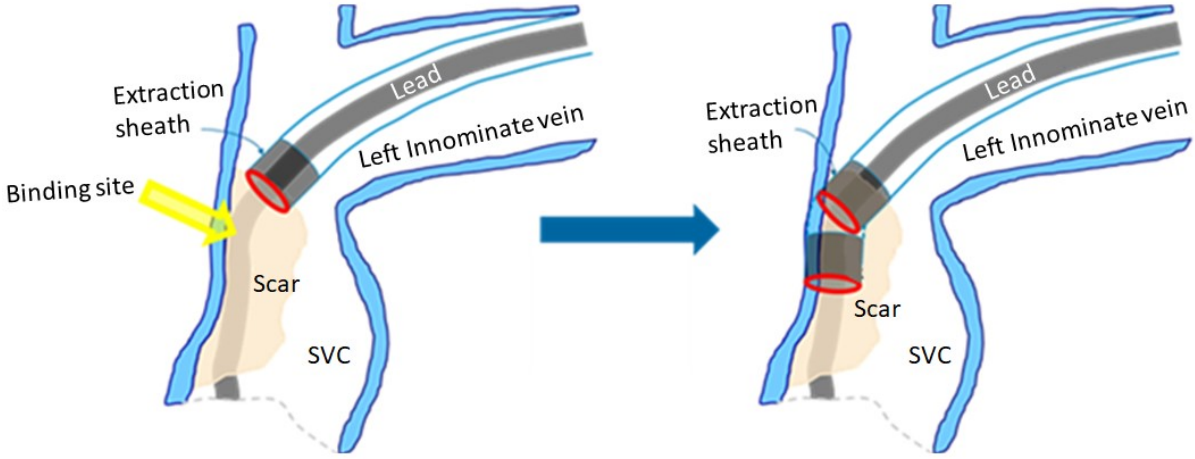

Figure 1. Inducing laceration in the SVC

Left: Encapsulation of the lead body by scar tissue. To disrupt the lead adhesions an extraction sheath is used that advances over the lead. Right: Inducing a dissection of the SVC wall over time with the sheath. Image acquired from: IBS, Philips Research Eindhoven, and subsequently modified.

Given the limitations of fluoroscopy, performing a TLE is not without risk and requires high skilled operators. Particularly, in case of endovascular scar tissue, which may encapsulate the lead body at several places, complexity and risk of extraction are increased as well as procedural and fluoroscopic exposure time [11]. This is because the lead adhesions should be disrupted first to extract the lead from the vascular system. However, the binding sites are most often located proximate to the venous wall (Figure 1). Since the operator is not able to identify the venous wall, nor the lead adhesions on fluoroscopy (Figure 2) and given that the venous system is tortuous and tight, there is a risk of advancing the tip of the sheath into the venous wall with corresponding complications (Figure 1).

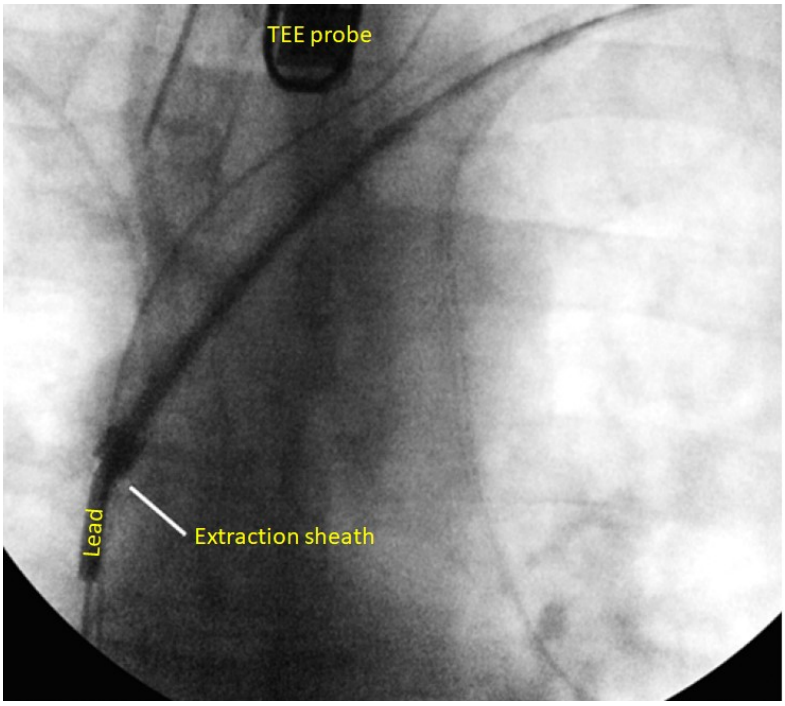

Figure 2. Fluoroscopy image of the SVC [18]

TEE = transesophageal echocardiography; probe to monitor complications. How does the operator know in which direction the extraction sheath should be oriented to disrupt the adhesions between the lead and the SVC wall, given that resistance of scar tissue can push the tip of the sheath towards the wrong direction with subsequent vascular laceration?

Although there are several factors (Table 11 of Appendix A) that increase the difficulty and risk of extraction, procedural outcomes of TLE's primarily depend on operator experience [18]. From literature, it has been reported that success rates of TLE have increased over time but the problem is that most of these reports originate from high volume extraction centres where the operators are highly experienced and receive referrals from smaller volume extraction centres [5, 9, 19-23]. In the smaller centres where the number of annual extractions per operator is much less, also the success rate is likely to be lower and the risk of major complications greater since little practice may lead to unnecessary complications [24]. Given the potentially serious complications that may arise, this procedure can even trigger anxiety in the most experienced operators [16]. As perception of risk of major complications can increase up to 5% [25], which is about 2.5 times as high as in practice, this may reduce the number of operators willing and able to perform the procedure while simultaneously the demand for lead extractions keeps growing in a population with greater risk of infection [18]. As endocarditis is associated with high morbidity and mortality [26-29], it is crucial to seek for methods that could encourage operators to do a TLE.

CLINICAL NEED

Performing a TLE carries a small but distinct risk of serious complications including vascular laceration, bleeding and death. In order to prevent adverse effects during lead management there is need for a guiding tool that allows the operator to identify the venous wall (for maintaining proper sheath positioning) and areas of high risk. Furthermore, it should enable early detection of complications so that when adverse effects emerge, they can be managed and controlled more properly by the operator.

1.3. PROPOSED SOLUTION

At Philips Research (In-Body Systems, Eindhoven) a phased-array intracardiac echocardiography (ICE) catheter (Viewflex, St Jude Medical, St Paul, MN, USA) is available to image the lead-tissue interface (i.e. the lead binding sites) and to evaluate its utility to reduce adverse effects during a TLE procedure. In order to perform these measurements, a specific lead extraction environment (e.g. a SVC with lead binding sites) is required. However, within this orientation phase, solely pre-clinical tests can be performed either in animal models or phantoms, serving as substitute for human tissue. Although porcine hearts closely resemble human hearts, their use is not a matter of course due to practical and ethical reasons. Furthermore, they are not pulsated which means that the veins will be collapsed, resulting in geometries other than when naturally pulsated. On top of that, porcine hearts are not generally diseased, which makes it challenging to obtain realistic patient scenarios of intravascular lead binding sites. As alternative to animal models, phantoms are considered a helpful method to mimic human tissue and allow technology testing in a patient-safe and environment-friendly manner [30]. Hence, within this thesis project an ultrasound compatible vascular phantom model will be developed to allow simulation of a lead extraction environment and subsequently to evaluate the utility of ICE for TLE procedures.

1.4. OBJECTIVE

The objective of this research project is twofold. First, the goal is to design and construct a vascular phantom model with realistic geometry and echogenicity to simulate a real-life lead extraction environment suitable for ultrasound imaging.

Second, the aim is to evaluate the utility of a ViewFlex phased-array ICE catheter, for the prevention of SVC injury during lead management. This will be accomplished by using in-vitro porcine tissue and the constructed vascular phantom model. Subsequently, various visualization planes of the ICE catheter will be investigated to determine which plane provides the most valuable insight into the lead-tissue interface.

Eventually, future research should perform clinical evaluation in an echo-patient study to assess whether the findings of this study are also valid in practice.

1.5. CURRENT STATE OF THE ART

Vascular phantom models

Commercial available phantoms are relatively expensive, intended for a broad market and often do not provide the desired test environment tailored to the needs of the user. Therefore, this thesis project aims for the development of a 'home made' vascular phantom model that will specifically simulate a real-life lead extraction environment, and with compatibility to ultrasound to allow for ICE evaluation. To the best of my knowledge, phantoms intended for this purpose have not been developed previously, neither commercially nor in academic setting. Hence, this phantom model would be valuable to examine the utility of ICE for TLE procedures. Simultaneously, it may stimulate other researchers to prepare these customized 'home made' phantoms as well since they are made more affordable and accessible and as a result it may accelerate pre-clinical and clinical research on cardiovascular diseases.

Echocardiography

A literature study conducted prior to this thesis project, has shown that transesophageal echocardiography (TEE) as adjunctive to fluoroscopy, is well established ultrasound imaging tool to detect complications during lead management [14]. Although TEE imaging has essential capabilities, such that it allows early detection of vegetations (e.g. endocarditis) and complications (e.g. pericardial effusion), it has a poor patient tolerance and therefore commonly requires general anaesthesia. Furthermore, it has a limited view since it images from the oesophagus, which means that it may not adequately show anatomic structures in the far field and lead adhesions in the SVC or heart [31]. As alternative to TEE, transthoracic echocardiography (TTE) and intracardiac echocardiography (ICE) are available ultrasound modalities that can be used for lead management. However, using TTE during fluoroscopy is difficult since it images from the chest. On top of that, it does not provide continuous intraprocedural monitoring and is also limited in visualizing far-field anatomic structures [16, 31]. In contrast to TEE, ICE has an excellent patient tolerance and only requires conscious sedation. It can be performed by the primary operator (i.e. no need for a sonographer) and eliminates the risk of inducing oesophageal trauma [17, 32].

Despite these promising advantages, only few studies are currently available that showed the clinical utility of ICE during lead management [3, 16, 31]. Bongiorni and colleagues already showed the safety and feasibility of ICE in 2008 [16]. The authors reported that ICE provided outstanding visualization of cardiac leads and areas of adherences but only applied radial ICE rather than phased-array ICE, which has practical limitations regarding penetration depth (i.e. fixed frequency) and steer mechanism. Due to technological advancement, phased-array ICE catheters have been developed that provided multidirectional tip-deflection, a deeper penetration depth and greater ability to image cardiac structures than radial ICE.

Because of these advantages, phased-array ICE is currently a dominant modality during electrophysiological procedures, and one study [33] even showed an increased diagnostic yield of cardiac device-related endocarditis compared with TEE. Recently, Sadek et al. 2017 [31] for the first time evaluated the utility of phased-array ICE during TLE and successfully detected areas of lead adherences in the right atrium (RA), right ventricle (RV) and SVC using an AcuNav catheter (ACUSON Corporation, Mountain View, CA). Within this study, the authors primarily focused on the detection of lead adhesion sites and complications. However, it is also critical to know how the lead adhesions are located with respect to the venous/cardiac wall to determine how the extraction sheath should be oriented (particularly in the SVC) to avoid vascular tears. Analysis of the lead-tissue interface, in

the ICE images presented by Sadek et al., showed that the SVC wall could not be identified and clearly not be discriminated from the lead adhesion sites (see section 2.2.2.3 of Chapter 2). As these measurements were solely taken from one image plane (i.e. inside the SVC and perpendicular to the SVC wall), it would be valuable to examine whether other visualization planes would give more insight into the lead-tissue interface with ICE.

1.6. APPROACH

In order to accomplish the objectives of this thesis project, the following steps were taken:

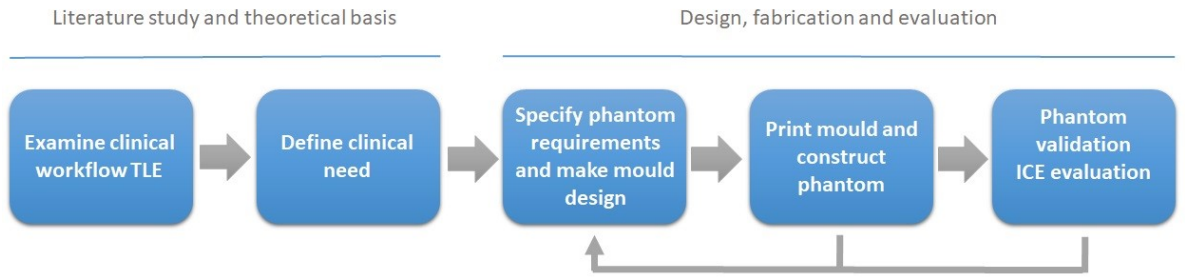

Figure 3. Schematic overview of the steps taken during the course of this thesis project

Prior to this thesis project a literature study was conducted to examine the clinical workflow of TLE and to find out what clinical problems currently exist, particularly with respect to image guidance. Along with the findings of this study, interviews were arranged with experts in the field to clarify the clinical needs.

Specification of the phantom requirements occurred at Philips Research (In-Body Systems, Eindhoven) with colleagues that were involved in the lead management project. Based on these requirements various mould designs were created following numerous iterations, ranging from basic vessel tubes to more realistic vascular trees.

The mould designs were 3D printed and allowed for phantom construction by means of material pouring. When the constructed phantom did not meet the design requirements following phantom construction or ICE evaluation, optimization occurred through either redesigning the mould or changing the properties (with respect to echogenic characteristics) of the pouring material.

The constructed vascular phantom was made suitable for ultrasound imaging, therefore ICE data could be acquired and subsequently compared to porcine data to perform phantom validation. Subsequently, the suitability of the phantom model to simulate a lead extraction environment was assessed by comparing its results with findings from prior reported clinical studies.

In the last phase of this project, ICE evaluation could be performed using the vascular phantom and porcine hearts.

1.7. ORGANIZATION OF THE THESIS

This thesis is organized as follow:

Chapter 2 is a theoretical background about lead extractions and intracardiac echocardiography. It will also provide important vascular geometry necessary to construct the phantom model and will explain the development of endovascular scar tissue.

Chapter 3 describes different methodologies to design and construct several vascular phantom models. It will provide a protocol to prepare the phantom with polyvinyl alcohol (PVA) and will give tips and tricks for PVA pouring.

Chapter 4 describes a validation experiment in which the SVC of the phantom is compared to porcine SVC in terms echogenicity.

Chapter 5 first assesses the suitability of the constructed vascular phantom model to simulate a lead extraction environment and subsequently describes numerous experiments in which the utility of ICE is evaluated using the phantom model and porcine tissue.

Chapter 6-7 Are an overall discussion of the results with current limitations of this study and recommendations for future research, followed by a final conclusion.

2

THEORETICAL BACKGROUND

This chapter provides the background information necessary to understand how a lead extraction procedure is performed nowadays. Furthermore, it will explain the basic principles of intracardiac echocardiography and some related concepts important to interpret the results, which will be presented in the following chapters. In the current chapter also an overview is given of relevant vascular geometry that will serve as a basis to construct the phantom model.

2.1. LEAD EXTRACTIONS

2.1.1. CARDIOVASCULAR ELECTRONIC IMPLANTABLE DEVICES

Cardiac arrhythmias are characterized by a disruption in either the rate (number) or rhythm (pattern) of the heartbeat. People that are severely affected by this life-threatening cardiovascular disease, usually got treated by means of a cardiovascular electronic implantable device (CIED), which is implanted in the person's body in order to restore the heartbeat when irregularities are sensed. Among CIEDs a distinction can be made between pacemakers, implantable cardioverter-defibrillators (ICDs) and cardiac resynchronization therapy (CRT) devices. A distinct difference between these devices is that pacemakers solely give low-energy electrical pulses whereas ICDs also give high-energy pulses when the prior is not effective. CRT devices function in a similar manner as pacemakers but often send electrical pulses to both ventricles of the heart. Some CRT devices also contain a built-in ICD device, thus intended for heart failure patients at high risk for sudden cardiac death [34]. In all devices, the electrical pulses are delivered through so-called leads, which are the wires that go through the veins to connect the CIED to a location in the heart, illustrated in Figure 4.

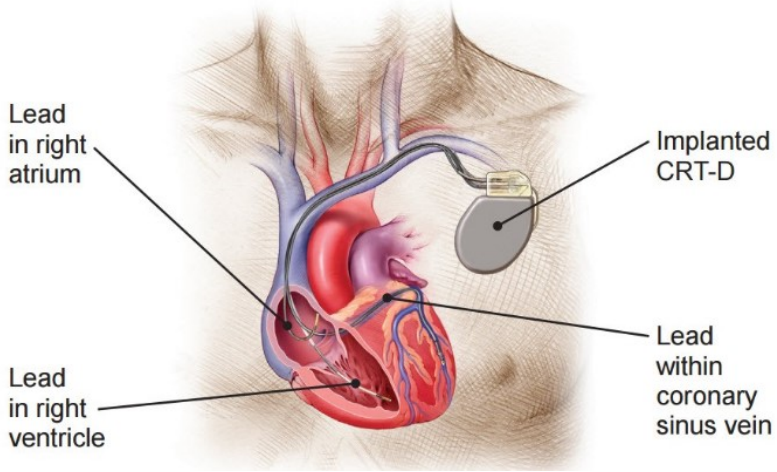

Figure 4. Leads that connect a CRT device to the heart [34]

2.1.2. TRANSVENOUS LEAD EXTRACTIONS

Sometimes the implanted pacing and defibrillator leads require to be extracted, for instance because of an infection or lead failure which necessitates the patient to undergo a lead extraction. This is an electrophysiological intervention under guidance of 2D X-ray fluoroscopy and is most commonly performed in a transvenous manner. A transvenous lead extraction (TLE) is considered the 'gold' standard because it is percutaneous and less invasive than a surgical approach. The generic clinical workflow of a TLE is presented in Figure 5, which is intended to provide a fast and concise idea of the various steps involved. In addition, a thorough description of its procedure protocol and corresponding clinical workflow is presented in Appendix A. For more information regarding TLEs the reader is referred to [14], which comprises a comprehensive literature study on lead extractions.

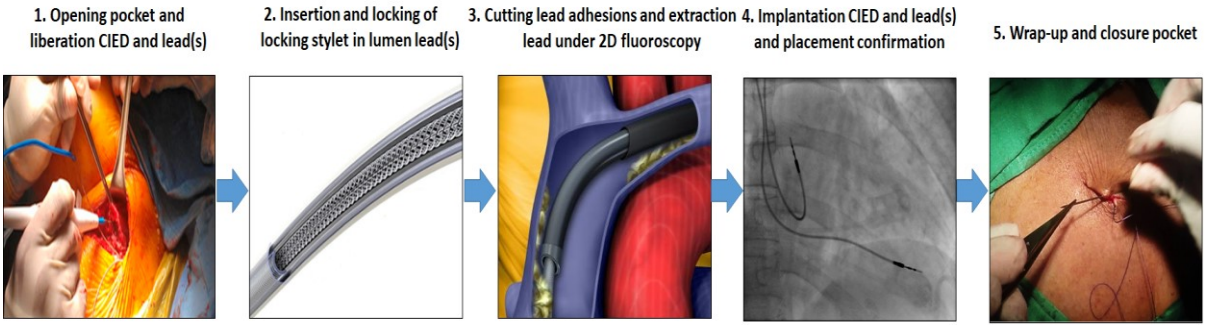

Figure 5. Generic clinical workflow of a TLE

When the CIED and lead(s) are liberated, the lead(s) are cut to allow access into their lumen. A locking stylet is inserted in the lumen to distribute the attachment forces along the lead body to facilitate extraction of the lead and to avoid the risk of coil lengthening or lead damage. Lead extraction is performed by applying push and pull forces with a mechanical or powered extraction catheter sheath (see Figure 43 for a more elaborate illustration). In case of an infection, the CIED and lead(s) are implanted a few weeks later. Images adopted from: [35-39].

2.2. INTRACARDIAC ECHOCARDIOGRAPHY IMAGING

ICE is a non-fluoroscopic imaging modality, based on the characteristics of ultrasound. It is usually inserted via a venous sheath positioned percutaneously into the femoral vein and allows for real-time imaging of cardiac structures and blood flow within the heart. Its basic principles are briefly explained.

2.2.1. PHYSICAL PRINCIPLES OF ULTRASOUND

Ultrasound is expressed as an acoustic or sound wave that includes frequencies larger than the maximum frequency audible by humans, which is 20 kHz. These sound waves, travel through a medium, are reflected at tissue boundaries and subsequently enable the generation of ultrasound images.

Concerning these sound waves, there is an inverse relation between their frequency and wavelength: With higher frequency, the wavelength becomes shorter, which requires a trade-off between resolution and penetration depth when selecting a frequency. This is because higher-frequency US waves produce images with a higher resolution. However, due to their shorter wavelength they are unable to penetrate through deep tissue structures and vice-versa.

Speed of sound highly depends on the medium in which it travels. It is influenced by the medium's rigidity or compressibility and density. When the medium is more rigid or less compressible (i.e. liquid and solids), this will result in a faster speed of sound. Alternatively, the larger the density of the medium, the slower the speed of sound. As density is affected by temperature, the speed of sound changes partially with the temperature of the medium [40].

Speed of sound is considered independent of the frequency since all frequencies approximately travel at a similar speed. However, it is affected by the wavelength and can be expressed in the following formula

$$v = f\lambda \quad (2.1)$$

where v is the speed of sound in meters per seconds [m/s], f the frequency in hertz [Hz] and λ the wavelength in meters [m]. Since the frequency remains unchanged, the wavelength should increase with higher speed at given frequency.

2.2.2. IMAGE FORMATION

2.2.2.1. Transducers

In order to generate and receive the echoes necessary to create an image, ultrasound transducers (also called probes) are used. These devices usually consist of piezoelectric crystals, which enable conversion of electrical energy into sound waves and vice-versa. Various transducers are available in different shape and size.

Within this study, a commercial available Viewflex ICE catheter (St. Jude Medical, Inc., St. Paul, MN, USA) is used (Figure 6) which comprises a 64 element linear phased-array transducer with a frequency range between 4.5 MHz and 8.5 MHz, thus containing a relatively low but sufficient image resolution to visualize cardiac structures whilst being able to penetrate through deep vasculature. Linear phased-array transducers are relatively small in size (i.e. 2-3 cm long) compared to a sequential array, which enable them to be used in small spaces. Their crystal elements are piled in a pyramid shape and produce sector-shaped images with side-firing arrays, see Figure 7. Due to the multiple elements, the

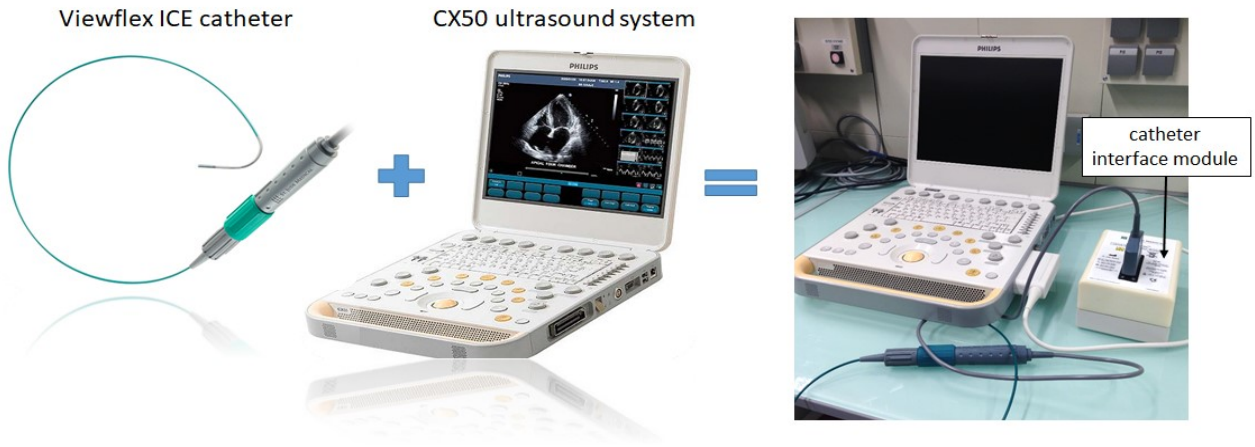

Figure 6. Connection of a Viewflex ICE catheter to a CX50 US system

The 9-Fr Viewflex ICE catheter can be connected to a CX50 ultrasound system (Philips Medical Systems, Andover, MA, USA) via a catheter interface module (St. Jude Medical, Inc., St. Paul, MN) to produce images. Images adopted from IBS, Philips Research Eindhoven and modified.

US beam can be steered by changing the time delay in element firing which is important to visualize cardiac structures. However, when steering to the outer boundaries, the sensitivity of the images is reduced. To obtain the best rest lateral resolution (i.e. the ability to distinguish structures perpendicular to the US beam), the structure of interest should be imaged in the centre of the field of view because of a larger effective aperture [41, 42].

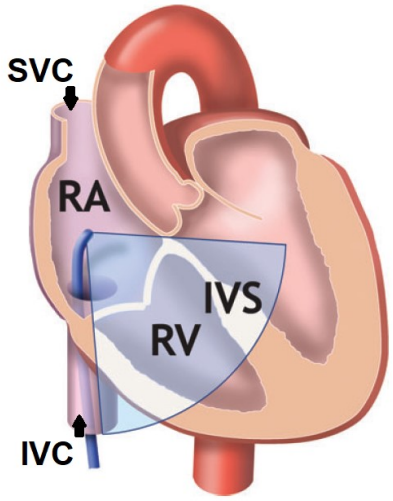

Figure 7. Producing a sector-shaped beam with a linear phased-array ICE transducer [17]

Home view of the ICE probe in the mid-right atrium. The probe has 120° of tip flexion, enabling it to be steered anterior/posterior. IVC = Inferior Vena Cava; IVS = Interventricular Septum; RA = Right Atrium; RV = Right Ventricle; SVC = Superior Vena Cava.

2.2.2.2. Interaction with tissue

When the transducer emits an echo in a medium, interaction occurs with different tissue structures. This interaction can be primary expressed in terms of attenuation and refraction.

Attenuation

This occurs when the US beam is weakened in amplitude as it encounters tissue and is described by the attenuation coefficient. Attenuation is due to reflection (back bouncing of US beam), scattering (change direction US beam) and absorption (conversion of US beam into heat). The amount of US

waves being reflected is determined by the difference in acoustic impedance between adjacent tissue structures [43].

The acoustic impedance is the resistance of a structure to US waves and is affected by the tissue's density and the speed of sound waves penetrating through this structure. At an interface of two distinct structures (e.g. dense and soft tissue or dense tissue and air) there will be a large difference in acoustic impedance, which gives a strong reflection of US echoes, whereas an interface of two soft tissue structures with a small difference in acoustic impedance, will solely reflect few echoes. A high amount of reflection will result in a high echogenicity (which refers to the ability to produce US echoes) and is visualized in the image as a bright echo. Since distinct tissue structures differ in echogenicity, there will also be clear difference in contrast visible, which allows them to be distinguished. The differences in echogenicity are explained in Figure 8. Among others, the acoustic impedance of water and blood is presented in Table 1.

Refraction

When the US beam penetrates a structure at a certain angle, there will be a transition in tissue density, which changes the speed of sound and subsequently causes the beam to bend or refract. As refraction may induce unwanted artifacts (explained in section 2.2.3) it is crucial to identify this concept [43].

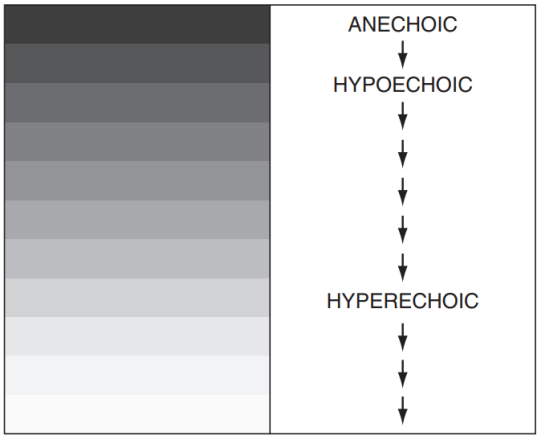

Figure 8. Differences in echogenicity [44]

Table 1. Acoustic properties of water and blood [45, 46]

Acoustic properties	Water	Blood
Speed of sound (m/s)	1480	1550-1560
Acoustic Impedance (MRayl*)	1.48	1.61-1.65
Attenuation coefficient (dB/cm at 1 MHz)	0.0022	0.17

*1 MRayl = 10^6 Pa·s·m^{-1}.

2.2.2.3. Lead-tissue interface visualized on echocardiography

On echocardiography, areas of fibrous and calcified tissue are visualized as echo-dense or hyperechoic structures, which are located along the lead-tissue interface (i.e. lead binding sites). They are characterized by a linear echogenic shadow. Leads are considered as mobile structures attached to cardiac tissue, either visualized as circular (lead transversal view) or linear (lead longitudinal view) [16, 31]. They often appear as hyperechoic, equivalent to the binding sites in terms of contrast. Figure 9 presents the lead-tissue interface.

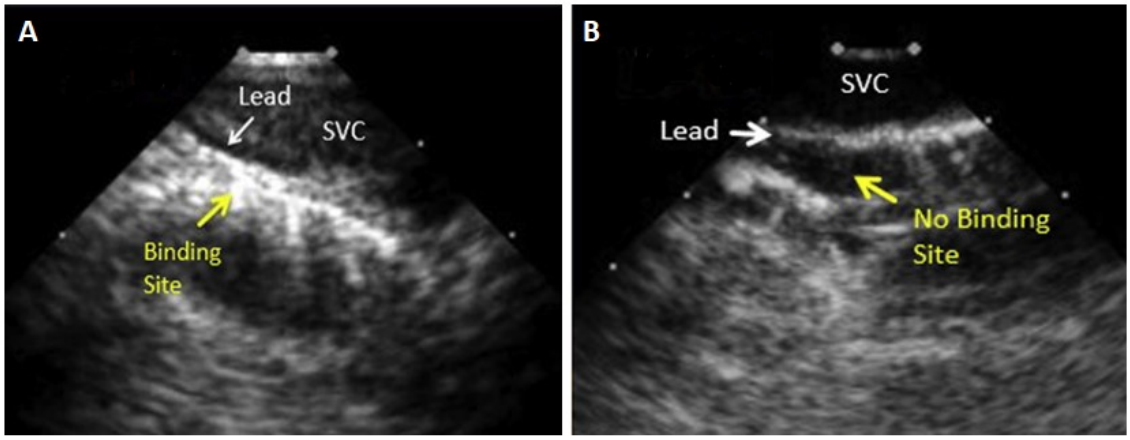

Figure 9. ICE image of the lead-tissue interface [31]

Longitudinal view of the SVC showing the lead-tissue interface in image A. In image B no binding sites are present, which allows the US beam to penetrate through this area. As a result, this area contains more echo signal than in A, where primarily a linear echogenic shadow is shown.

2.2.2.4. Ultrasound contrast agents

Ultrasound contrast agents are able to increase the echogenicity of a structure evidently. They comprise microbubbles, which are made of either air or an inert gas and usually coated by a layer of protein, lipid or polymer and sometimes quartz glass microspheres [30, 47, 48]. When the microbubbles are captured in an US field, they compress and expand by differences in acoustic pressure. This results in non-linear oscillations producing an increased echo signal, which can be discriminated from normal tissue. The microbubbles can be administered to the systemic circulation to produce contrast-enhanced ultrasound but can also be added to phantom structures to increase the echogenicity of a particular structure locally.

2.2.3. IMAGE ARTIFACTS

Artifacts include features of an acquired US image, which are not a true representative of the area being investigated [43, 49]. When analyzing US images, it is essential to recognize these artifacts and subsequently to understand the reason behind their evolvement, so that when necessary one knows how to eliminate them. Within the scope of this thesis, two artifacts are relevant which will be explained as follow:

Mirror image artifact

This artifact occurs when the primary US beam encounters another structure in its path, causing it to be reflected again while it actually should return back to the transducer. In other words, the beam first reflects from the tissue surface (e.g. phantom) and subsequently encounters a highly reflective most often rounded surface, such as a glass beaker. This causes the US beam to be reflected back again, giving a delayed echo when returning back towards the transducer. Since the transducer incorrectly assumes the returning echo has solely been reflected once rather than twice, it assesses the delayed echo as being returned from a deeper structure. As a result, this gives a mirror artifact on the other side of the highly reflective surface. Imaging from a different angle may possibly eliminate this artifact [43, 50].

Sibe Lobe Artifact

This artifact occurs when echoes are generated from sound waves that have travelled from another direction than the primary US beam. However, they are positioned in the image as that they originated from the primary beam. These artifacts are associated with round and highly reflective structures and

usually emerge as faint echoes. Usually, reducing the gain or adjusting the penetration depth will eliminate side lobes.

2.2.4. ULTRASOUND GLOSSARY

Adopted from [43] and [44].

Anechoic	Free of echoes; area appears black on US
Echocardiography	Ultrasound examination of the heart
Echogenic	The ability of a structure to produce US echoes
Hyperechoic	Highly reflective, having strong echoes. Describes an area of great signal amplitude compared with surrounding structures. Appears as varying shades of lighter grey
Hypoechoic	Less reflective, having relatively weak echoes. Describes an area of lower signal amplitude compared with surrounding structures. Appears as varying shades of darker grey
Isoechoic	Having a similar echogenicity to a surrounding structure
Resolution	Ability to separate in space, time or strength

2.3. VASCULAR GEOMETRY

The geometric dimensions of the human vascular structures of interest were acquired from literature. These measures, presented in Table 2 and Table 3, provide a reference of how the vascular phantom geometrically should be. In Figure 10 an illustration is given of the heart and its corresponding vessels.

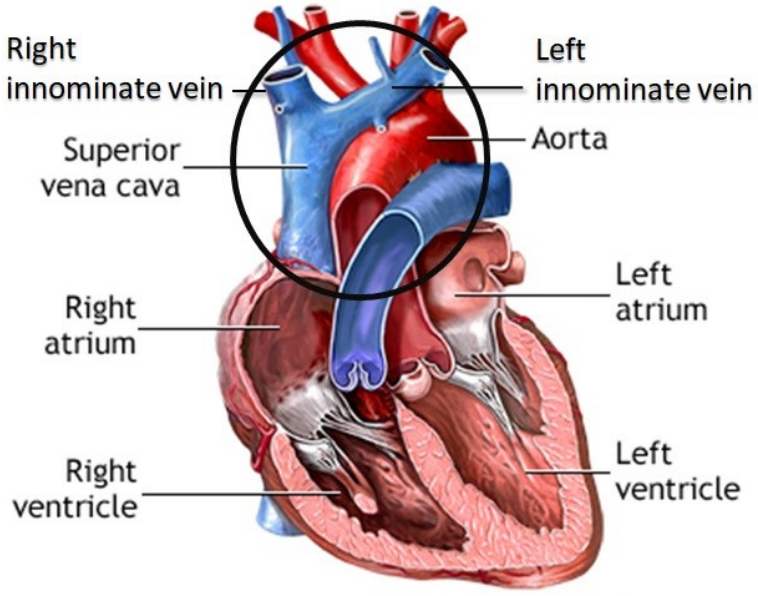

Figure 10. The heart including the SVC and innominate veins

The circle shows the vasculature of interest. This shape will be adopted to create a phantom model, described in Chapter 3. Sometimes the innominate veins are also called brachiocephalic veins. The image has originated from [51] and has been modified.

Table 2. Geometry of different vascular structures

Type of vein	Length (cm)	Diameter (cm)	Source
Superior Vena Cava	7.1 ± 1.4	2.1 ± 0.7	[52, 53]
Left Innominate vein	± 6.0*	1.2 cm ± 0.3	[54-56]
Right Innominate vein	± 2.0-3.0*	1.5 ± 0.4	[54-56]

* No standard deviation was provided.

Table 3. Angulation between the SVC and innominate veins

Angulation	Left Innominate vein (degrees)	Right Innominate vein (degrees)	Source
Superior Vena Cava	116 (± 7)	Descends directly into the SVC	[57, 58]

Vessel wall

The SVC has a thinner vessel wall compared to for instance the aorta. This is because this vein only returns the blood to the heart, resulting in a much lower pressure and risk of vessel rupture. Contrary, the aorta carries the blood away from the heart, which means that it has a higher pressure due to the pumping force of the heart and thus requires a thicker vessel wall (of about 2 mm to resist the higher force on the artery [59].

Type of vein	Superior Vena Cava	Left Innominate vein	Right Innominate vein	Source
Wall thickness (mm)	1.0[1] - 1.5	Not provided[2]	Not provided[2]	[59]

[1]According cardiosurgeon S. Hakmi (University Medical Center Hamburg-Eppendorf) the vessel wall of the SVC is approximately the thickness of a paper sheet to 1 mm. [2]These wall thicknesses could not be found from literature. However, in general the thickness of a vein is 0.5 mm [59].

2.3.1. ENDOVASCULAR SCAR TISSUE

Pathology

The presence of endovascular scar tissue in the patient is significantly associated with increased difficulty and risk of a TLE [2] and grows with time of implantation. Its evolvement can be particularly explained by the body's foreign response to endovascular leads. Initial response starts directly after implantation and can be characterized by thrombus formation along various sites of the lead body. Subsequently, it proceeds with fibrosis of the thrombus and corresponding development of fibrin bridges, resulting in encapsulation of the lead a few days later [60-62]. Primary, at sites where there is direct contact between the lead and vasculature as well as the endocardium, robust fibrosis may develop. Over time, evolvement of calcification, which occurs concentrically close to the lead, further increases complexity and risk of the procedure [2]. Figure 11 provides an illustration of endovascular scar tissue.

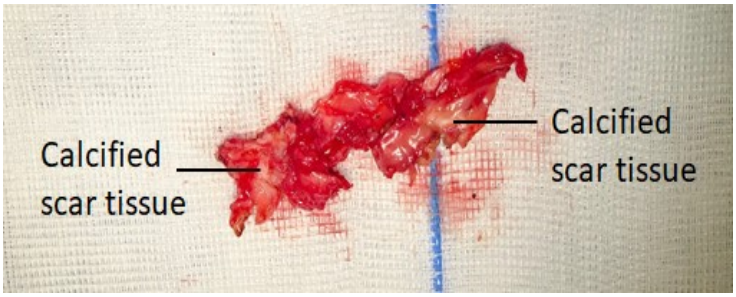

Figure 11. Endovascular scar tissue from a patient

Fibrosis (red tissue) sometimes include areas of calcium (whitish tissue). These calcifications are felt solid and dense and comprise sharp edges. This photo was taken during an attendance of a TLE procedure at Erasmus Medical Centre Rotterdam.

Scar Severity

To obtain an indication of realistic scar thicknesses, a paper from Maytin et al. 2015 [2] was consulted in which the writers evaluated the severity of pocket scar. Classification (i.e. mild, moderate, severe) was performed based on three subjective measures: The operator's assessment of scar thickness, quantity of scar tissue and difficulty of lead dissection. When there was calcified scar present, this was automatically classified as severe. Tissue was also sent to pathology for further investigation. The mean measured scar thickness was 0.4 ± 0.2 cm (with a range of 0.1–1.1 cm). Table 4 presents the findings of this study.

Table 4. Severity of scar tissue and corresponding measured thickness [2]

Scar severity	Mild (cm)	Moderate (cm)	Severe (cm)
Scar thickness (cm)	0.28 ± 0.16	0.42 ± 0.23	0.49 ± 0.29

3

VASCULAR PHANTOM: DESIGN AND CONSTRUCTION

3.1. INTRODUCTION

This chapter will describe the design and construction processes necessary to create the vascular phantom of interest. It will first describe the mould design and construction methods and subsequently the iteration steps undertaken to fabricate the final version of the vascular phantom model.

3.2. DESIGN CRITERIA

Specification of the phantom requirements occurred at Philips Research (In-Body Systems) with colleagues that were involved in the lead management project. In agreement with them, the following requirements were composed to fulfil the objectives of this thesis project.

The vascular phantom to be constructed should meet the following general requirements:

- Low cost
- Durable
- No toxic resources
- Easy construction
- Standardized construction

To simulate the lead extraction environment, the vascular phantom should meet the following composition requirements:

- It contains a vessel wall and lumen (with the ability to position a lead inside)
- It resembles the SVC and approximate innominate veins with realistic geometry
- It contains scar tissue at the inner wall of the SVC

To allow ICE evaluation, the vascular phantom should meet the following imaging requirements:

- Suitable for ultrasound imaging
- It contains different echogenic structures to allow (tissue) structure discrimination on ultrasound (i.e. vessel wall, scar tissue and lead)

3.3. MATERIALS AND METHODS

3.3.1. MOULD DESIGN AND CONSTRUCTION

In order to allow construction of the vascular phantom model, a specific mould was necessary which could be made in design software Solidworks (Dassault Systèmes, France). With this software several computer-aided design (CAD) models were created, which were all saved as stereolithography (STL) file format to allow import to 3D printing software (Cura, Ultimaker, Netherlands). Thermoplastic polylactic acid (PLA) was the chosen print material because it had a low printing temperature that allowed for easy and rapid printing and also because of its availability in the MISIT lab (Department of Biomechanical Engineering, Delft University of Technology, Netherlands). The print settings are presented in Table 12 of Appendix B.

3.3.2. PHANTOM CONSTRUCTION

3.3.2.1. Material selection

Three constituents were selected to construct the vascular phantom:

1. Polyvinyl alcohol – to create the vessel
2. Calcium carbonate – to create calcified scar tissue
3. Acoustic scatterer – to increase the echogenicity of both the vessel and scar tissue

1. Polyvinyl Alcohol

Polyvinyl alcohol (PVA) gels are chemically synthesized polymers that are widely adopted to mimic soft tissue [63-67]. When this gel undergoes a number of freeze thaw (FT) cycles, mechanical properties such as the elastic modulus can be altered, allowing PVA phantoms to be mechanically tailored to the needs of the user. With freezing, crystal nuclei are formed whereas on thawing crosslinking formation occurs, the latter increases mechanical strength. Hence, crosslinking sites increase with the number of FT cycles, resulting in a rubber-like material of variable stiffness and suitable for both ultrasound (US) and magnetic resonance imaging (MRI). Since PVA gels can be blended with additives, such as US contrast agents, the acoustic reflectance can be enhanced (see section 2.2.2.4 of Chapter 2) [48, 67, 68]. In Table 5, the advantages and disadvantages of PVA are listed.

Table 5. Advantages and disadvantages of PVA gels

Advantages	Disadvantages
Tailor mechanical properties	Bacterial growth
Low cost	Long preparation time (i.e. FT cycles, precise temperature control)
Non-toxic	Should be covered in water to prevent dehydration
More stable and durable compared to biopolymers*	
Fewer ingredients required compared to agarose-based tissue substitutes	
Heterogeneous layers possible	
Compatible with US and MRI imaging	

* Agar, agarose, gelatin and gellan gum are commonly used biopolymers.

From Table 5 it can be noticed that some of the listed advantages (i.e. low cost, non-toxic, durable, compatible with US) are included in section 3.2. Design Criteria. Particularly, durability was one of the reasons to exclude biopolymers from the choice of materials since they are not stable in the long term. This is due to the evaporation of their water content and susceptibility to bacterial growth [48, 68].

PVA was chosen over other common chemically synthesized polymers such as polymerized siloxanes (silicone) and polyvinyl chloride because it is equivalent to various types of soft tissue in terms of acoustic properties, while silicone and polyvinyl chloride have a much lower speed of sound [64, 69]. Furthermore, PVA allows precise modelling of its mechanical properties and construction of multiple heterogeneous layer structures, useful to create scar tissue in a vessel.

PVA powder (Selvol PVOH 165, Sekisui Chemical Group NJ, USA) with a high degree of hydrolysis (99%+) was selected to obtain strong hydrogen bond formations, thus for optimal crosslinking in the sample. All samples were created with a 7 wt% PVA since this was the maximum recommended soluble concentration [70, 71]. For specifications of this type of PVA, see Table 13 of Appendix B.

2. Calcium Carbonate

PVA was blended with powdered calcium carbonate $CaCO_3$ (500 g Calciumcarbonat, Original Rügener Schlämmkreide, Germany) to create calcified scar tissue. Calcium carbonate was chosen because it has the ability to increase material density with creation of specific internal structures, often resulting in a higher texture strength [72]. A higher texture strength, which is desired to mimic scar tissue, may also produce an increased echogenicity on US. The scar tissue was prepared using a mix of 7 wt% PVA, 5 or 50 wt% CaCO3 and 0.5 wt% acoustic scatterer concentration.

3. Acoustic Scatterer

Within the samples a small amount of acoustic scatterer, made of harmless powdered silicon dioxide glass spheres in particle size between 15 to 40 µm (Silica gel 60, KGaA, Darmstadt, Germany), was added to increase the acoustic reflectance on US. Particularly in a multilayer phantom, varying the scatterer concentration per layer could be useful to create distinct echogenic structures, to allow discrimination of tissue (e.g. vessel, scar tissue) on US imaging. Most of the vessel wall structures contained a concentration between 0.05 wt% and 0.3 wt% while the scar tissue consisted of a concentration of 0.5 wt%. An overview of the concentrations used is presented in Table 6.

Table 6. Phantom materials and their concentration

Constituent	Concentration (wt %)
PVA	7
$CaCO_3$	5, 50
Acoustic scatterer	
- Vessel wall	0.05, 0.1, 0.2, 0.3
- Scar tissue	0.5

3.3.2.2. Standardized construction - Preparation protocol PVA

Preparation of the PVA gel was performed according a developed protocol, see Appendix C: Preparation Protocol PVA. This protocol was based on a methodology described by T. de Jong et al. 2017 [71] and on personal conversations with T. de Jong (Delft University of Technology, MISIT group Biomechanical Engineering, Delft) and A. Kolen (Philips Research, In-Body Systems, Eindhoven). Furthermore, previous preparation protocols (Philips Research, In-Body Systems, Eindhoven) were studied to acquire relevant information.

All steps of the preparation protocol were followed in a consistent manner. Subsequently, the next step was to pour the PVA gel into the 3D printed mould. Since this step was quite critical, a second protocol was developed to provide some practical insights regarding pouring (see Appendix D: Protocol PVA pouring – tips and tricks). After the PVA gel was poured into the mould, the entirety was put in a temperature controllable freezer set at -19 °C. Subsequently, it underwent a number of FT

cycles (varying from 2 for the vessel wall to 4 for the scar tissue) of which one cycle included 16 hours of freezing and 8 hours of thawing at room temperature.

3.4. PHANTOM 1: BASIC VESSEL

3.4.1. DESIGN

The first mould was designed with the intention to allow vertical PVA pouring around a tube so that a straight blood vessel phantom could be created. This mould, illustrated in Figure 12A, consisted of an upper and lower part, which can be detached from each other. The upper part (Figure 12B) contained an open circular space in the centre whereas the lower part (Figure 12C) consisted of a fixed inner tube with a diameter of 20 mm. This latter was intended to create the lumen of the vessel. When attaching the upper and lower part, a resulting circular opening with a thickness of 5 mm can be observed (presented in Figure 12A) separating the fixed inner tube from the outer side of the mould. Within this opening, the PVA material could be poured to create a phantom with a 5 mm thick vessel wall.

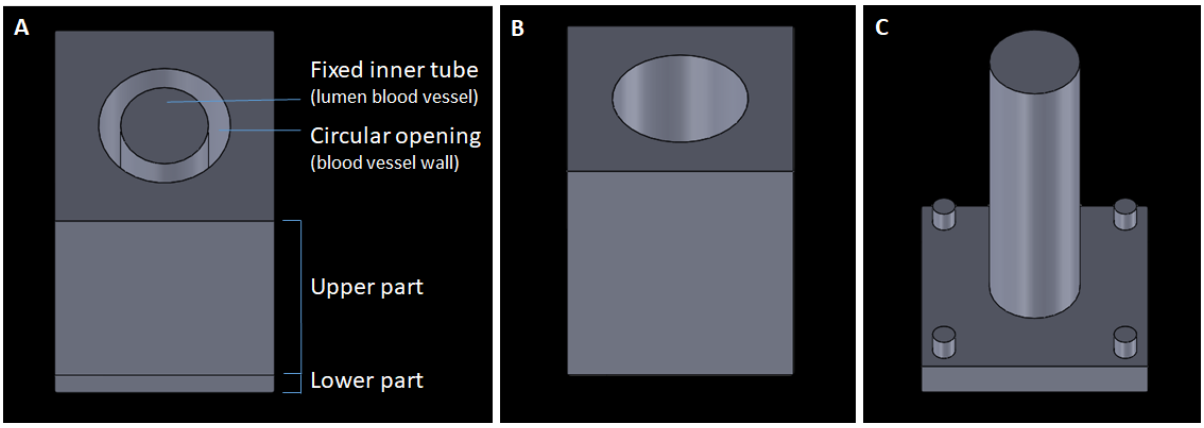

Figure 12. Design of a basic mould for PVA pouring

A: The entire mould including a circular opening with 5 mm thickness. B: Upper part of the mould with open circular space in the centre. C: Lower part of the mould with a 20 mm fixed inner tube.

Since a vascular phantom with a 5 mm thick vessel wall does not represent a realistic blood vessel, it was examined whether phantoms could be constructed with a smaller wall thickness. Therefore, external tubes of various diameters were designed that could be positioned in the open circular space to create phantoms with a smaller vessel wall thickness as illustrated in Figure 13. Table 7 summarizes the (external) tube dimensions and the corresponding wall thicknesses.

Table 7. Tube dimensions and corresponding wall thickness

Type of tube	Length (mm)	Inner diameter (mm)	Outer diameter (mm)	Corresponding wall thickness (mm)[2]
Upper part basic mould (Figure 14A)	70	30	-	5
External tube 1 (Figure 14B)	80[1]	24	30	2
External tube 2 (Figure 14C)	80[1]	22	30	1

[1] The external tubes were made slightly longer than the upper part to allow easy extraction from the mould
[2] Wall thickness = inner diameter tube – diameter fixed inner tube (20 mm) / 2.

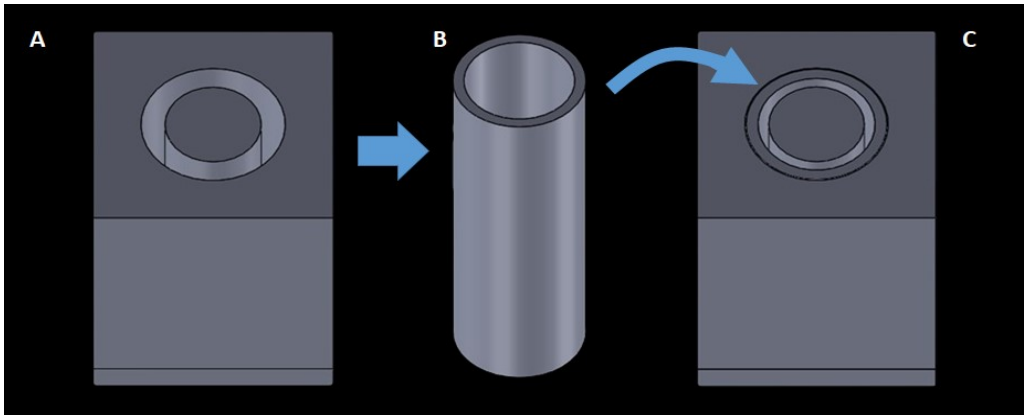

Figure 13. Creating vessel phantoms with a smaller wall thickness

A. Basic mould B. External tube C. Placement of external tube into mould to create a smaller wall thickness. By placing the tube into the open circular space, the distance to the fixed inner tube is reduced.

3.4.2. CONSTRUCTION

After designing the basic mould and external tubes of variable diameters, the concepts were 3D printed and subsequently used to construct the phantoms, shown in Figure 14. From this figure, it can be observed that the basic mould could be used to create 70 mm long vessel phantoms including a lumen and wall with equal thicknesses of 5, 2 and 1 mm.

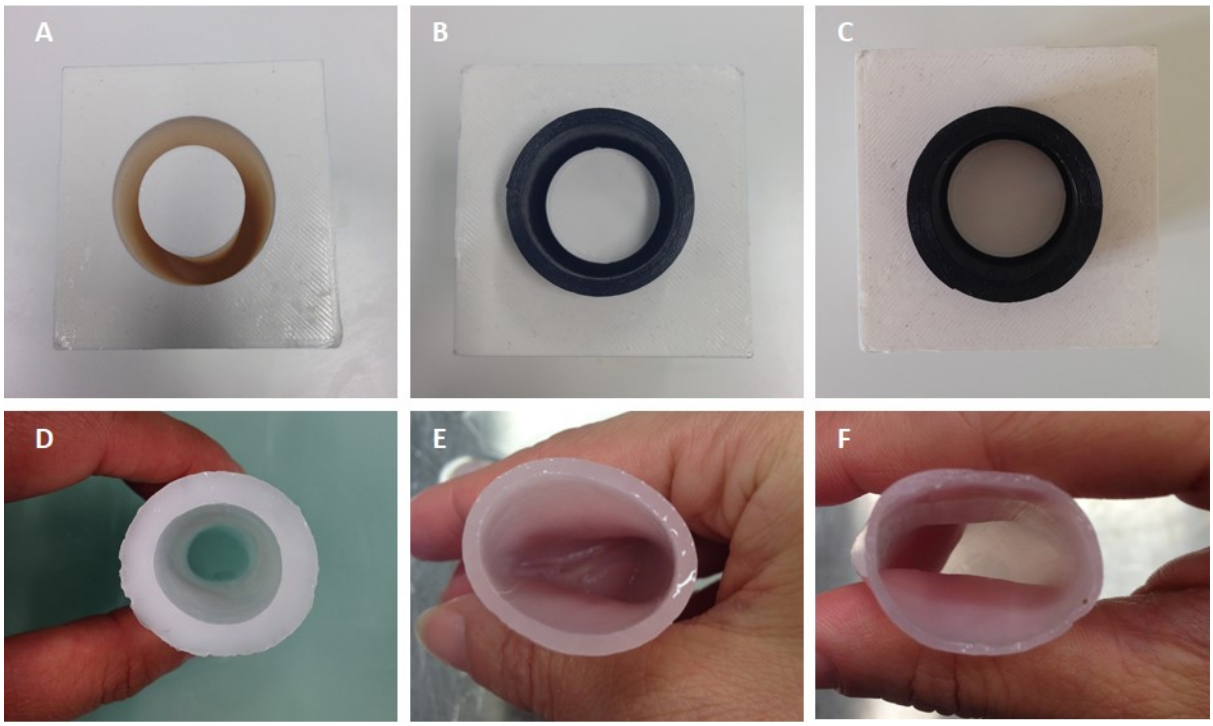

Figure 14. Construction of the basic mould and straight vessel phantoms.

Top: Mould with wall thickness of 5, 2 and 1 mm, shown in A, B and C respectively. Bottom: Phantoms with a wall thickness of 5, 2 and 1 mm, shown in D, E and F respectively. The phantom shown in F has a length of 70 mm, diameter of 20 mm and vessel wall of 1 mm, which is equivalent to a human SVC.

3.5. PHANTOM 2: BASIC VESSEL WITH SCAR TISSUE

3.5.1. DESIGN

Based on the results of the previous phantom, it was examined whether a similar basic vessel could be designed but with an extension of a second layer inside the lumen of the tube, to create scar tissue. In order to perform this, a second mould with a new inner tube (illustrated in Figure 15B) was designed. This mould consisted of two open spaces suitable for PVA-$CaCO_3$ pouring to add a layer of scar tissue within the lumen of the vessel (Figure 15C).

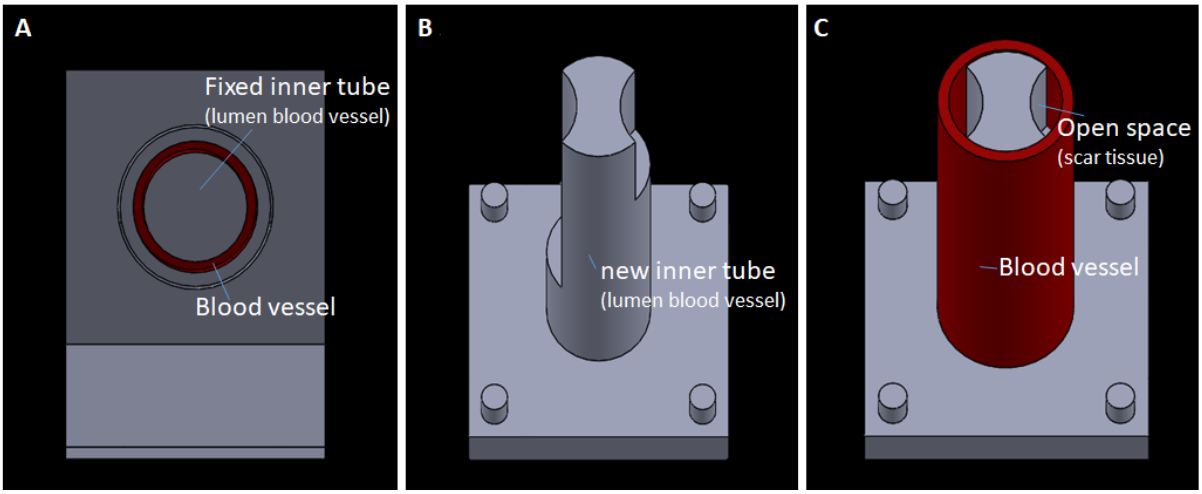

Figure 15. Design of new inner tube mould to create a vessel with scar tissue

A. Construction of a blood vessel (as described in section 3.4.2). B: Replacement of the fixed inner tube by a new inner tube with open spaces. C: Simulation of a blood vessel surrounding the new inner tube.

3.5.2. CONSTRUCTION

Following 3D printing of the new inner tube and construction of the vessel phantom, as described in section 3.4.2, the blood vessel was placed around the new inner tube (Figure 16A). Subsequently, the PVA-$CaCO_3$ mixture could be poured in the open space of the mould to add a layer of scar tissue. Figure 16B shows the constructed basic vessel with scar tissue.

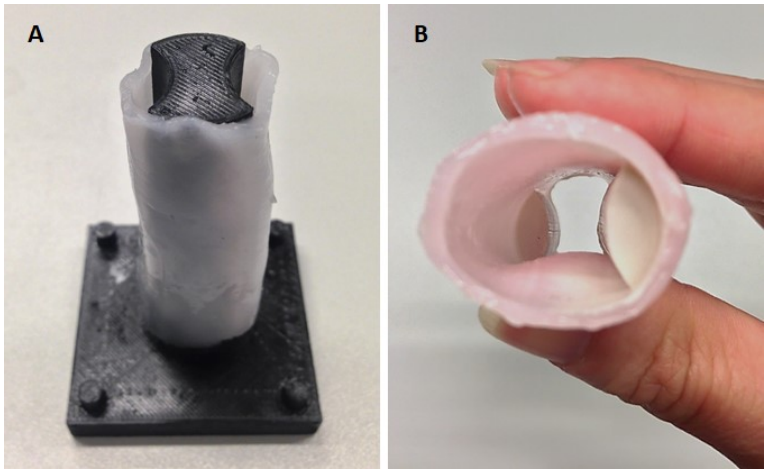

Figure 16. Basic vessel with scar tissue

A: Blood vessel surrounding the new inner tube. B: Basic vessel phantom with scar tissue in the lumen. The thickness of the scar tissue is 5 mm at the centre, which is comparable to severe scar conditions in humans (section 2.3.1).

3.6. PHANTOM 3 & 4: VASCULAR TREE

After successful construction of the basic and multilayer phantom, mentioned in section 3.4 and 3.5 respectively, it was examined whether the phantom could be extended to a vascular tree. Similar to the previous phantoms, the moulds were 3D printed and subsequently utilised for PVA pouring. However, during construction of the phantoms, several complications were encountered due to design constraints. Therefore, some iteration steps were applied that eventually resulted in the final version of the vascular tree. A complete description of the mould design and construction processes of phantom 3 and 4 can be found in Appendix E: Phantom 3 & 4: Vascular Tree.

3.7. PHANTOM 5: FINAL VASCULAR TREE

3.7.1. DESIGN

As aforementioned, a couple of design iterations were undertaken to create the final vascular phantom of interest. Although phantom 4 included some problems that could be solved through design optimization, its corresponding mould was still not sufficiently convenient to achieve easy phantom construction. Therefore, it was decided to create a complete new mould design while taking learnings from previous editions into account. In contrast to mould design 3 and 4, the current design was created vertically to minimize the likelihood of air bubbles remaining present within the PVA solution. On top of that, this design primarily consisted of one part to prevent PVA leakage. In order to obtain a representative vascular tree model of the SVC and approximate innominate veins, the mould was designed such that the constructed phantom would be equivalent to a human junction of the SVC and innominate veins in terms of geometry (Figure 17C).

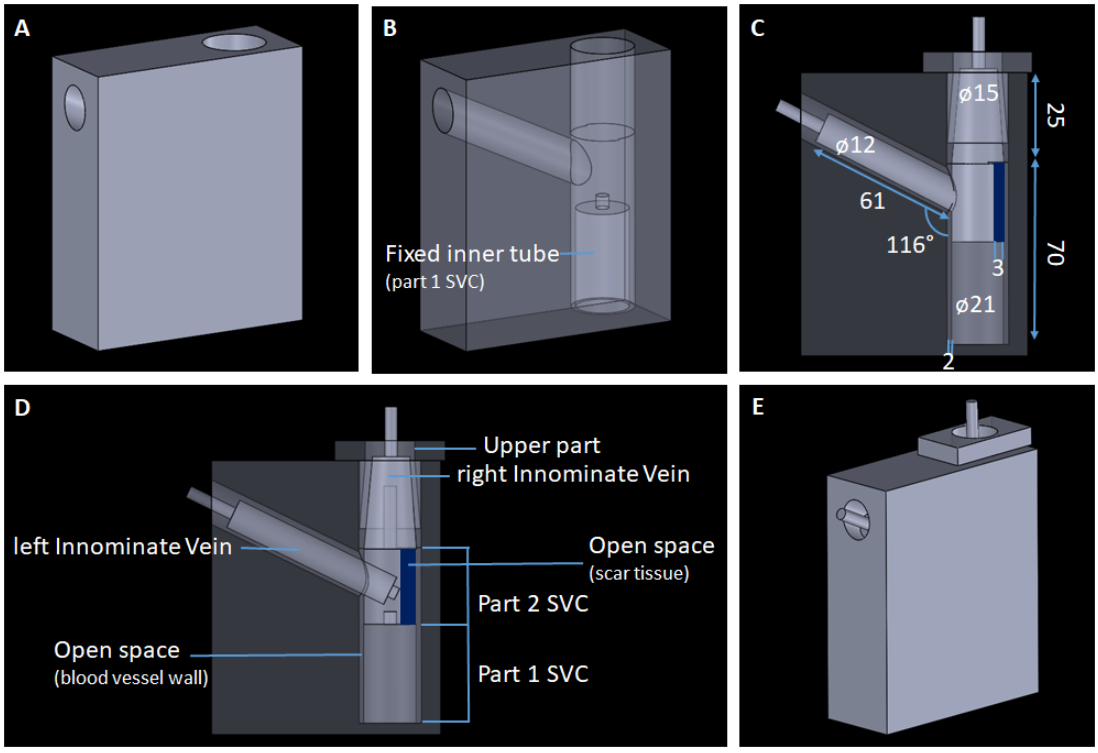

Figure 17. Final design of the vascular tree mould

A: Final design mould with two openings located at the top and side. B: Inner side of the mould comprising a fixed inner tube. C: Geometry (length, inner diameter, thickness in mm) of the vascular tree. D: Description of the mould. E: Mould ready for pouring. All tubular structures can be (dis)connected from each other, in a similar manner as in Figure 46B.

From Figure 17A it can be observed that the mould only consists of two openings through which the PVA gel can be poured. At the inside, it comprises a fixed inner tube (Figure 17B), which is the first part of the SVC. The second part of the SVC can be attached to the fixed inner tube (see Figure 46B for a more elaborate representation of inner tube connections) and contains an open space with 3 mm thickness at the centre, intended for scar tissue (Figure 17D). This latter can be prepared in advance by pouring of the CaCO3 mixture (see preparation protocol in Appendix C) into the open space of a tubular mould, which is similar in shape to the second part of the SVC (Figure 17D) but closed at the side and bottom. After subjection of 2 FT cycles, the scar tissue can be positioned at the open space of the second part of the SVC, prior to connection of the other tubular parts (i.e. left and right innominate vein, upper part) and PVA pouring of the vessel wall. From Figure 17D it can be also noticed that when the scar tissue is put in place, there is still capacity to create a vessel wall. When connecting the tubular structures to the second part of the SVC, it can be observed that the left innominate vein is sharply angulated with respect to the SVC whereas the right innominate vein directly descends into the SVC. To induce a gradual transition in terms of diameter from the SVC towards the right innominate vein (Figure 17C), an upper part has been constructed which adopts the desired geometry and simultaneously allows maintenance of the 2 mm thin vessel wall. Figure 17E presents the mould from sideways.

3.7.2. CONSTRUCTION

The results of the final mould design and phantom are presented in Figure 18. As shown, a complete vascular tree phantom was created that contained a vessel wall, lumen and scar tissue at the inner wall of the SVC (Figure 18C and Figure 18D).

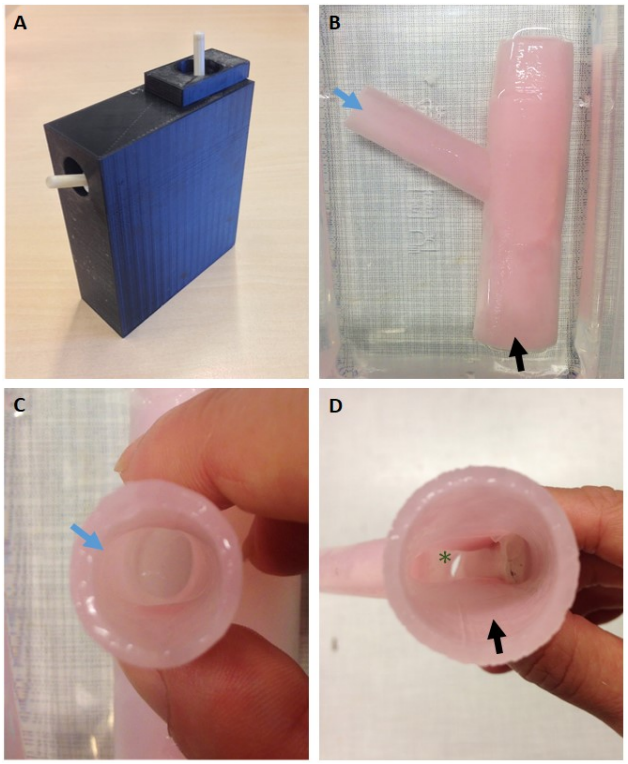

Figure 18. Construction of the final vascular tree mould and phantom

A: Final mould after 3D printing. B: Vascular tree phantom. The blue arrow represents the entrance of the left innominate vein whereas the black arrow is the entrance to the SVC. The right innominate vein directly descends into the SVC. C: Left innominate vein. D: SVC with scar tissue at the inner wall. Green asterisk: Stenosis between the SVC and right innominate vein. This is due to inflow of PVA gel to the connection points of the tubular structures during pouring and can be easily avoided by proper sealing of the edges prior to pouring. Note that for an appropriate anatomy interpretation the phantom should be horizontally rotated by an angle of 180°.

3.8. DISCUSSION AND CONCLUSION

In this chapter the design and constructing methods of the vascular phantom model were described. To assess whether the design criteria of this phantom model were fulfilled, the general and composition features of the phantom will be first discussed (chapter 5 will discuss the imaging features). On top of that, the limitations of the current vascular phantom model will be evaluated.

DESIGN CRITERIA

General Requirements

The general requirements for the vascular phantom included low costs, durable, no toxic sources, ease of construction and standardized construction.

Costs

The costs were calculated based on the amount of PVA required per sample and are presented in Table 8:

Table 8. Costs per sample of PVA

Material	Price per unit	Content of unit	Required amount	Costs per sample
PVA	€31,10	100 g	7,5 g	€2,33

As can be observed, the costs per sample are €2,33. However, one sample is sufficient to construct about four vascular phantoms, which makes the price €0,58 per phantom.

Durability

Durability was defined by the extent to which the vascular phantom could withstand time and repeated US measurements.

Given that PVA phantoms become rapidly dehydrated when exposed to air, they were placed in water and subsequently stored in a fridge to reduce the risk of fast degradation. Although PVA phantoms are susceptible to bacterial growth, this could not be noticed during six months of visual observation. Furthermore, inspection showed that the phantoms were still usable after numerous US measurements.

Toxicity

No toxic resourced were used to construct the vascular phantoms. Hence, no precautionary measures were taken to test the phantoms.

Ease of construction

Ease of construction depended on the amount of time required to construct the vascular phantom as well as the complexity of the preparation process.

Construction of the PVA phantoms in a vascular shape first required the design and construction of a mould in which the PVA solution could be poured to. This took quite a lot of time since it depended on the number of iteration steps.

After this, the phantoms could be prepared which was rather a time consuming than complex process. Preparation of the PVA solution only took about 1,5 hour in which the mixture was made, completely dissoluted (and hold for 30 minutes at 93°C) and subsequently cooled down to a temperature below 60°C. However, after preparation of the PVA, the material required to be poured into a mould and subjected to prolonged FT cycles, comprising 24 hours per cycle. Depending on the number of FT cycles, which varied between to 2 (for constructing the vessel) and 4 (for constructing the scar tissue), this took 48 to 96 hours respectively.

Standardized construction

This referred to the ability to produce vascular phantoms in a consistent manner so that all phantoms could be reproduced.

A preparation protocol (Appendix C: Preparation Protocol PVA) was developed and followed consistently. Despite a few issues were encountered (see Limitations), the phantoms could be made quite equivalent to each other.

Composition Requirements

To simulate the lead extraction environment, the requirements regarding composition of the vascular phantom were:

- The phantom should have a vessel wall and lumen
- The phantom should be equivalent to the SVC and innominate veins with realistic geometry
- The phantom should contain scar tissue at the inner wall of the SVC

Due to the number of iteration steps taken during this project, the vascular phantom could be adjusted such that the final version contained all features that were required with regard to composition. Nevertheless, the vessel wall was not optimal in terms of thickness. This will be discussed in the following section 'Limitations'.

CONCLUSION

Based on the aforementioned results, a brief assessment of the vascular phantom can be made regarding its general and composition features. This is presented in Table 9.

Table 9. Assessment of the vascular phantom with regard to its general and composition features

General requirements of the vascular phantom	Assessment
Low cost	+
Durable	+
No toxic resources	N/A
Easy construction	+/-
Standardized construction	+/-
Composition requirements of the vascular phantom	**Assessment**
Vessel wall and lumen	+
Equivalent to SVC and innominate veins with realistic geometry	+/-
Scar tissue at the inner wall of the SVC	+

+ = good; +/- = sufficient; - = poor.

It can be concluded that the vascular phantom made of PVA has fulfilled the general and composition requirements of this chapter. Despite its time consuming manufacturing process, this phantom model can be made relatively easy with low costs (€0,58 per phantom) whilst being reproducible and durable. However, to reach this latter, the phantom should be stored properly to prevent dehydration, which is one of the drawbacks of PVA. Due to undertaken iteration steps, the vascular phantom contains all features necessary to simulate a real-life lead extraction environment. Whether this environment is also suitable to perform proper ICE evaluation, will be discussed in Chapter 5.

LIMITATIONS

During the construction process of the phantom, a few practical issues were encountered that have primarily influenced the ease of construction and the ability to perform standardized construction. These will be further explained below.

Preparation protocol

This chapter has demonstrated that customized 'home made' phantoms can be reproduced by following a standardized protocol. Although this protocol was based on previous preparation protocols and own experiences, there are some points that require more attention.

First, the temperature to heat the PVA solution was set at 93°C. This was adopted from a previous protocol [71] in which 93°C was found to be the maximum temperature up to where the PVA solution could be heated using a hot plate (IKA RET Control-Visc S1 Digital Hot Plate). However, it has been indicated from literature that the minimum temperature reached, has an effect on the physical properties of the phantom [63]. From literature provided by Sekisui [70], it was found that polyvinyl alcohols with a super hydrolysis grade (i.e. 99+% hydrolysis) require minimum heating temperatures of 96°C to reach complete dissolution. When the solution is not entirely solubilized, it will not reach its optimum performance. Since 93°C is below this criterion, it should be worth investigating what the effect is of using a slightly higher temperature from 96°C and above.

Second, PVA particles tend to swell and rapidly clump together when added to hot water [70]. Therefore, it is recommended to first slowly add the particles to cold water to reach complete dissolution. However, despite these particles were slowly added, clumping of the particles could not be avoided in almost all cases of preparation. Given that the clumped particles do not dissolve optimally, this may influence PVA performance. Furthermore, when larger PVA volumes are used, the particles tend to clump faster. As these clumps are difficult to eliminate from the glass beaker, it could be a cumbersome process, particularly in case of upscaled production.

On top of the aforementioned points, the properties of PVA are dependent on several variables such as the added weight percentage of PVA, degree of polymerization (number of cross-linked monomers) and hydrolysis as well as the number of FT cycles and their corresponding freeze thaw time/rate [63, 64]. Although these variables likely have influenced the physical properties of the PVA phantom, this was not investigated during this study and therefore necessitates further research to enable proper standardized construction.

Furthermore, this study was limited to PVA as tissue mimicking material. Although PVA was chosen because of its durability, compatibility with US imaging and ability to create heterogeneous layers, it remains susceptible to prolonged preparation times, dehydration and bacterial growth. Hence, it would be interesting to consider other tissue mimicking materials to overcome these limitations. However, it should be kept in mind that the aforementioned advantages of PVA are crucial to enable construction of the described vascular phantom of this chapter. Using another material might

overcome the limitations of PVA but will likely go at the expense of one of the aforementioned advantages.

Mould design

The current mould is constructed with the intention to comprise two openings of which one located at the side. However, during pouring it was observed that, when the mould was placed in its normal standing state, there was a lot of PVA leakage from the side opening. Therefore, the mould was angulated to prevent leakage, as shown in Figure 19A. Nonetheless, this problem could be solved relatively easy through design optimization by angulating the mould and subsequently extending the bottom downwards.

Another limitation of the current mould was the fact that it primarily consisted of one solid part, which increased difficulty regarding extraction of the phantom. Consequently, the phantom was prone to rupture when it was not extracted with caution (Figure 19B). In order to facilitate this process, sufficient Vaseline was used to grease the inside of the mould prior to pouring, whilst unknown whether or not this has influenced the mechanical properties of the phantom. Furthermore, it was found that, to extract the phantom entirely, the left tubular part (i.e. left innominate vein) should be extracted first from the mould and subsequently the other parts (i.e. in order of upper part, right innominate vein and second part SVC). When applying this order of extraction, the phantom already slightly appeared from the mould whilst removing the other parts. As a result, this piece was used to pull the entire phantom out of the mould through the opening of the top. Subsequently, the left innominate vein could be easily extracted through the same opening (due to its smaller diameter than the rest of the veins).

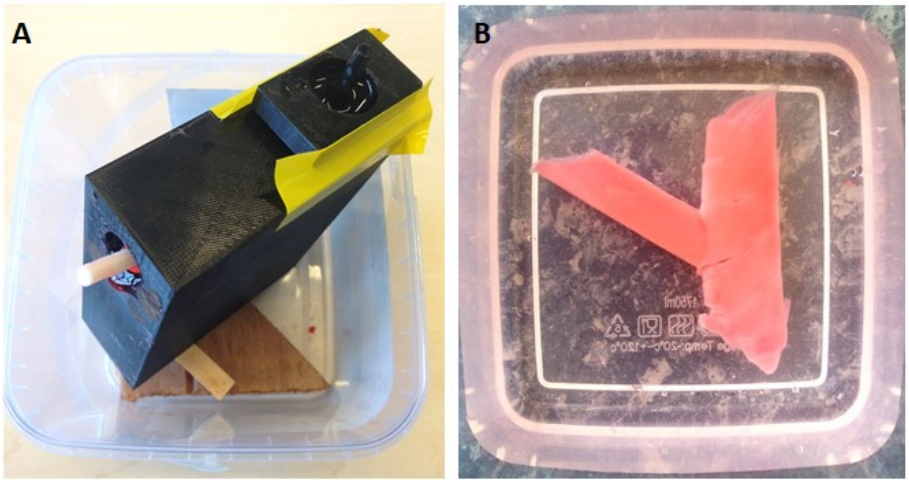

Figure 19. Limitations of the current mould design

A: Positioning the mould under a 20° angle to prevent PVA leakage. The yellow tape was used to fix the upper part to the mould. This was done to ensure that the upper part remained fixated without the risk of being pushed outwards by the PVA fluid inside the mould. B: Ruptured vascular tree phantom.

Furthermore, the final mould is designed to create a vascular tree with a vessel wall thickness of 2 mm rather than the desired thickness of 1 mm (Chapter 2 section 2.3). This thickness was chosen to minimize the risk of vessel rupturing during extraction. Since the goal is to strive towards realistic vessel geometries, the mould should be optimized with a geometry that allows creation of a 1 mm thin vessel wall, particularly to obtain a realistic SVC. Additionally, it should be examined whether the optimized version still allows for complete phantom construction and extraction. Ideally, its corresponding geometry should be based on anatomical data (i.e. digital imaging and communications

in medicine (DICOM) images of the SVC and innominate veins). However, during this project, it was not feasible to extract a vascular model from available computed tomography (CT) data. This was due to the presence of leads, which induced many artifacts on the images. Besides, the vessel wall could not be discriminated from surrounding vessel structure, hindering segmentation of the vessel wall. Given these constraints, this dataset was not adequate for segmentation of the SVC or innominate veins.

Multilayer phantoms require more FT cycles

This chapter has demonstrated that PVA phantoms can be constructed with scar tissue inside the lumen of a vessel. Although this was crucial to simulate a lead extraction environment, it has significantly reduced the ease of construction in terms of time. This was because experiments showed that in order to obtain distinct structures (i.e. vessel and scar tissue), the solutions should be poured separately from each other rather than simultaneously to avoid complete mixing. However, to attach the structures without the consequence of mixing them, one structure already required to be subjected to minimally one FT cycle. As a result, there was a difference of at least one FT cycle between the structures. Depending on the desired number of FT cycles, this will increase the amount of time evidently. Furthermore, it was noticed that a phantom with a 1 mm vessel wall, subjected to solely one FT cycle, could not be extracted properly without rupturing. Therefore, these phantoms required a minimal number of two FT cycles (see section 3.3.2.2). However, this was also desired because the phantom would then have elastic properties comparable to 'healthy' human vascular tissue [65, 67], although its type of PVA and concentration slightly differed from the ones described in [65] and [67]. Nevertheless, it might still provide an approximation of 'healthy' elastic tissue whereas a higher number of FT cycles would be more convenient to model 'diseased' stiff tissue (e.g. scar tissue) [65].

3.8.1. RECOMMENDATIONS

Cryogenic 3D printing

As mentioned above, the fabrication process of the vascular phantom is time consuming, especially when the design and 3D printing of the mould are part of the process. To reduce the amount of time it would be interesting to consider 3D printing methods to produce vascular phantom models rather than constructing them with conventional cast moulding. Recently, Tan and colleagues [73] presented a new cryogenic 3D printing method that is able to print stable soft tissue structures. The ink that they used is a composite of existing tissue mimicking materials PVA and gellan gum, which makes adoption on larger scale more accessible. Validation of this method could be performed by means of compression tests and the results showed that the 3D printed material was equivalent to cast-moulded samples in terms of mechanical properties. Additionally, the printed material was also compared to real brain tissue, examined in literature, and the results showed to be well within the range of reported brain tissue results. Since these authors were even able to print complex hollow and cylindrical structures, it could be worth investigating how this 3D printing method can be extended to produce vascular phantom models.

4

PHANTOM VALIDATION

4.1. INTRODUCTION

As demonstrated in the previous chapter, a vascular phantom model with realistic geometry can be constructed for the simulation of a real-life lead extraction environment. In order to assess whether this model also resembles realistic tissue in terms of echogenicity, this chapter will focus on the validation of the phantom model.

Since porcine hearts are equivalent to human hearts, the approach of this experiment was to image a 'healthy' SVC (i.e. without scar tissue) of a porcine heart and of phantom models with variable weight percentages of acoustic scatterer in both a water and blood pool. Subsequently the purpose was to quantitatively measure the contrast-to-noise ratio (CNR) signal intensity values in the corresponding images to allow for direct comparison between the porcine and phantom models. This parameter was chosen because of the reason that interpretation of US images in general is quite a difficult task and every human being perceives images differently. Therefore using the CNR as quantitative measure (see Appendix F for explanation of its formula) would allow for objective measurement with the ability to perform statistical analysis, whilst being simple and easily comparable. The study focused on the influence of acoustic scatterer on echogenicity in the phantom models, to find out which phantom most closely resembled porcine tissue in terms of echogenicity by using CNR values.

4.2. MATERIALS AND METHODS

4.2.1 EXPERIMENTAL SET-UP

The experimental set-up consisted of an ultrasound probe holder, mounted on a plastic box, and a circular glass beaker that was placed inside the box. Within the holder, a 9 french (Fr) linear phased-array ViewFlex ICE catheter (St. Jude Medical, Inc., St. Paul, MN) was positioned at a fixed depth to consistently image either the phantoms or the porcine tissue. The ICE catheter was coupled to a catheter interface module (St. Jude Medical, Inc., St. Paul, MN) which was connected to a CX50 ultrasound system (Philips Medical Systems, Andover, MA, USA), see Figure 6. The medium (i.e. water or blood) was added to the glass beaker. In this medium, the SVC of either the porcine or phantoms with variable weight percentages of acoustic scatterer (i.e. 0.1, 0.2 and 0.3 wt%) could be horizontally placed in front of the ICE probe and remained in position, solely by floating. The characteristics of the specimens are presented in Table 14 of Appendix F. Figure 20 illustrates the experimental set-up whereas Figure 21 shows the porcine SVC.

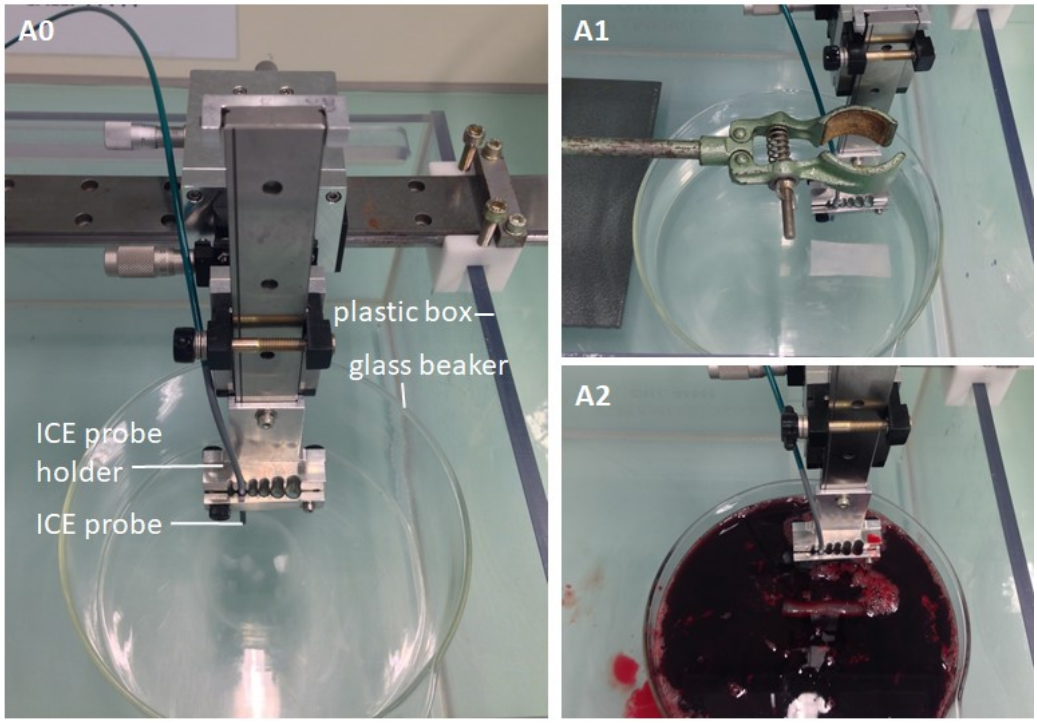

Figure 20. Experimental set-up of the validation experiment

A0: The set-up without addition of the medium in the glass beaker. A1: Addition of water to the glass beaker, creating a water pool in which a SVC phantom is placed. Note the presence of another holder above the set-up. This holder was solely for orientation purposes and did not belong to the actual set-up. A2: Addition of fresh porcine whole blood to the glass beaker, creating a blood pool in which a SVC phantom is placed.

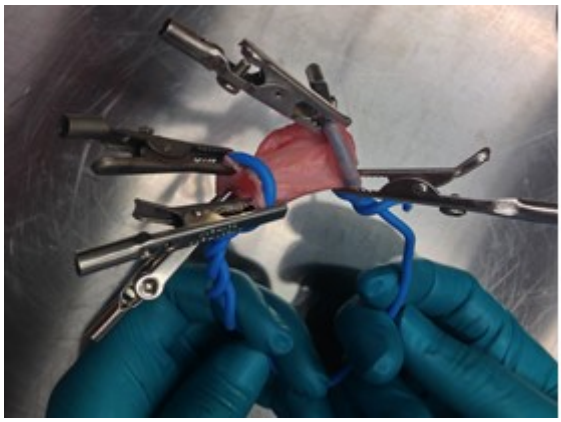

Figure 21. Porcine SVC

Notice how the SVC is clamped around a blue wire to avoid the vein from collapsing. This construction could be put in the medium while holding the blue wire up, above the surface of the medium, to enable imaging of the SVC with the ICE probe.

4.2.2. EXPERIMENTAL DESIGN

The ICE probe was positioned perpendicular to the porcine and phantom samples in the medium so that cross-sectional or transversal images could be taken at a frequency of 6.25 MHz, as presented in Figure 22. Due to this method, in which solely the circular shape of the specimen required to be visualized in the field of view (FOV), it was easy to position the specimens in the visualization plane without fixation. In order words, the specimens did not require to be hold in a fixed position but instead could rather float in the medium whilst still enabling proper acquisition of the images at the same depth. Additionally, because of this manner, the length of the specimens could be neglected, which was advantageous since they differed in length. Per specimen, minimally two cross-sectional

images were taken with the ICE probe, all with the same US settings (Table 15 of Appendix F), first in water and subsequently in porcine whole blood.

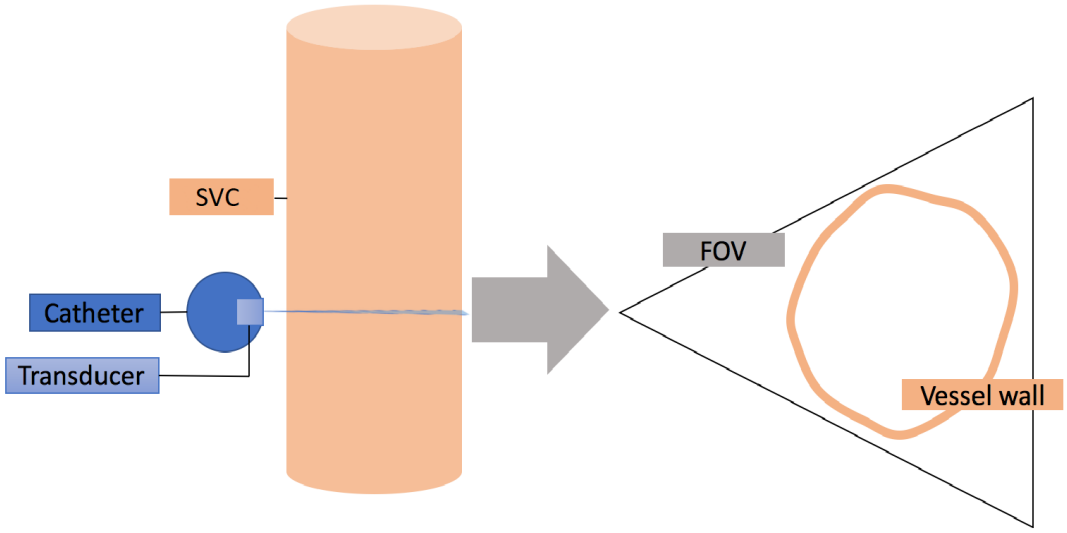

Figure 22. Cross-sectional view of the SVC in the image plane

For the sake of clarity, this image was presented in a standing position of the SVC. Notice that in the experimental set-up (Figure 20) both the catheter and SVC were rotated under an angle of 90°, first vertically anticlockwise and subsequently horizontally clockwise.

4.3. RESULTS

The cross-sectional ICE images of the porcine and phantom SVCs are presented in Figure 23.

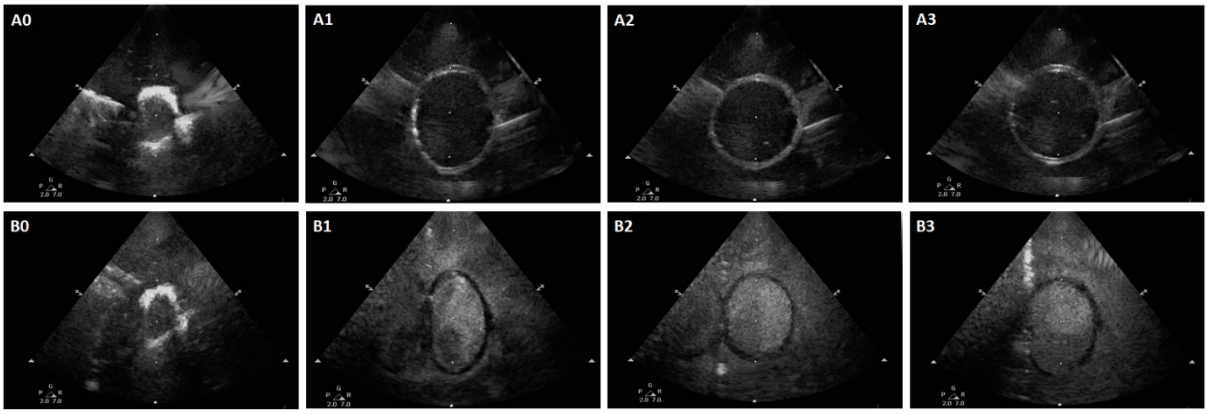

Figure 23. Comparison of porcine SVC with phantom SVCs

The letters represent the medium in which the specimen was placed; A: water. B: Blood.
The numbers represent either porcine (nr. 0) or phantom (nr. 1-3). The latter are composed of acoustic scatterers with weight percentage; 1: 0.1 wt%. 2: 0.2 wt%. 3: 0.3 wt%.

Figure 23 shows cross-sectional images of the porcine and phantoms in both a water and blood pool. From these images, it can be observed that the porcine and phantom SVC are not equivalent in shape and echogenicity. Although the shape of the specimens remain equal in both water and blood, it can be noticed that the echogenicity, particularly of the phantoms, remarkably changes when switching from water to blood. In water, the porcine SVC appears relatively bright in colour (i.e. hyperechoic) as opposed to the phantoms. When comparing the phantoms to each other, no clear differences can be

observed in terms of echogenicity. In blood, the porcine SVC still gives a hyperechoic signal. However, the phantoms are represented in a dark colour, which is even darker than the echo signal of the blood. As this 'inverse' signal (relatively to the signal given in water) of the phantoms appears completely dark in blood, it is considered anechoic.

Image artifacts

Besides the specimens, also a few image artifacts are illustrated in Figure 23. In the images presenting the porcine SVC (Figure 23A0 and Figure 23B0), a hyperechoic signal can be observed at the left side of the image plane. This may be due to the hyperreflection of the metal clips that clamped the SVC around the wire. Furthermore, there are some faint echoes surrounding the SVC, which could be due to the presence of grating lobes (see section 2.2.3 of chapter 2, which explains artifacts). Also, in Figure 23A1-A3 a similar pattern is visible. In Figure 23B0-B3, distortion of the signal by the glass beaker is evident and can be characterized by a so-called mirror image artifact.

4.4. FOLLOW-UP EXPERIMENTS

In response to the anechoic signal of the phantoms in blood, a fast test was performed by increasing the time gain compensation control significantly to examine whether the acoustic enhancement of the phantoms was masked but without result. Since the anoechoic signal could not be explained, it was necessary to conduct additional measurements to find out what parameters could have influenced the signal during the experiment. A couple of hypotheses can be drawn with respect to the hypoechoic signal of the phantoms in blood:

- The phantoms were not able to reflect an echo due to little difference in acoustic impedance between the phantom material and blood.
  Proposed solution: Since the acoustic impedance depends on the structure's density and speed of sound passing through this structure, this could be altered by changing the mechanical properties of the phantoms, by means of the number of FT cycles.

- The circumstances in which was measured were not optimal and created too much noise. As a result, the echo signals of the phantoms were distorted.
  Proposed solution: Gas bubbles for instance give an increased hyperechoic signal, which could have governed the echo signal of the phantoms. By attempting to avoid these (by simply storing the fluid after stirring) when present, faint echo signals of the phantoms can be better visualized.

- The weight percentage of acoustic scatterer added to the phantoms was not sufficient to produce a proper echogenic signal.
  Proposed solution: Increasing the concentration of acoustic scatterer in the phantoms.

4.4.1. FOLLOW-UP EXPERIMENT 1: CHANGING THE MEDIUM

Since it is unknown which hypothesis is true and which parameters have most strongly influenced the echo signal, multiple and repetitive experiments were required to test the hypotheses. It was therefore decided to use blood-mimicking fluid (BMF) as alternative to animal blood. This was because of the fact that blood should solely be used when fresh in order to obtain reliable results. However, since continuous supply was not a matter of choice, BMF as replacement to blood was considered a better option since it contained similar acoustical and physical properties as blood, thus still providing a stable and reliable medium to perform the follow-up experiments. Furthermore, this fluid was not hazardous and could be supplied more easily. The specifications of the BMF fluid used (CIRS blood mimicking fluid model 046, Norfolk, VA, USA) as well as those of water and human blood are presented in Table 16 of Appendix F.

Materials and Methods

Similar to the previous measurements, the circumstances in which was measured (i.e. experimental set-up and design outlined in section 4.2.) were kept the same but BMF was used as medium, rather than water or porcine blood. In addition, solely the phantoms were used in these measurements and to obtain the first results with BMF (as comparison to porcine blood) no parameters except the medium were changed.

Results

The results are illustrated in Figure 24 in which array A and C presents the phantoms in water and blood respectively (as already shown previously) whereas array B shows the additional images of the phantoms in BMF.

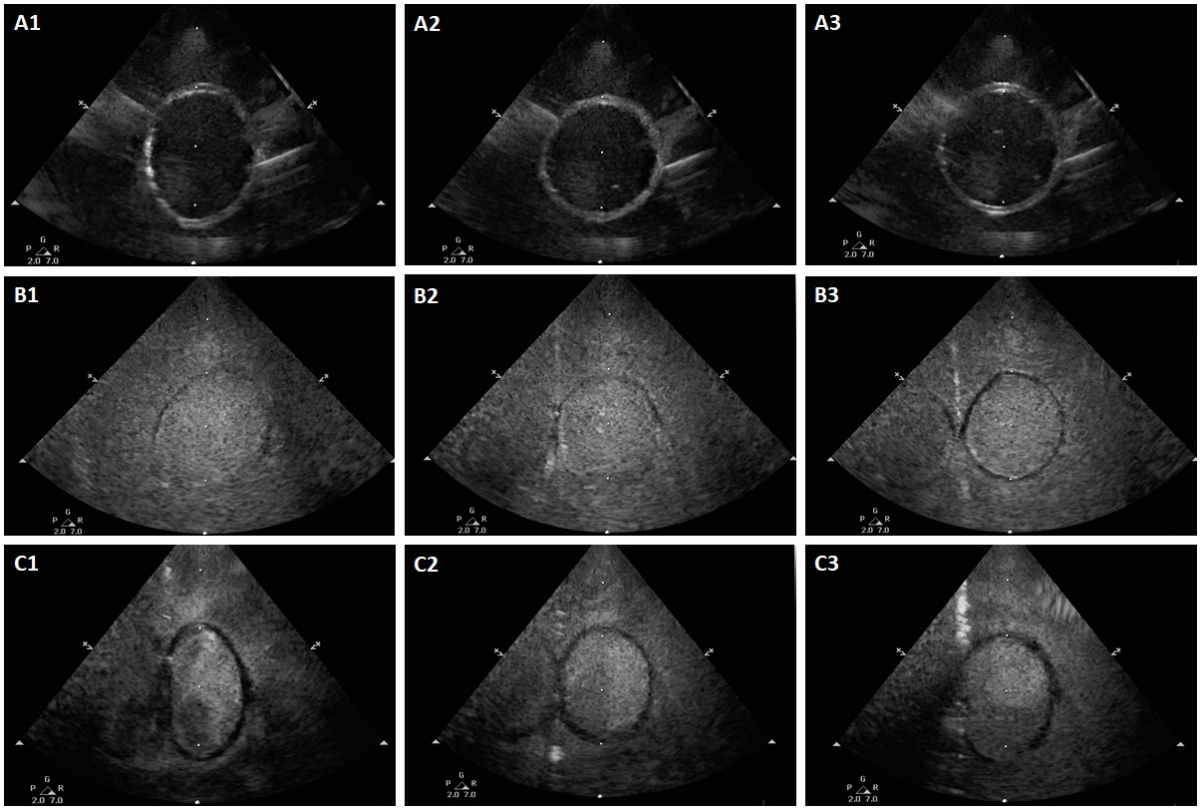

Figure 24. Cross-sectional view of three basic phantoms in water, BMF and blood

The letters represent the medium in which the phantom was placed; A: water. B: BMF. C: Blood. The numbers represent phantoms, which are composed of acoustic scatterers in weight percentage; 1: 0.1 wt%. 2: 0.2 wt%. 3: 0.3 wt%.

From Figure 24 it can be observed that the phantoms give a similar anechoic signal in BMF as in porcine blood, which is also likely because of the equivalent properties [74]. Besides the present mirror image artifacts, it can be noticed that both BMF and porcine blood seem to give a higher echo signal than water. Since blood is a poor ultrasound reflector and usually appears completely dark on echography (i.e. anechoic), this observation is not in line with presented literature [47, 75].

Because this observation was remarkable and could not be explained, it was decided to first investigate the circumstances in which the measurements were performed. A reason to focus on this latter was that the BMF and porcine blood gave such an evident echo that it almost seemed that an US contrast agent was added to the medium. Since US contrast agents comprise gas bubbles which are highly echogenic (See section 2.2.2.4 of Chapter 2) [47], it was interesting to examine whether these microbubbles were also present in BMF.

4.4.2. FOLLOW-UP EXPERIMENT 2: EFFECT OF MICROBUBBLES

In general, BMF is completely degassed prior to packaging to minimize the presence of noise caused by air bubbles. However, when one uses BMF as medium, it should be considered that settling of the particles might occur during prolonged storage with resulting clumping [74]. In order to avoid this, the fluid requires to be stirred sufficiently prior to use. However, with stirring there is a risk of producing unwanted gas bubbles, which are known to amplify the acoustic signal on echography.

Materials and Methods

Since gas bubbles will rise out to the surface over time when solely storing, an interesting parameter to investigate was the time range in which the BMF could restore from gas bubbles after stirring, followed by use of the BMF to perform the US measurements and with the purpose to find out what the effect was of present gas bubbles. Therefore, three times differences were taken of 30 minutes, 24 hours and 48 hours. Visual observation showed that with 30 minutes, still a lot of gas bubbles were present in the BMF, whereas with 24 hours or 48 hours the bubbles were not clearly observable anymore. With these observations, the assumption was made that primarily the transition time from 30 minutes to 24 hours would give a distinct difference between the images in terms of echogenicity. Again, measurements were conducted in a similar manner as mentioned in section 4.2. The results are presented in Figure 25.

Results

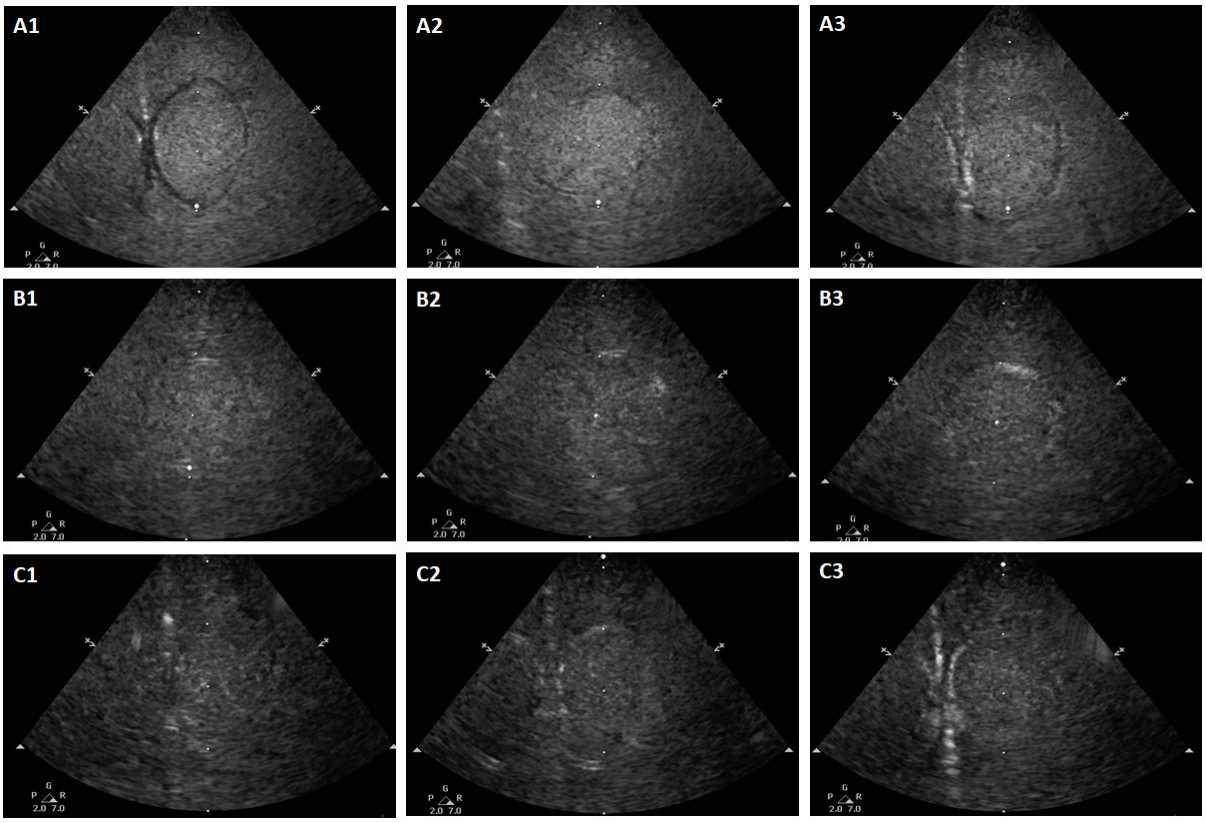

Figure 25. Increasing the time range between BMF recovery and performance of the US measurements

The letters represent the time range between stirring of the BMF and performance of the US measurements; A: 30 minutes. B: 24 hours. C: 48 hours. The numbers represent phantoms, which are imaged from a cross-sectional view and composed of acoustic scatterers in weight percentage; 1: 0.1 wt%. 2: 0.2 wt%. 3: 0.3 wt%.

In array A of Figure 25 the dark or anechoic signal of the phantoms is still visible. However, the signal appears to become more echogenic with increasing time difference between stirring of the BMF and performance of the US measurements, primarily when switching from 30 minutes (array A) to 24 hours (array B). No distinct differences can be observed in terms of echogenicity between the images with a time difference of 24 hours and 48 hours (array C). Evident is the mirror image artifact, present in most of the images.

4.4.3. FOLLOW-UP EXPERIMENT 3: CHANGING THE NUMBER OF FT CYCLES

As the gas bubbles in the previous experiment did not seem to strongly affect the echo signal of the phantoms, another interesting parameter to investigate was the number of FT cycles of the phantoms. With an increasing number of FT cycles it was assumed that the mechanical strength would increase and so the density. This latter, which influences the acoustic impedance of a structure, would result in a larger acoustic impedance. The hypothesis was that there was little difference in acoustic impedance between the phantoms and blood. Hence, it was expected that an increased acoustic impedance of the phantoms (as a result of more FT cycles), would also give a larger difference in acoustic impedance between the phantoms and BMF, thus providing a higher echogenic signal.

Materials and Methods

The phantoms from the previous studies were also used within this experiment. However, after each run of US measurements, they underwent another FT cycle to increase the mechanical strength, followed by a new run of measurements. This proceeded until a number of 5 FT cycles was reached. The experiment was conducted in a similar manner as previously described, however the glass beaker was alternated by a plastic beaker because the latter was not available at the time of measurement. Additionally, the BMF was stored (i.e. without stirring) for 48 hours prior to the start of the US measurements to avoid the presence of possible gas bubbles in the fluid.

Results

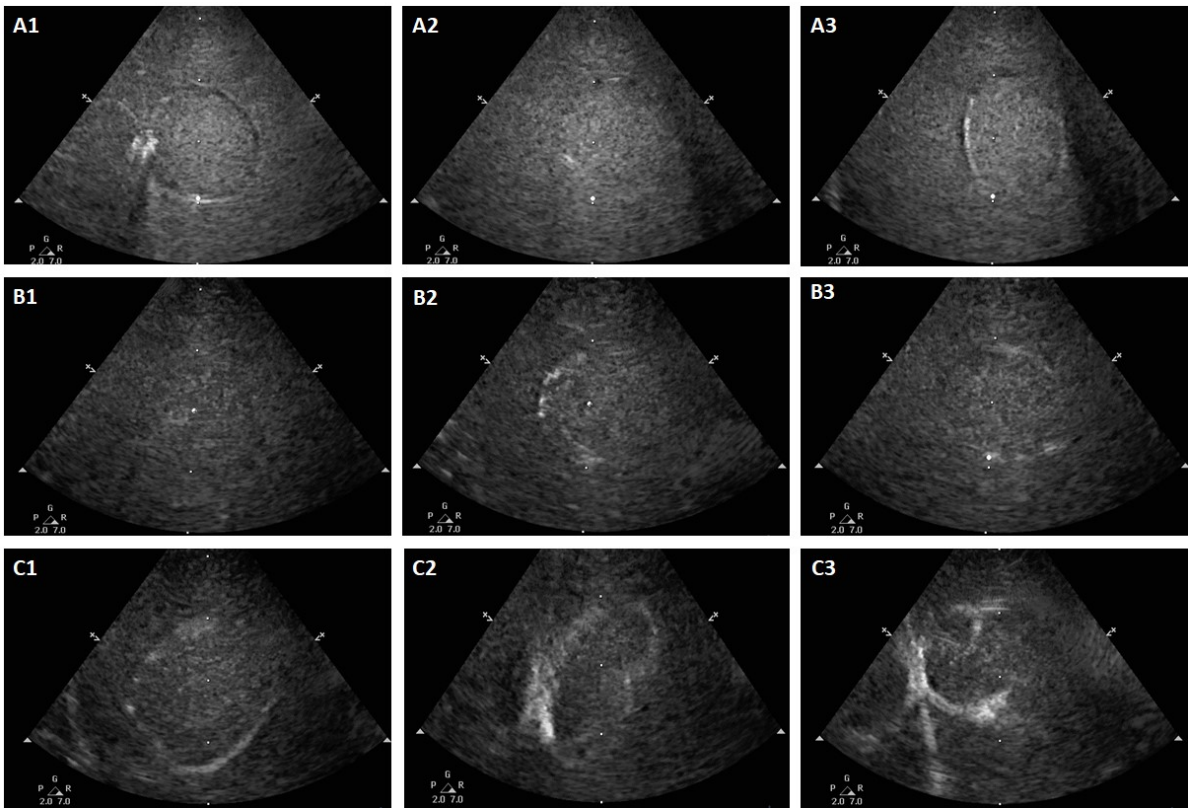

Figure 26. Increasing the number of FT cycles of the phantoms

The letters represent the number of FT cycles of the phantoms; A: 3 FT cycles B: 4 FT cycles. C: 5 FT cycles. The numbers represent phantoms, which are imaged from a cross-sectional view and composed of acoustic scatterers in weight percentage; 1: 0.1 wt%. 2: 0.2 wt%. 3: 0.3 wt%.

Figure 26 shows the result of increased number of FT cycles. With a number of 3 FT cycles, still a hypoechoic signal is observed for all three phantoms whereas a number of 5 FT cycles clearly gives an increased echogenicity. It appears that with a number of 4 FT cycles, the signal of the phantoms is somehow equivalent to the signal of BMF, making it difficult to distinguish between the specimen and medium. The phantom shown in Figure 26C2 has a peculiar shape compared to its initial circular shape presented in Figure 26A2 and Figure 26B2. This can be explained by the manner in which the phantoms were frozen after the first two FT cycles. None of the phantoms were hold in their original shape (i.e. around a tube to remain circular, see Figure 12C) but they were rather put in the freezer without support. As shown, other phantoms remained circular, as opposed to the phantom in Figure 26C2 which has slightly modified. Furthermore, several images present mirror image artifacts. In Figure 26A2-A3 a clear shadow is present which might be explained by a strong attenuation of the signal, possibly due to the plastic material of the beaker in which the phantoms were positioned.

4.5. DISCUSSION

This chapter has proposed an experiment to validate phantom models with respect to their echogenicity expressed in terms of CNR values. From the results, it could be observed that direct comparison between the SVC of the porcine and phantoms models was not doable due to the remarkable anechoic signal of the phantoms in both BMF and porcine blood, as opposed to the hyperechoic signal of the porcine tissue. Since this could not be explained, this chapter got another focus than the initial purpose of validating the phantom models. Also because comparison of completely different echo signals, expressed in quantitative CNR values, would neither give reliable results nor insights to proceed further validation. Hence, in order to examine the cause beyond this observation, two parameters were investigated that could have influenced the echogenicity of the phantoms. The first parameter included the time range between recovery of the BMF and performance of the US measurements, and the second parameter comprised the number of FT cycles undertaken by the phantoms.

Parameter 1: Time range between recovery of the BMF and performance of the US measurements

With the first parameter, it was primarily assumed that a distinction could be made between the images in the transition time from 30 minutes to 24 hours. From the results, solely a small difference in echo signal was observable but it seemed to increase slightly with 24 hours and up. This suggests that the circumstances of measuring (in this case the condition of the BMF, either with or without gas bubbles) do add to image quality but do certainly not affect the echogenicity distinctly. As a high image quality is always desired, it is important to stir BMF sufficiently prior to use in order to avoid settling of the particles. Simultaneously, it should be considered that the fluid should be temporarily stored to avoid the presence of noise caused by gas bubbles. Although not evident in BMF, it remains questionable to which degree the presence of gas bubbles has influenced the quality of the images in porcine blood as they were clearly present, see Figure 27.

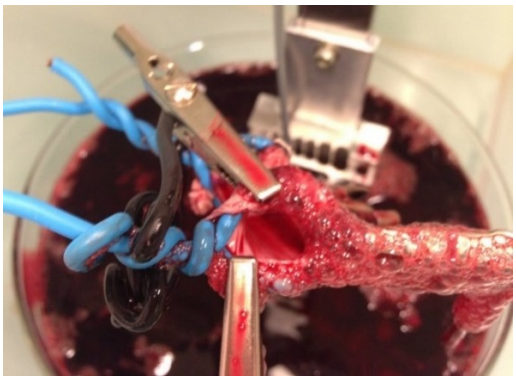

Figure 27. Gas bubbles surrounding porcine SVC

Figure 20A2 also shows the formation of fibrin networks, which occurred because the anticoagulant heparin was not administered either sufficiently or properly. Several studies have comprehensively investigated the effect of blood clotting on echogenicity [76-81]. They quantitatively demonstrated that both coagulating human and porcine whole blood show an increased backscatter signal during the clotting process. This is due to the formation of fibrin fibers, which increase the size and change the shape of blood cells (e.g. red blood cell aggregation). As a result, this increases the echogenicity of the blood during clotting, and might explain the results of Figure 23, which show an enhanced signal of the porcine blood rather than an expected regular anechoic signal [47, 75]. Despite the enhanced

signal of the blood, the SVC of the porcine still gives a hyperechoic signal, which indicates that the porcine's echo signal was not evidently governed by the blood's signal.

Parameter 2: The number of FT cycles undertaken by the phantoms

The second parameter, which examined the number of FT cycles of the phantoms, has demonstrated to affect the echogenicity of the phantoms in BMF. While a number of 2 FT cycles gave an anechoic signal, characterized by a completely dark echo, a number of 5 FT cycles distinctly showed an increased echogenicity of the phantoms. Although these measurements were quite evident, they solely provided a basis for further research in which it should be investigated whether the echogenicity enlarges even more after a number of 5 FT cycles or that it already has reached its maximum at this number. This latter is important to know since currently the echogenicity of the phantoms was still not sufficient (showed from visual observation) to enable comparison with porcine tissue in terms of CNR values. Although theoretically the CNR values of the phantom and porcine images, acquired in water, could already be compared statistically, it would not add to representative results since they do not reflect a realistic setting with measurements taken in either human or animal blood. Therefore, examining the number of FT cycles of phantoms in BMF would be more interesting for further validation. However, it should be also considered that BMF may not entirely represent human or animal blood despite its equivalent acoustical and physical properties. Although it is likely that a phantom with a number of 5 FT cycles gives an equivalent echogenicity in porcine blood, this assumption should be confirmed in a later study.

This chapter has shown that with increasing FT cycles also the phantom's echo signal changes. However, it is crucial to know what the underlying mechanism is beyond this observation. Regarding this, a study performed by Fromageau et al. 2007 [63] examined the mean density and the speed of sound as a function of the number of FT cycles in PVA samples. When varying the number of FT cycles from 1 to 10, they observed a logarithmic increasing relationship with the mean density, which varied from 1028 (1 FT cycle) to 1054 kgm^{-3} (10 FT cycles). Also for the speed of sound a logarithmic increasing relationship was found with an increasing number of FT cycles. This varied between 1525 ms^{-1} and 1560 ms^{-1}. Although the type of PVA and corresponding concentration used were slightly different, it is likely that the relationships observed by Fromageau et al. 2007 [63] are also valid within this study and may therefore provide a possible explanation for the observed anechoic signal of the phantoms. It was namely assumed that there was little difference in acoustic impedance between the phantom material and the blood, which may have resulted in few echoes being returned to the transducer (see section 2.2.2.2 of Chapter 2). As with a number of 5 FT cycles the phantom's mean density and speed of sound have increased, the acoustic impedance of the phantom became larger, and likely did the difference between the phantom material and the blood. Subsequently, the increased difference in acoustic impedance might have resulted in stronger reflected US echoes and thus a higher echogenicity of the phantoms.

In order to verify this hypothesis, additional experiments would be valuable in which the focus should be on either measuring the difference in acoustic impedance between the phantom material and blood after for example 2 and 5 FT cycles, or changing the properties of the medium rather than of the phantom itself. For instance, the viscosity of the blood could be reduced by adding another medium such as water to examine whether the echogenicity of the phantoms would increase. Hereby the underlying thought is that reducing the viscosity would increase the difference in acoustic impedance again, allowing more echoes to be reflected to the transducer which would give an increased signal. However, it should be considered as well that adding water to blood is not ideal since addition of water could burst the blood cells since they would fill up with water. Therefore, it would

be more convenient to test another medium, such as BMF, although at this stage it cannot be anticipated whether or not the latter would encounter similar problems.

Other study limitations and recommendations for future research

Within this study, porcine tissue was compared to phantoms on echocardiography and subsequently the images were used to validate the phantoms. As could be observed from the results (see Figure 23), the SVC of porcine clearly differs from the constructed phantoms in geometry as well as in echogenicity. A first explanation for the smaller diameter of the porcine SVC than actually expected from literature, is that the vein was not pulsated. Because this was already known prior to the experiment, the SVC was clamped around a wire to prevent total collapse of the vessel wall. However, the result was still not as desired. Hence, in a next experiment it is recommended to expand the vein by putting it under internal pressure (e.g. using an inflation/deflation cuff) to obtain a diameter equivalent to a realistic setting. Nevertheless, ultrasound systems are developed with the intention to be used for tissue structures with a body temperature of 37 °C rather than thawed tissue at room temperature. Therefore, the speed of sound within the structures may have differed as well since density is affected by temperature (section 2.2.1). As 'dead' and thawed tissue may provide a distinct different signal than 'living' tissue, it would be more convenient to conduct this experiment on living animals, also to prevent collapsible veins.

Two aforementioned parameters were investigated during this study which could have influenced the echogenicity of the phantoms in BMF. Besides these, another parameter namely the weight percentage of acoustic scatterer added to the phantoms, was assumed to affect the echogenicity. Although this parameter was not directly examined, it could be observed that there were no distinct differences in echogenicity between the phantoms with a weight percentage of 0.1 to 0.3 acoustic scatterer. Hence, when examining this parameter, larger concentration differences should be taken to find out whether this would add to increased echogenicity.

5

ICE EVALUATION

This chapter will evaluate the utility of ICE in porcine tissue and in a simulated lead extraction environment. Therefore, different visualization planes will be adopted to examine the lead-tissue interface. However, to perform these measurements, the vascular phantom model that will be used to simulate the lead extraction environment should comply with the imaging requirements outlined in section 3.2 of Chapter 3. Hence, the following section will first assess the suitability of the phantom model for ultrasound imaging and a lead extraction environment.

5.1. SUITABILITY OF THE VASCULAR PHANTOM MODEL

The objective of this experiment was to assess the suitability of the vascular phantom model. In order to accomplish this, it was examined whether it complied with the following imaging requirements:

- Suitable for US imaging
- It contains different echogenic structures to allow (tissue) structure discrimination on ultrasound (i.e. vessel wall, scar tissue and lead)

5.1.1. MATERIALS AND METHODS

Experimental Set-Up

Within this experiment, two customized vascular phantom models in terms of geometry (elaborated in section 3.7 of Chapter 3) were used with a PVA concentration of 7 wt%, and a $CaCO_3$ concentration of either 5 wt% or 50 wt%. They consisted of different structures with the following concentration of acoustic scatterer and number of FT cycles:

- PVA Vessel wall 0.1 wt% - 2 FT cycles
- $CaCO_3$ Scar tissue 0.5 wt% - 4 FT cycles

First, the 5 wt% $CaCO_3$ phantom was placed in a circular glass beaker, which was filled with water. The SVC of this model was attached to a holder through metal wires and clips. A 9-Fr Viewflex ICE catheter (Viewflex, St Jude Medical, St Paul, MN, USA) was used to produce the images at 6.25 MHz. This catheter was coupled to a catheter interface module (St. Jude Medical, Inc., St. Paul, MN, USA) which was connected to a CX50 ultrasound system (Philips Medical Systems, Andover, MA, USA), see Figure 6. After the images were taken, the first phantom was alternated by the second phantom with a $CaCO_3$ concentration of 50 wt%. In Figure 28 the experimental set-up is shown.

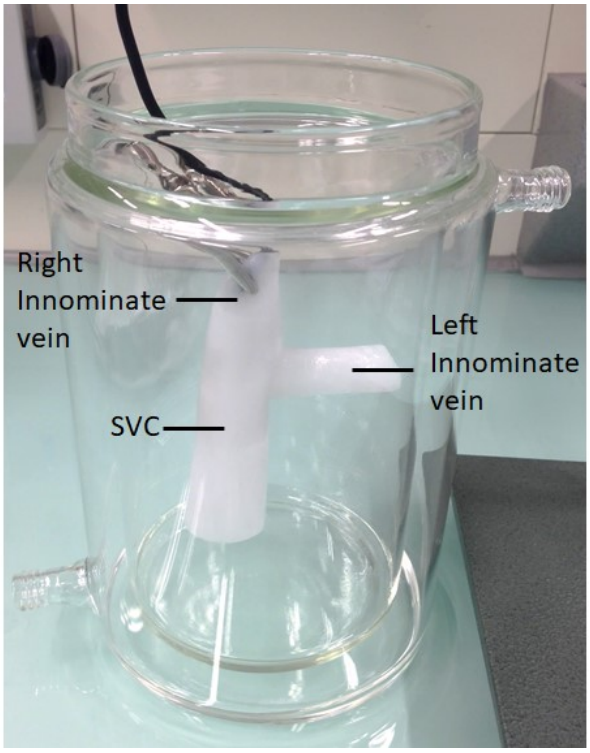

Figure 28. Experimental set-up of a vascular phantom model in water

Experimental Design

The SVC of the models was taken as FOV, since this area consisted of different structures (i.e. vessel wall and scar tissue), which were interesting to examine with ICE. Subsequently, the ICE probe was hold manually to take images from one view:

- Parallel (longitudinal) view outside the SVC

Its corresponding visualization plane is presented in Figure 29.

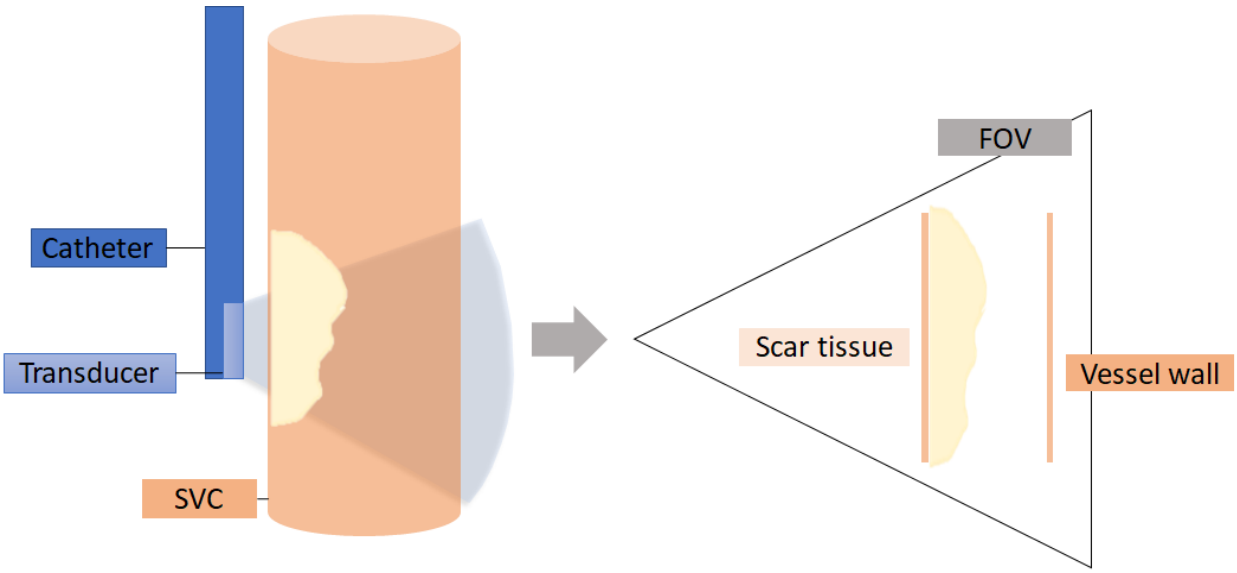

Figure 29. Parallel view outside the SVC

5.1.2. RESULTS

The results of this experiment are presented in Figure 30.

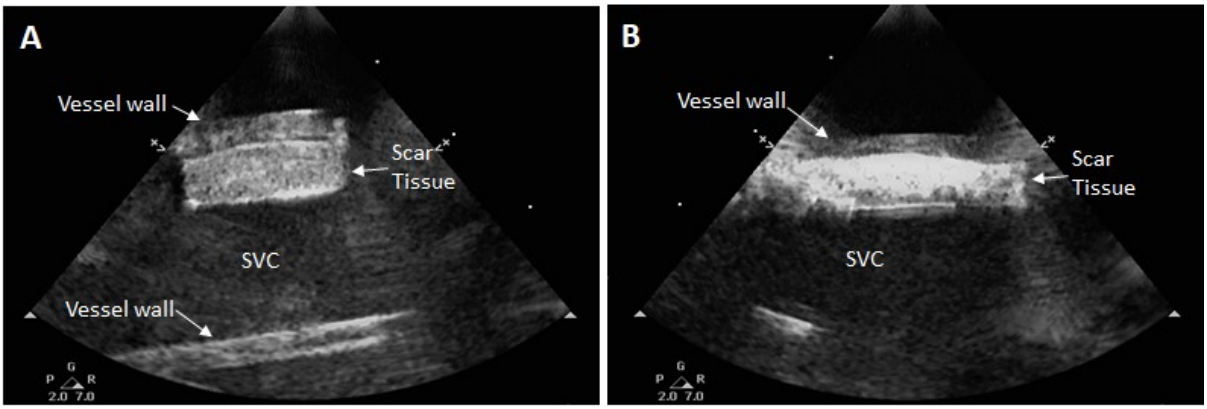

Figure 30. Comparison of SVC phantoms with different echogenicity

A: Phantom with scar tissue comprising 5 wt % of $CaCO_3$. B: Phantom with scar tissue comprising 50 wt % of $CaCO_3$. Image A clearly shows both sides of the vessel wall in the image plane whereas image B solely shows the vessel wall at one side, in the near field proximate to the transducer.

From Figure 30a and Figure 30b it can be observed that both phantoms show a distinct signal on echocardiography and comprise different echogenic structures. As a result, a clear discrimination can be made between the vessel wall and scar tissue, adherent to the wall. Figure 30a visualizes both sides of the vessel wall whereby primarily the wall at the distal end of the image plane is depicted with sharp echogenic edges. Conversely, Figure 30b solely shows one side of the vessel wall at the proximal end of the image plane. The area beyond the scar tissue appears more dark or anechoic. However, the scar tissue gives a hyperechoic signal, which is distinctly brighter than shown in Figure 30a. On top of that, it seems to be unequal in shape at the interface with the vessel wall, particularly at the right side of the image plane.

Comparison with prior clinical observations

When comparing these results to reported images from literature (see also section 2.2.2.3 of Chapter 2), it can be observed that Figure 30b is consistent with prior observations. Within these clinical studies it was reported that highly dense structures (i.e. fibrotic and calcified tissue) cause the US beam to be attenuated entirely. As a result, these areas are characterized by a linear echogenic shadow [16, 31], leaving a black area beyond the adherence site which can be also identified in Figure 30b.

5.1.3. FOLLOW-UP EXPERIMENT

Since the phantom with a concentration of 50 wt% $CaCO_3$, presented distinct echogenic differences between the vessel wall and scar tissue on ICE and also appeared to be equivalent to observations from literature, this model was solely used to proceed further measurements. Hereby the purpose was to evaluate whether the insertion of a lead could be identified in a similar view as previously described. In order to verify this, a 2-mm thin pacing lead was inserted in the phantom, first in a free-floating setting and subsequently in scar tissue. The experimental set-up is shown in Figure 31 and the results are presented in Figure 32.

Experimental Set-Up

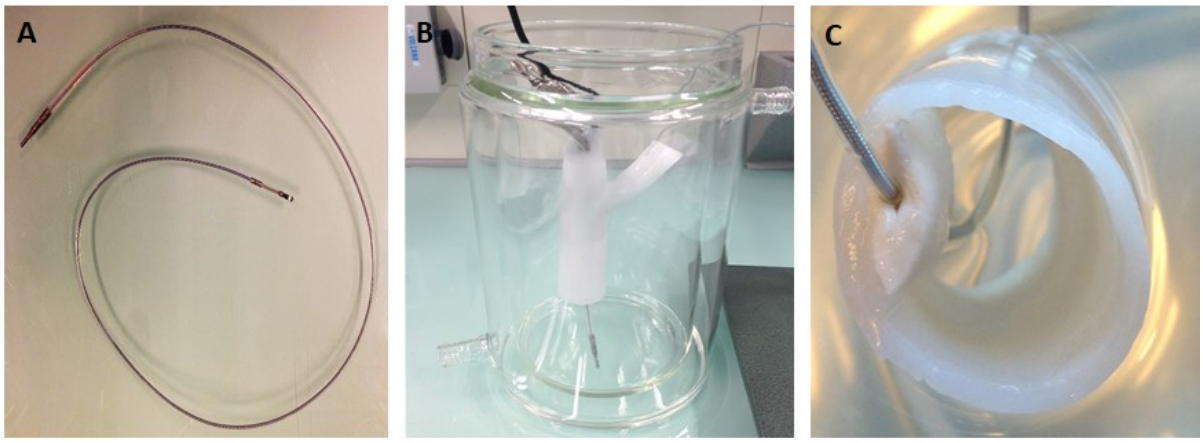

Figure 31. Pacing lead inserted in the vascular phantom

A: 2-mm thin pacing lead. B: Experimental set-up of a pacing lead in the vascular phantom. C: Cross-section of the pacing lead in scar tissue, adherent to the SVC wall.

Results

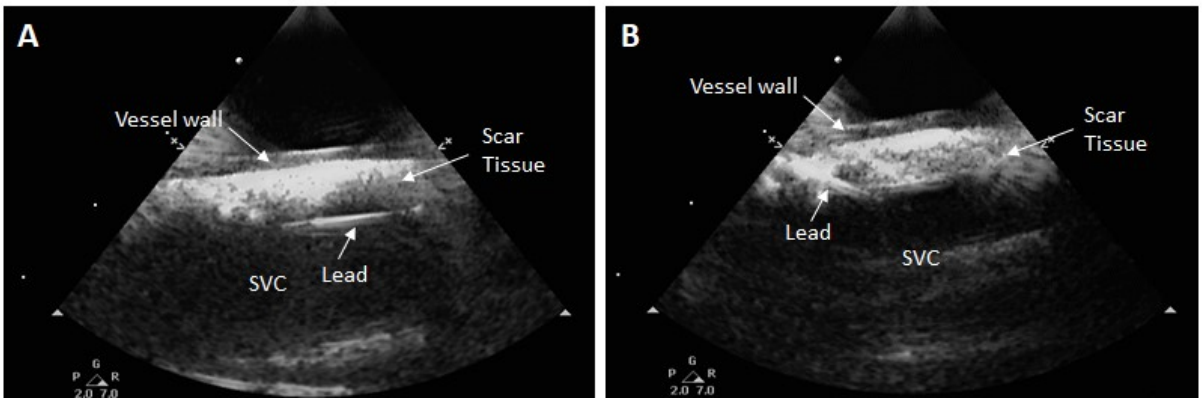

Figure 32. Parallel view of a pacing lead in a SVC phantom

A: free-floating lead. B: lead in scar tissue adherent to the vessel wall

Figure 32 shows the insertion of a pacing lead in the SVC phantom. An easy distinction can be made between a free-floating lead (Figure 32a) and a lead in scar tissue, adherent to the wall of the SVC (Figure 32b). The lead is highly reflective and gives a hyperechoic signal. In terms of contrast, it appears to be isoechoic to scar tissue, which can also be observed in prior results (see Figure 9 of Chapter 2).

5.1.4. DISCUSSION AND CONCLUSION

The results of this section have illustrated that a vascular phantom model with a concentration of 5 wt% $CaCO_3$ allows visualization of both vessel walls in a longitudinal view on intracardiac echocardiography. This means that the echo signal was able to penetrate through all structures of the phantom and subsequently to return to the transducer, even when passing through the area of scar tissue. In other words, no strong attenuation has occurred at the area of scar tissue which might be due to a low acoustic impedance and likely because the 5 wt% $CaCO_3$ scar tissue was not highly dense. As a result, also the vessel wall at the distal end of the image plane could be visualized. This was depicted with sharp echogenic edges, which might be explained because of a distinct acoustic impedance difference between the water and the phantom material, although unknown what the acoustic impedance of the phantom is.

As opposed to the 5 wt% $CaCO_3$ phantom, a 50 wt% $CaCO_3$ vascular phantom solely showed one vessel wall at the proximate end of the image plane, indicating that there was a strong attenuation of the signal at the area of scar tissue. This latter was unequal in shape at the interface with the vessel wall, which might be due to differences in its structure's density. When the density of a structure is larger (which is the case with 50 wt% $CaCO_3$), the speed of sound that passes through this structure is slower (see section 2.2.1 of Chapter 2). Since the scar tissue was not made homogeneous during the fabrication process (a PVA solution in water with an additional concentration of 50 wt% $CaCO_3$ was not entirely soluble), the scar tissue was likely denser at this interface (i.e. particularly the right side of the image plane) compared to other sites within the scar tissue. Because the signal of the scar tissue at this interface was slightly further away in the image plane than expected this observed delay might confirm the hypothesis. Alternatively, the unequal shape of the scar tissue might be also due to the unevenness of construction as result of inaccurately pouring.

Despite the aforementioned visualization differences, this section has demonstrated that the constructed vascular phantom models with both a concentration of 5 wt% and 50 wt% $CaCO_3$ are compatible with ultrasound imaging and enable tissue discrimination in terms of echogenicity. Thus, it can be concluded that all requirements of Chapter 3 were fulfilled, allowing the phantom models to be used as a lead extraction environment for the evaluation of ICE. Since the phantom with a concentration of 50 wt% $CaCO_3$ showed equivalent results to those from prior clinical studies [16, 31], this model was assessed more suitable for follow-up measurements. Although being quite isoechoic to calcified tissue, this section has still demonstrated that leads can be easily identified with ICE.

5.2. EVALUATING THE UTILITY OF ICE

The previous section has assessed the suitability of constructed vascular phantom models for the evaluation of ICE. Simultaneously, it showed that ICE was able to detect a venous wall, area of scar tissue as well as cardiac leads in a longitudinal view. This section will analyse the lead-tissue interface by examining multiple visualization planes with ICE. Subsequently, it has the purpose of determining which view provides the most valuable insight to reduce adverse effects during a TLE.

Approach

In order to accomplish this purpose, multiple experiments were conducted consecutively of which the overview is presented in Table 10. In these experiments, it was examined from different views whether ICE could detect the following structures:

- Venous wall
- Cardiac leads
- Area of scar tissue
- Extraction sheath

Table 10. Overview of conducted experiments

Experiment 1	Three views of a porcine IVC with free-floating lead
Experiment 2	Three views of a phantom SVC with lead adherent to scar tissue
Experiment 3	One view of a phantom SVC with insertion extraction sheath

5.2.1. EXPERIMENT 1: THREE VIEWS OF A PORCINE IVC WITH FREE-FLOATING LEAD

Prior to evaluating the utility of ICE for TLE procedures in realistic patient scenarios, multiple pre-clinical experiments are required which can be conducted on either animals or phantoms. Since porcine hearts closely resemble human hearts [82], they serve as a reliable measure to evaluate ICE performance. Therefore, this porcine heart experiment was conducted with the objective to examine whether a side-looking ICE catheter could be used to visualize free-floating leads and the vessel wall of a porcine heart in both a water and blood pool. This experiment has solely used a porcine heart obtained from a slaughterhouse, and was conducted with the lead extraction team from In-Body Systems (IBS), Philips Research Eindhoven.

MATERIAL AND METHODS

Experimental Set-Up

A porcine heart was placed in a circular glass beaker, which was first filled with water and subsequently with porcine whole blood. The inferior vena cava (IVC) of the porcine heart was attached to a holder through metal wires and clips. A 9-Fr Viewflex ICE catheter (Viewflex, St Jude Medical, St Paul, MN, USA) was used to produce the images at a frequency of 6.25 MHz. This catheter was coupled to a catheter interface module (St. Jude Medical, Inc., St. Paul, MN, USA) which was connected to a CX50 ultrasound system (Philips Medical Systems, Andover, MA, USA), see Figure 6. In Figure 33 the experimental set-up is shown.

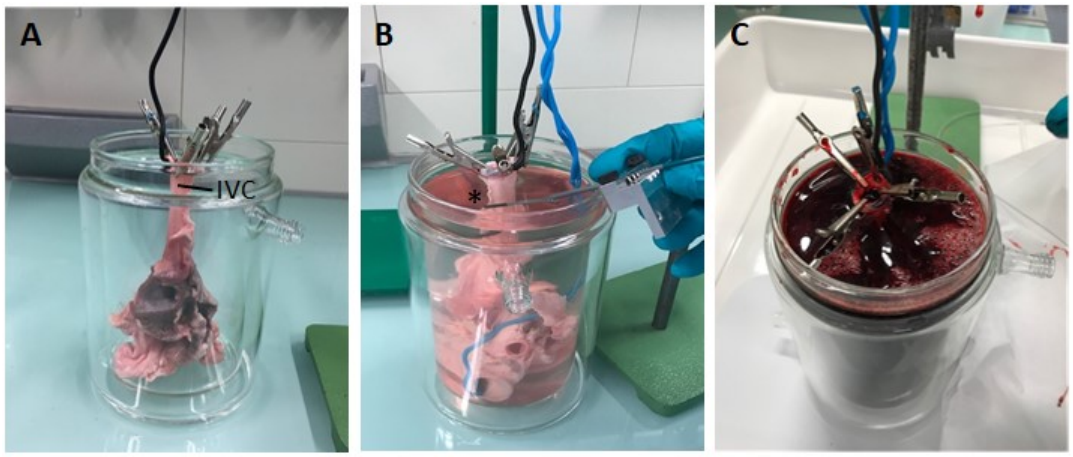

Figure 33. Experimental set-up of a porcine heart in a water and blood pool

A: Porcine heart in a glass beaker. B: Porcine heart submerged in water. Asterisk: ICE probe closely placed to the IVC to take a cross-section. C: Porcine heart submerged in blood. Images acquired from IBS, Philips Research Eindhoven and subsequently modified.

Experimental Design

The IVC of the porcine heart was used as region of interest because this structure was most convenient to mount and image. A 2-mm thin pacing lead was inserted in the IVC. Subsequently, the ICE probe was hold manually to take images (first in water and then in blood) from three different views:

- Parallel (longitudinal) lead view outside the IVC
- Cross-sectional (transversal) lead view outside the IVC
- Parallel (longitudinal) lead view inside the IVC

The corresponding visualization planes are illustrated in Figure 34.

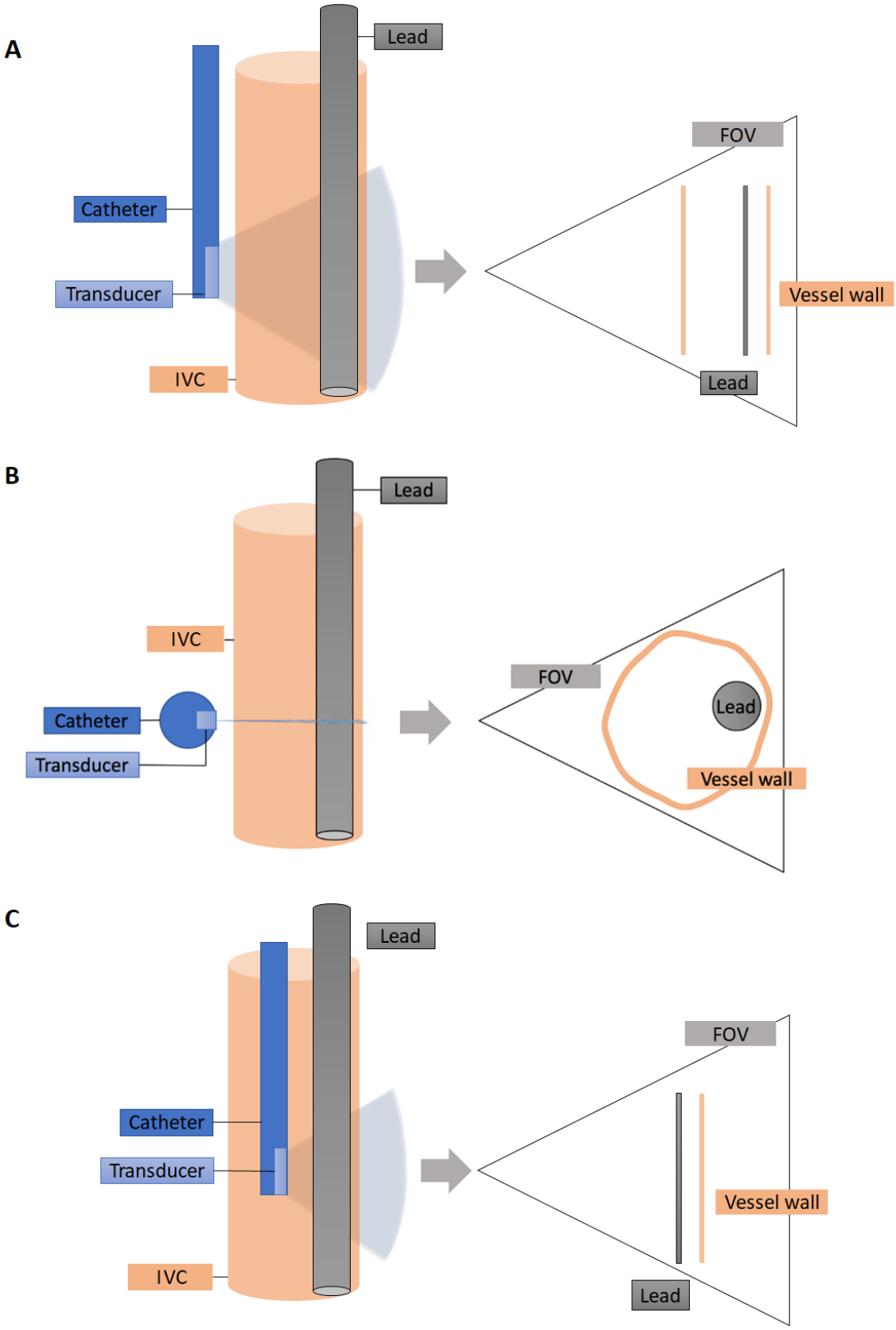

Figure 34. Three different visualization planes

Imaging of three different views with a Viewflex ICE catheter. A: Parallel lead view outside the IVC. B: Cross-sectional lead view outside the IVC. C: Parallel lead view inside the IVC.

RESULTS

The results of experiment 1 are presented in Figure 35.

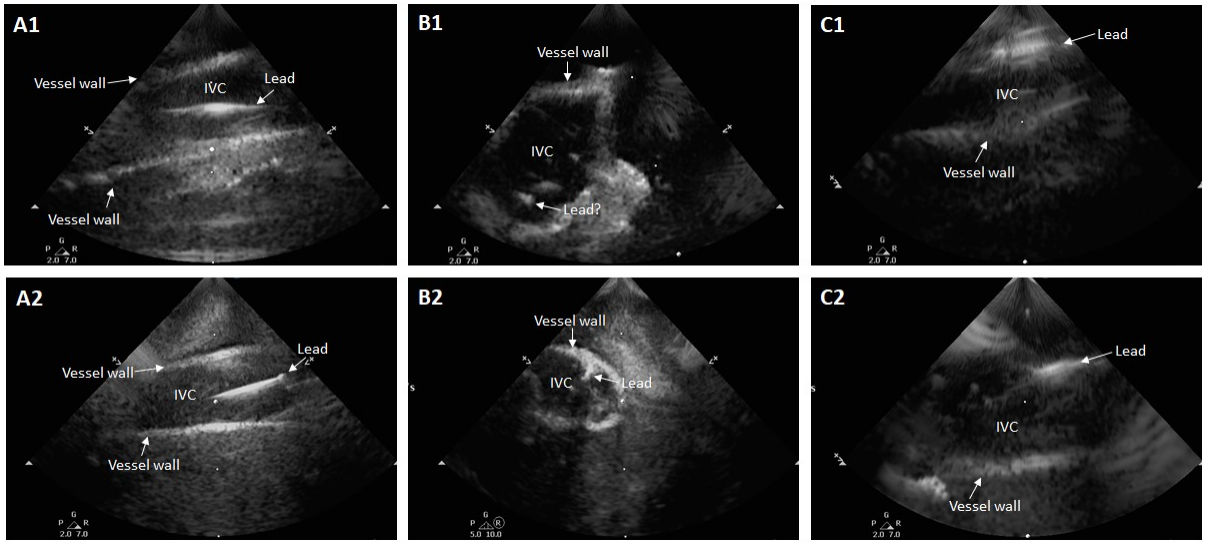

Figure 35. Three different views of free-floating leads in a porcine IVC with ICE

The letters represent the visualization plane in which was imaged; A: Parallel lead view outside the IVC. B: Cross-sectional lead view outside the IVC. C: Parallel lead view inside the IVC. The numbers represent the medium; 1: Water. 2: Blood.

Figure 35 shows that the IVC wall and pacing lead can be identified for three different views in both a water and blood pool. In Figure 35C1-2, the linear lead seems to partially block the echo signal, which gives a relatively weak echo of the vessel wall compared to the signal amplitude of the vessel wall presented in Figure 35A1-2. Furthermore, the circular lead in Figure 35B1 cannot be clearly identified. Primarily in Figure 35B1-2, there are some lumps of surrounding tissue (e.g. fat) visible which give an echogenic signal besides the signal of the IVC wall. On top of that, all images are illustrated with grating lobe artifacts, located at the side of the FOV.

5.2.2. EXPERIMENT 2: THREE VIEWS OF A PHANTOM SVC WITH LEAD ADHERENT TO SCAR TISSUE

In the previous experiment it was shown that a side-looking ICE catheter was able to detect the vessel wall and free-floating leads in the IVC of a porcine heart from multiple views. Since this experiment solely included a 'healthy' porcine heart with no areas of scar tissue, the current experiment was conducted in a vascular phantom model with lead adhesions to scar tissue, serving as alternative to mimic 'diseased' human vasculature. The objective was to examine whether a side-looking ICE catheter could be used to visualize the SVC of a phantom model with lead binding sites for three different views in water. This study was an extension of a previous described experiment (elaborated in section 5.1) where only one visualization plane was used.

MATERIAL AND METHODS

Experimental Set-Up

A similar set-up was adopted as the one described in section 5.1.1. However, solely the vascular phantom model with a concentration of 50 wt% $CaCO_3$ was used.

Experimental Design

The SVC of a phantom model was used as region of interest because this structure consisted of calcified scar tissue through which a 2-mm thin pacing lead could be inserted. Subsequently, the ICE probe was hold manually to take images from three different views in water:

- Parallel (longitudinal) lead-tissue view outside the SVC
- Cross-sectional (transversal) lead-tissue view outside the SVC
- Parallel (longitudinal) lead-tissue view inside the SVC

In the latter view, the ICE probe was introduced into the entry of the right innominate vein to approach the SVC. The corresponding visualization planes are illustrated in Figure 36. For each view, multiple images were taken from either a stationary lead or moving lead.

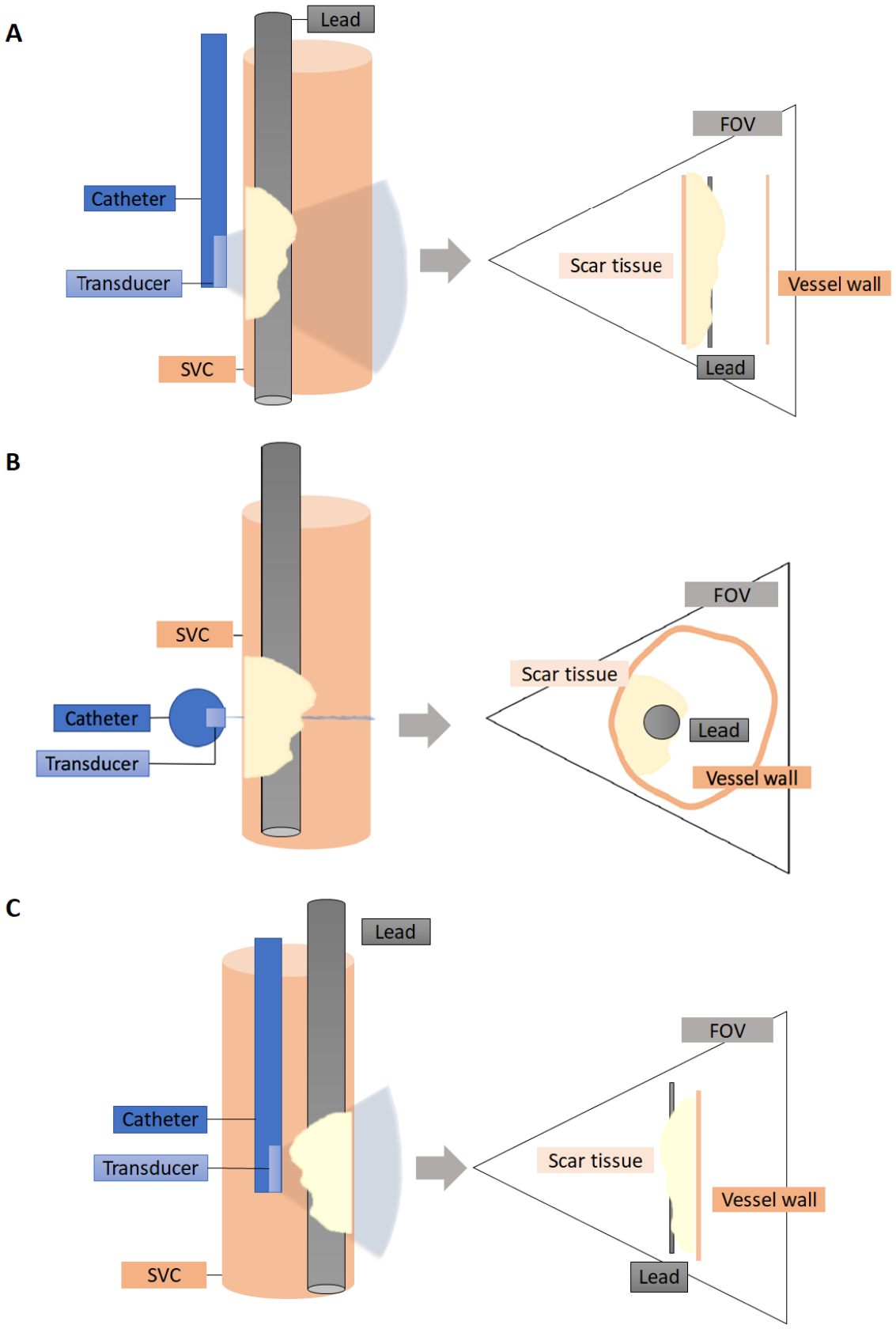

Figure 36. Three different visualization planes of the lead-tissue interface

Imaging of three different views with a Viewflex ICE catheter. A: Parallel lead-tissue view outside the SVC. B: Cross-sectional lead-tissue view outside the SVC. C: Parallel lead-tissue view inside the SVC. To obtain a representative image of the experimental set-up, view C should be horizontally rotated by an angle of 180°.

RESULTS

The results of experiment 2 are presented in Figure 37.

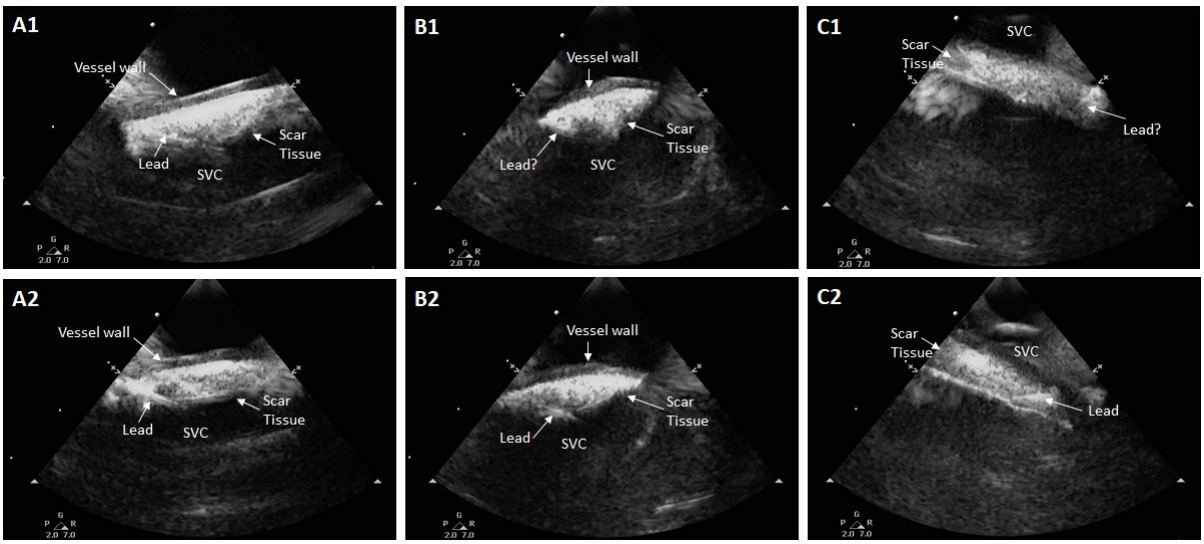

Figure 37. Three different views of leads adherent to scar tissue in a phantom SVC with ICE

The letters represent the visualization plane in which was imaged; A: Parallel lead-tissue view outside the SVC. B: Cross-sectional lead-tissue view outside the SVC. C: Parallel lead-tissue view inside the SVC. The numbers represent the state of the lead; 1: Stationary. 2: Moving.

Figure 37 shows that the lead-tissue interface can be clearly identified for all three different views in water. Although the images per view appear to be similar, it can be observed that a moving lead (array 2 of Figure 37) provides a slightly increased signal in terms of echogenicity than a stationary lead. Particularly in Figure 37B1 and Figure 37C1 it is more difficult to identify the lead. Notice that a parallel view inside the SVC does not show any vessel wall but rather gives a linear echogenic shadow beyond the scar tissue. Both a parallel and cross-sectional view outside the SVC also give this typical shadow but do present the vessel wall and its position with respect to the lead binding site at the proximal end of the image plane. Furthermore, in Figure 37C the lead is visualized twice, both as free-floating and adhered to scar tissue. This is because the lead body was solely encapsulated at a few sites. Consequently, both its free-floating and adhered part were in the image plane of the ICE transducer. Moreover, the images are illustrated with side lobe artifacts, located at the side of the FOV.

5.2.3. EXPERIMENT 3: ONE VIEW OF A PHANTOM SVC WITH INSERTION EXTRACTION SHEATH

Experiment 2 has demonstrated that a side-looking ICE catheter is able to visualize the lead-tissue interface in a phantom model for three different views in water. Besides visualization of the lead-tissue interface, which is important to assess the difficulty and risk of extraction [31], another crucial point of attention is the alignment of the extraction sheath when disrupting the lead adhesions. Since vascular laceration, particularly of the SVC, may result in serious complications, it is important for the operator to know how the extraction sheath should be positioned to disrupt lead adhesions without inducing lacerations. Hence, this third and last experiment was conducted with the objective to examine whether a side-looking ICE catheter could be used to visualize the advancement of an extraction sheath over a lead, adherent to scar tissue.

MATERIAL AND METHODS

Experimental Set-Up

A vascular phantom model with a scar concentration of 50 wt% $CaCO_3$ (described in section 5.1.1) was placed in a circular glass beaker, which was filled with water. The SVC of this model was attached to a holder through metal wires and clips. A 2-mm thin pacing lead was inserted through the left innominate vein into the scar tissue. Subsequently, a 13-Fr Tightrail mechanical rotating extraction sheath (The Spectranetics Corporation, Colorado Springs, CO, USA) was advanced over the lead to the area of scar tissue. A 9-Fr Viewflex ICE catheter (St Jude Medical, St Paul, MN, USA) was used to produce the images at 6.25 MHz. This catheter was coupled to a catheter interface module (St. Jude Medical, Inc., St. Paul, MN, USA) which was connected to a CX50 ultrasound system (Philips Medical Systems, Andover, MA, USA), see Figure 6. In Figure 38 the experimental set-up is shown.

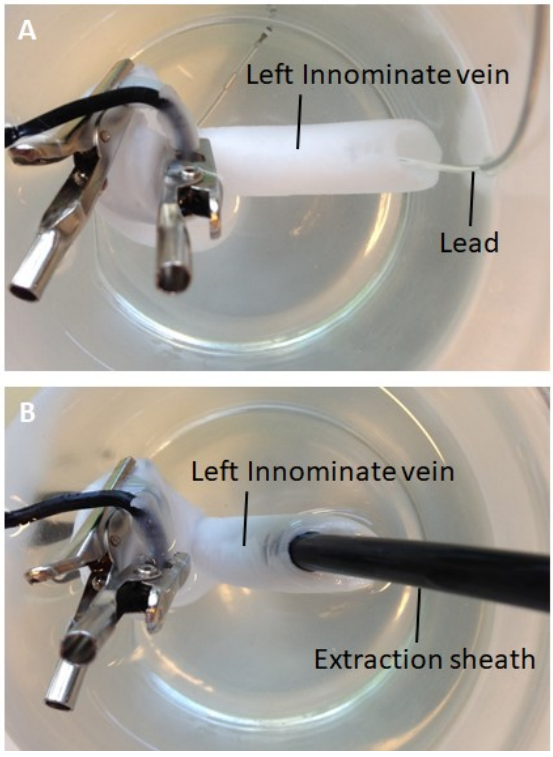

Figure 38. Experimental set-up of an extraction sheath in a vascular phantom

A: Top view of the phantom with a pacing lead inserted through the left innominate vein into scar tissue. B: Insertion of an extraction sheath into the left innominate vein, which is advanced over the lead to reach the area of scar tissue in the SVC.

Experimental Design

The ICE probe was hold manually at the left side of the phantom to take images from one view:

- Parallel (longitudinal) lead-tissue view outside the SVC

The corresponding visualization plane is illustrated in Figure 39.

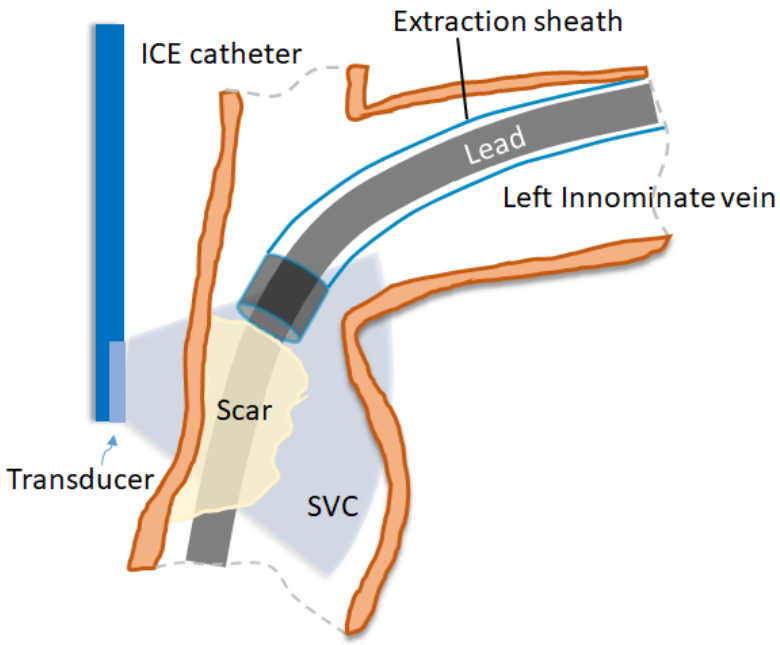

Figure 39. Visualization plane of the lead-tissue interface with an extraction sheath

A parallel lead-tissue view outside the SVC, which shows the advancement of an extraction sheath over a lead to approach the area of scar tissue.

RESULTS

In Figure 40 the results of experiment 3 are presented.

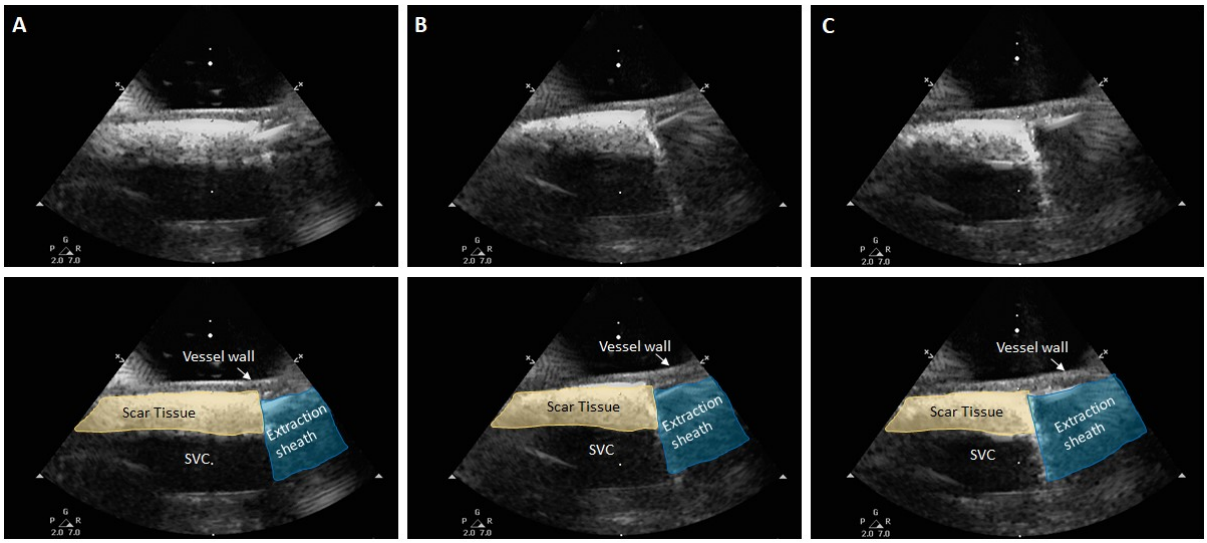

Figure 40. Advancement of an extraction sheath to approach the lead-tissue interface

The upper row shows the ICE images, which present the advancement of an extraction sheath over time. The lower row provides the same images but with a description of the present structures in the images.

Figure 40 shows the advancement of an extraction sheath to approach the area of scar tissue. The extraction sheath can be clearly identified, although it appears to be larger in geometry than its original diameter of about 1.3 cm (the distance between two points in the centre of the plane is equal to 1 cm). The marked blue area approximately indicates it original size. Due to this parallel view, the position of the extraction sheath can be properly presented with respect to the vessel wall and lead-tissue interface. Notice the presence of side lobe artifacts, located at the side of the FOV in all images.

5.2.4. DISCUSSION AND CONCLUSION

Within this chapter, the goal was to evaluate the utility of a side-looking Viewflex ICE catheter for TLE procedures by examination of its visualization capabilities, particularly with regard to the vessel wall, lead-tissue interface and an extraction sheath in a porcine heart and vascular phantom model. Subsequently, the goal was determine which catheter position gave the most insight into the lead-tissue interface. To accomplish this, multiple experiments were conducted of which the results will be discussed per experiment.

Experiment 1

The first experiment has illustrated that vessel walls and free-floating leads can be clearly visualized from different views in the IVC of a porcine heart when submerged in both a water and blood pool. Although, the circular lead within the cross-sectional view could not be properly identified in water, it was clearly visible in blood. Therefore, this was rather due to pollution of the water (e.g. as result of skin contact or oxidation of the metal clips that clamped the porcine IVC) than the limitation of this view in general. When contaminants float in water, they tend to move faster when an acoustic wave passes by and thus sometimes provide an echogenic signal. Within this view, these particles likely provided a signal equivalent to the free-floating lead in water, which increased the difficulty to discriminate between the lead and particles. From this experiment it appeared that a parallel and cross-sectional image from outside the IVC gave a better visualization of the lead and the IVC wall than a parallel image inside the IVC.

Experiment 2

Instead of a porcine heart, the second experiment has used a vascular phantom model with lead adhesions to scar tissue, to examine whether a side-looking ICE probe could visualize a lead-tissue interface in water. It has shown that for all examined views the area of scar tissue and leads can be clearly visualized, although it appeared that a moving lead in scar tissue provided a slightly increased echogenicity than a stationary lead, which enabled for better and faster identification. Hence, to properly identify the lead in a realistic patient scenario with ICE, it requires to be moved around, which can be easily performed through exertion of push and pull forces. Furthermore, this experiment has demonstrated that for all examined views the scar tissue along the lead-tissue interface was visualized as an echo dense signal, characterized by a linear echogenic shadow. For a parallel view inside the SVC, this finding is equivalent to prior clinical observations [16, 31] but not optimal in terms of assessing the lead-tissue interface. This is because the corresponding shadow was the result of the scar tissue's high density, which attenuated the signal completely and subsequently induced a complete disappearance of the vessel wall, although visualization of the latter is important to avoid vascular tears. While a parallel and cross-sectional view outside the SVC encountered the same problem, they showed the vessel wall at the proximate end of the image plane where the area of scar tissue was located. Hence, this led to more insight into the lead-tissue interface.

Experiment 3

The third experiment was conducted with the goal to examine whether the advancement of an extraction sheath in a phantom model could be visualized with a side-looking ICE probe in water. It illustrated that the advancement of an extraction sheath could be clearly visualized from a parallel view outside the SVC of the phantom. The tip of the extraction sheath did not seem to affect image negatively, neither did movement of the sheath seem to disturb the image plane. Although these results are quite promising, this should be also investigated for a cross-sectional outside the SVC and a parallel view inside the SVC. This latter was not feasible at the time of measurement because this view required the ICE probe to be inserted from below into the SVC, to obtain a proper lead-tissue-sheath view. However, this was not possible due to the bottom of the beaker glass, which obstructed the insertion. Additionally, at this time the experiment could solely conducted by one person whilst actually requiring more hands to perform the measurements properly.

Based on the findings of the described experiments, this section has demonstrated that a side-looking Viewflex ICE catheter is able to identify a vessel wall and cardiac leads in a porcine IVC as well as to visualize areas of scar tissue and an extraction sheath in a vascular phantom model with sufficient resolution. Although the examined visualization planes all present the lead-tissue interface, it can concluded that both a parallel and cross-sectional view outside the SVC, give more insight into the lead-tissue interface than a parallel view inside the SVC. This is because the former show the vessel wall, which is crucial to determine how an extraction sheath should be (re)positioned in the desired image plane, whilst disrupting the lead adhesions and simultaneously avoiding laceration. Nevertheless, the question remains whether the other two views outside the SVC could be applied since they currently do not seem anatomically possible, as opposed to a parallel view inside the SVC that has already been applied in a few clinical studies [3, 31]. Overall, from this section it can be concluded that the use of a side-looking ICE catheter for TLE procedures is valuable to assess the lead-tissue interface to predict the difficulty and risk of extraction, and to improve sheath alignment to reduce adverse effects.

6

OVERALL DISCUSSION

The objective of this study was to design and construct a vascular phantom model and to use this model to evaluate the utility of ICE for TLE procedures. This was an explorative study performed with the reason to examine how ICE could reduce serious adverse effects during lead management, as TLE procedures are still associated with a small but distinct rate of major complications and mortality.

The following major steps were taken to accomplish the objective: Several mould prototypes intended for the phantom were designed and constructed based on data of vascular geometry from literature. Then following a couple of prototype iterations and according a developed protocol, a vascular phantom model was constructed with realistic geometry and echogenicity. After construction, the SVC of the phantom was compared to the SVC of a porcine heart in a validation experiment. Subsequently, its suitability to serve as a real-life lead extraction environment was assessed by comparison of its results with findings from previous conducted clinical studies. Ultimately, both the constructed phantom and a porcine model were used to evaluate the performance of ICE in three experiments whereby several visualization planes of the lead-tissue interface were examined.

STUDY OUTCOMES

Within this study, some distinct efforts were made regarding the construction of a non-biological tissue-mimicking vascular phantom model to simulate a real-life lead extraction environment and the evaluation of ICE for TLE procedures. To my knowledge, this is the first study that proposed an affordable and accessible customized 'home made' vascular phantom model for the simulation of a real-life lead extraction environment, and demonstrated that ICE evaluation for TLE procedures can be also performed on a tissue-mimicking phantom as alternative to animals or patients. This has the advantage of saving costs and ethical issues on animal experiments and possibly even early clinical evaluations in the longer term but may also accelerate pre-clinical and clinical research on this topic. Furthermore, the results of this study illustrated that a side-looking phased-array ICE probe is able to visualize the lead-tissue interface from different visualization planes and might therefore be of clinical significance for TLE procedures to reduce major complications. Despite the promising results, this study was subjected to several limitations, which will be discussed in the following section.

STUDY LIMITATIONS

Although the constructed phantom model appeared to be a suitable method to simulate a lead extraction environment in terms of geometry and echogenicity, it was not statistically validated. Within the validation experiment, it became clear that the constructed phantom could not be quantitatively compared to porcine tissue in terms of CNR values. This was because the phantom gave a complete anechoic signal in blood, likely due to little difference in acoustic impedance between the

phantom material and the porcine blood in which the measurement were performed. Since the acoustic impedance of the specimens (i.e. phantom, porcine tissue and blood) was not examined within this study, it remains unknown what the cause was behind the anechoic signal and therefore necessitates further investigation. In addition, knowing the acoustic impedance is also important to perform validation in terms of acoustic properties. Ideally, the constructed phantom model would include highly lifelike mechanical, optical, mobile and acoustic properties to enable adequate testing of ICE and to provide the feedback necessary to proceed further implementation. However, this was not feasible in terms of time and beyond the scope of this project.

Since the phantom was not suitable for use in BMF and porcine blood, all measurements were performed in water. Although the obtained results in water appeared to be promising and provided a good framework to continue further work, they do not represent realistic patient scenarios in which measurements are performed in human blood. Furthermore, this study solely focused on the utility of 2D ICE rather than 3D ICE. Although physicians are already used to 2D views and are well familiar with the anatomy of a patient, 3D ICE may provide better views of the lead-tissue interface and may also enable faster and easier identification of, for example, entwined leads or how the lead adhesions are located with respect to the vessel wall. The former often occurs in patients and may increase the difficulty with regard to extraction. However, within this study solely a basic setting of one lead was applied to visualize with ICE, rather than multiple (entwined) leads.

Moreover, the constructed phantom model solely represented the SVC and approximate innominate veins, which was useful to obtain local insight of the lead-tissue interface. However, one should keep in mind that the ultimate goal is to avoid complications and otherwise to identify them fast enough to intervene on time. Therefore, the phantom model should be extended to an entire heart, so that complications (e.g. inducing a SVC perforation with an extraction sheath and a consequent pleural effusion/inducing a myocardial perforation with an inserting lead and a consequent pericardial effusion) can be simulated to examine whether ICE is able to detect them and to find out whether there are also ICE-related complications. According a study of Sadek et al. 2017 [31] a possible drawback of 2D ICE could be the low sensitivity of detecting pleural effusions, as opposed to its high sensitivity to pericardial effusions. Since this study solely focused on ICE, it would be interesting to investigate whether other US modalities can detect pleural effusions more easily whilst still providing a proper visualization of the lead-tissue interface. Although, studies already demonstrated that TEE can detect pleural effusions [83, 84], it is unlikely that it will properly visualize the lead-tissue interface due to its position in the oesophagus. Nevertheless, it still requires attention in future research.

Despite the fact that the implementation of ICE in TLE procedures is still in its infancy, an important point to consider in the longer term is the cost-benefit ratio. From an economic perspective, ICE avoids general anaesthesia and may result in shorter procedural times (due to better visualization of the targeted lead-tissue interface), fewer complications and use of extraction tools, which would all save costs distinctly. Conversely, these potential benefits should be weighed against the significant costs of an ICE catheter, which are not covered by health insurance agencies [17, 85, 86]. A potential method to reduce the costs is by re-sterilization and reuse of the catheter. However, this is currently only permitted in a few European countries [17]. On top of that, it is important to compare the overall cost-benefit ratio of ICE with TEE and conventional fluoroscopy, to examine whether ICE would worth structural implementation into TLE procedures.

FUTURE PERSPECTIVES

There are several aspects regarding both the vascular phantom model and intracardiac echocardiography, which are recommended to be investigated in future research. These recommendations are described within this section.

Vascular phantom model

1. Training of physicians
2. Constructing a multimodal phantom
3. Creating anisotropy

Intracardiac echocardiography

4. Implementation of forward-looking ICE in extraction sheath
5. Utilizing ICE to monitor the advancement of powered sheaths

1. Training of physicians

TLE procedures

Generally, phantoms are used with the purpose of either testing new medical instruments and tools or enabling training of a certain medical procedure. Within this study, the phantom model was specifically developed for the evaluation of ICE during TLE procedures. However, its application might be extended to training purposes as well. Given that a TLE is an invasive procedure, in which most serious adverse effects occur with the operator's early experience and little regular practice, it demands highly trained and experienced operators to consistently deliver safe and effective care [20, 24, 87]. Unfortunately, currently there is a lack of means to provide the training, practice and repetition necessary to acquire the desired technical expertise. Only few sites are available where practitioners could gain adequate clinical experience, and watching an instructional video demonstration or observing how another operator performs the extraction is not sufficient [4, 87]. As this could be problematic, alternative solutions are required, such as phantom models that serve as training tool. Particularly, with the current phantom it would be interesting to examine whether it is able to produce similar extraction forces such as those perceived in realistic patient scenarios, to acquire tactile skills as additive to the skills acquired from visual learning (ICE could also aid in this process by simultaneously providing visual feedback). This is because tactile skills are hard to teach, while excessive pulling and primarily pushing forces are a main malefactor of complications (e.g. SVC tears) [88]. Thus, the constructed phantom might be potentially utilized to provide adequate training and acquisition of these skills by offering realistic situations in an environment free of risk.

Plaque debulking therapies

Similar to TLEs, atherosclerotic plaque debulking therapies (e.g. percutaneous coronary or peripheral angioplasty) have a great patient risk and require high operator skills. Within these procedures, even a minimum training period of one year is required whilst encountering the same problems as TLE of limited training means [87]. Hence, the vascular phantom might also aid in these procedures but it should be examined whether the phantom could be adjusted to smaller diameter vessels such as the coronary and peripheral, and whether the calcified tissue still suffices to mimic atherosclerotic plaque or that it should be alternated with areas of softer plaque. Furthermore, it is interesting to examine whether multiple vessel layers (i.e. intima, media, adventitia) could be created. This is because the

incidence of restenosis (i.e. the recurrence of a stenosis) after treatment is still a major problem of debulking therapies. As restenosis may be due to dissection of deeper vessel layers [14], it could be valuable to examine, by using the phantom, how often dissection occurs and in which vessel layers. Subsequently, this could aid the process of finding out how dissection could be avoided to assure that excessive restenosis triggering remains absent.

2. Constructing a multimodal phantom

Within this study, it was important to construct a phantom model that was suitable for ultrasound imaging to evaluate the performance of ICE. When considering other imaging modalities or multimodalities (e.g. think of support using multimodal image registration) for guidance of TLE procedures in future research, it would be useful to extend this model to a multimodal phantom to enable testing of those (overlaid) modalities. Within this study, the phantom material consisted of PVA, which is also suitable for application in MRI. Hence, this phantom could already be used for MRI. Furthermore, to enable application of CT imaging, which is another prominent but ionizing radiation-dependent medical imaging modality, the phantom material could be blended with CT contrast agents such as iodine prior to subjection of FT cycles. Phantoms used for CT evaluation are commonly mixed with calcium chloride to mimic hard tissue (e.g. bone, calcified tissue) [89]. Within this study, $CaCO_3$ was used to mimic calcified tissue. Therefore, it should be examined whether it still could be utilized for application in CT or that it should be alternated with calcium chloride.

3. Creating anisotropy

When the properties of a material vary in different orientations, this is called anisotropic. Considering the constructed phantom of this study, this was made isotropic and solely represented the SVC and approximate veins in the heart. In order to study the entire lead-tissue interface with ICE, the phantom should be extended to a complete heart. However, since the heart muscle is composed of different fibre structures (e.g. filaments), which vary in different orientations and tend to give an 'anisotropic effect' on US [90], it is recommended to examine whether an anisotropic phantom can be constructed. This is important since anisotropy affects the US image in such a way that, measuring under a different insonation angle than perpendicular to the structure causes the hyperechoic signal of fibre structures to be changed into a hypoechoic signal. When one wants to study the lead-tissue interface from multiple insonation angles in the entire heart, this effect should be certainly taken into account.

4. Implementation of forward-looking ICE in extraction sheath

Based on the findings of this study it was shown that ICE provides insight into the lead-tissue interface, but that the extent to which it can image the FOV particularly depends on the location of the ICE probe. Anatomically, currently only a parallel view inside the SVC is feasible. However, with this view the main problem is that a side-looking phased-array ICE probe is not able to provide a proper signal of the vessel wall beyond the lead-tissue interface. A forward-looking phased-array ICE probe, that images in front of the probe, may clearly distinguish the wall from the lead-tissue interface and would be therefore worth to investigate. When this probe would be implemented in the extraction sheath, it would be even more optimal to provide local real-time monitoring of the lead-tissue interface whilst advancing the extraction sheath to disrupt the adhesions.

5. Utilizing ICE to monitor the advancement of powered sheaths

This study has demonstrated that ICE was able to image the advancement of a mechanical rotating extraction sheath over a lead. The advantages of using a mechanical sheath over a powered sheath (e.g. laser) is that it is easier to disrupt areas of (calcified) lead adhesions. However, it induces vascular laceration more rapidly than a powered sheath, which allows the adhesions to be disrupted in a controlled manner. As the latter is also a common TLE tool, it would be interesting to examine whether ICE is able to monitor the advancement of these types of sheaths. In a study of Schaller et al. [3] the laser sheath was already used in a patient study combined with ICE. Nevertheless, the authors did not report whether ICE was also able to visualize the lead-tissue interface at the time that the laser was turned on, or that ICE could be solely used in between the laser pulse durations.

7

FINAL CONCLUSION

This thesis project has demonstrated a methodology to design and construct an affordable and accessible customized 'home made' vascular phantom model for the simulation of a real-life lead extraction environment. It has shown that this ultrasound compatible and risk free phantom model of the SVC and approximate innominate veins provides an adequate testing environment in terms of geometry and echogenicity for the evaluation of ICE imaging. From the findings of this study, it can be concluded that ICE is able to image and assess the lead-tissue interface from different visualization planes, important to predict the difficulty and risk of extraction. However, it has demonstrated that a parallel view and cross-sectional view outside the SVC give more valuable insight into lead binding sites and their position with respect to the vessel wall than a conventional parallel view inside the SVC. Furthermore, ICE has shown to be a valuable tool to monitor the advancement of an extraction sheath at the lead-tissue interface, which is crucial information for the operator to improve sheath alignment and subsequently to avoid major complications such as tears in the SVC. Thus, implementation of ICE imaging into TLEs has the potential to add to a more effective and safer procedure.

BIBLIOGRAPHY

1. Marieb, M. *Procedures - AICD Implantation*. 2019 2 January 2019]; Available from: https://www.markmariebmd.com/procedures/.
2. Maytin, M., R. John, and L.M. Epstein, *Device pocket scar predicts transvenous lead extraction difficulty.* J Innov Card Rhythm Manage, 2015. **6**: p. 2173-2177.
3. Schaller, R.D., M.M. Sadek, and J.M. Cooper, *Simultaneous lead traction from above and below: A novel technique to reduce the risk of superior vena cava injury during transvenous lead extraction.* Heart Rhythm, 2018.
4. Kusumoto, F.M., et al., *2017 HRS expert consensus statement on cardiovascular implantable electronic device lead management and extraction.* Heart Rhythm, 2017. **14**(12): p. e503-e551.
5. Wazni, O., et al., *Lead extraction in the contemporary setting: the LExICon study: an observational retrospective study of consecutive laser lead extractions.* J Am Coll Cardiol, 2010. **55**(6): p. 579-86.
6. Oestreich, B.A., et al., *Use of Transesophageal Echocardiography to Improve the Safety of Transvenous Lead Extraction.* JACC Clin Electrophysiol, 2015. **1**(5): p. 442-448.
7. Endo, Y., et al., *Clinical utility of intraprocedural transesophageal echocardiography during transvenous lead extraction.* Journal of the American Society of Echocardiography, 2008. **21**(7): p. 861-867.
8. ROUX, J.F., et al., *Laser lead extraction: predictors of success and complications.* Pacing and clinical electrophysiology, 2007. **30**(2): p. 214-220.
9. Jones IV, S.O., et al., *Large, single-center, single-operator experience with transvenous lead extraction: outcomes and changing indications.* Heart Rhythm, 2008. **5**(4): p. 520-525.
10. Hauser, R.G., et al., *Deaths and cardiovascular injuries due to device-assisted implantable cardioverter–defibrillator and pacemaker lead extraction.* Europace, 2009. **12**(3): p. 395-401.
11. Lou, X., et al., *Successful stent implantation for superior vena cava injury during transvenous lead extraction.* HeartRhythm Case Rep, 2015. **1**(6): p. 394-396.
12. Wilkoff, B.L., et al., *Pacemaker lead extraction with the laser sheath: results of the pacing lead extraction with the excimer sheath (PLEXES) trial.* Journal of the American College of Cardiology, 1999. **33**(6): p. 1671-1676.
13. Brunner, M.P., et al., *Outcomes of patients requiring emergent surgical or endovascular intervention for catastrophic complications during transvenous lead extraction.* Heart Rhythm, 2014. **11**(3): p. 419-425.
14. Jong, L., *Lasers for Cardiovascular Interventions and the utility of In-Body Systems*, in *Systematic Literature Study*, D.U.o. Technology, Editor. 2018.
15. Hetterich, H., et al., *New X-ray imaging modalities and their integration with intravascular imaging and interventions.* Int J Cardiovasc Imaging, 2010. **26**(7): p. 797-808.
16. Bongiorni, M.G., et al., *Intracardiac echocardiography in patients with pacing and defibrillating leads: a feasibility study.* Echocardiography, 2008. **25**(6): p. 632-638.
17. Bartel, T., et al., *Why is intracardiac echocardiography helpful? Benefits, costs, and how to learn.* Eur Heart J, 2014. **35**(2): p. 69-76.
18. Topaz, O., *Lasers in cardiovascular interventions*. 2015: Springer.
19. Deharo, J.C., et al., *Pathways for training and accreditation for transvenous lead extraction: a European Heart Rhythm Association position paper.* Europace, 2012. **14**(1): p. 124-34.
20. Byrd, C.L., et al., *Clinical study of the laser sheath for lead extraction: the total experience in the United States.* Pacing and Clinical Electrophysiology, 2002. **25**(5): p. 804-808.
21. Bongiorni, M.G., et al., *Transvenous removal of pacing and implantable cardiac defibrillating leads using single sheath mechanical dilatation and multiple venous approaches: high success rate and safety in more than 2000 leads.* European heart journal, 2008. **29**(23): p. 2886-2893.

22. Kennergren, C., et al., *A single-centre experience of over one thousand lead extractions.* Europace, 2009. **11**(5): p. 612-617.
23. Byrd, C.L., et al., *Intravascular extraction of problematic or infected permanent pacemaker leads: 1994–1996.* Pacing and Clinical Electrophysiology, 1999. **22**(9): p. 1348-1357.
24. van Erven, L., J.M. Morgan, and C. Scientific Initiatives, *Attitude towards redundant leads and the practice of lead extractions: a European survey.* Europace, 2010. **12**(2): p. 275-6.
25. Henrikson, C.A., K. Zhang, and J.A. Brinker, *A survey of the practice of lead extraction in the United States.* Pacing Clin Electrophysiol, 2010. **33**(6): p. 721-6.
26. Ellis, C.R. *When Should We Extract a Lead?* ; Available from: http://ismics.org/summit/multimedia/files/2015/Presentations/Friday/session1/815_Ellis.pdf.
27. Greenspon, A.J., et al., *16-year trends in the infection burden for pacemakers and implantable cardioverter-defibrillators in the United States: 1993 to 2008.* Journal of the American College of Cardiology, 2011. **58**(10): p. 1001-1006.
28. Sohail, M.R., et al., *Management and outcome of permanent pacemaker and implantable cardioverter-defibrillator infections.* Journal of the American College of Cardiology, 2007. **49**(18): p. 1851-1859.
29. Baddour, L.M., et al., *Update on cardiovascular implantable electronic device infections and their management: a scientific statement from the American Heart Association.* Circulation, 2010. **121**(3): p. 458-477.
30. Chmarra, M.K., et al., *Multimodal phantom of liver tissue.* PLoS One, 2013. **8**(5): p. e64180.
31. Sadek, M.M., et al., *Utility of intracardiac echocardiography during transvenous lead extraction.* Heart Rhythm, 2017. **14**(12): p. 1779-1785.
32. Enriquez, A., et al., *Use of Intracardiac Echocardiography in Interventional Cardiology: Working With the Anatomy Rather Than Fighting It.* Circulation, 2018. **137**(21): p. 2278-2294.
33. Narducci, M.L., et al., *Usefulness of Intracardiac Echocardiography for the Diagnosis of Cardiovascular Implantable Electronic Device–Related Endocarditis.* Journal of the American College of Cardiology, 2013. **61**(13): p. 1398-1405.
34. Scientific, B. *How CRTs Work*. 2019 2 January 2019]; Available from: http://www.bostonscientific.com/en-US/patients/about-your-device/crt-devices/how-crts-work.html.
35. Lakkireddy, D., et al., *IMpact of pocKet rEvision on the rate of InfecTion and other CompLications in patients rEquiring pocket mAnipulation for generator replacement and/or lead replacement or revisioN (MAKE IT CLEAN): a prospective randomized study.* Heart Rhythm, 2015. **12**(5): p. 950-956.
36. Manolis, A.S., et al., *Cardiac implantable electronic device lead extraction using the lead-locking device system: keeping it simple, safe, and inexpensive with mechanical tools and local anesthesia.* Anatolian journal of cardiology, 2017. **18**(4): p. 289.
37. Dicardiology. *FDA Clears Spectranetics' Mechanical Lead Extraction Devices*. 2014 2 January 2019]; Available from: https://www.dicardiology.com/product/fda-clears-spectranetics%E2%80%99-mechanical-lead-extraction-devices.
38. Marcus, G. *Right atrial and right ventricular leads as visualized under X-ray during a pacemaker implant procedure.* 2008 2 January 2019]; Available from: https://commons.wikimedia.org/wiki/File:Fluoroscopy_pacemaker_leads_right_atrium_ventricle.png.
39. Pace, H.t. *Closure of Skin of Pacemaker Pocket - Example 3 (Subcuticular)*. 2016 2 January 2019]; Available from: http://www.howtopace.com/skin-closure/.
40. Gateway, T. *14.1. Speed of Sound, Frequency and Wavelength*. 2019 2 January 2019]; Available from: https://www.texasgateway.org/resource/141-speed-sound-frequency-and-wavelength.

41. Burnett, J.M., et al., *Intracardiac echocardiography 101: The beginner's guide to ICE imaging and cardiac structure recognition.* EP Lab Digest, 2005. **5**(5): p. 4148.
42. Thurston, M.N., R. *Phased array*. 2019 2 January 2019]; Available from: https://radiopaedia.org/articles/phased-array.
43. Secrest, S., *Basic Principles of Ultrasonography.* VETERINARY TECHNICIAN, 2006. **27**(12): p. 756.
44. Silowski, C. *Chapter 1: Ultrasound Nomenclature, Image Orientation and Basic Instrumentation*. 2019 2 January 2019]; Available from: http://samples.jbpub.com/9780763765583/65583_CH01_5378.pdf.
45. Zagzebski, J., *Essentials of ultrasound physics St Louis.* Mo: Mosby, 1996.
46. Shung, K.K., *Diagnostic ultrasound: Imaging and blood flow measurements*. 2015: CRC press.
47. MC, E. *Ultrasound Contrast Agents*. 2018 28 December 2018]; Available from: https://www.erasmusmc.nl/thoraxcenterbme/Current-Research/AgentsDiag/4678596/?lang=en.
48. Pogue, B.W. and M.S. Patterson, *Review of tissue simulating phantoms for optical spectroscopy, imaging and dosimetry.* J Biomed Opt, 2006. **11**(4): p. 041102.
49. Kremkau, F.W. and K. Taylor, *Artifacts in ultrasound imaging.* Journal of ultrasound in medicine, 1986. **5**(4): p. 227-237.
50. Bickle, I.G., A. *Radiopaedia - Mirror image artifact*. 2018 28 December 2018]; Available from: https://radiopaedia.org/articles/mirror-image-artifact.
51. didier-chantier. *Diagram Of S Four Chamber Heart*. 2019 2 January 2019]; Available from: http://didier-chantier.com/diagram-of-s-four-chamber-heart/diagram-of-s-four-chamber-heart-new-best-photo-gallery-websites-with-diagram-of-s-four-chamber-heart/.
52. Sonavane, S.K., et al., *Comprehensive imaging review of the superior vena cava.* Radiographics, 2015. **35**(7): p. 1873-1892.
53. Mahlon, M.A. and H.-C. Yoon, *CT angiography of the superior vena cava: normative values and implications for central venous catheter position.* Journal of Vascular and Interventional Radiology, 2007. **18**(9): p. 1106-1110.
54. Mozes, G. and P. Gloviczki, *Venous embryology and anatomy*, in *The Vein Book*. 2007, Elsevier. p. 15-25.
55. Gibson, F. and A. Bodenham, *Misplaced central venous catheters: applied anatomy and practical management.* Br J Anaesth, 2013. **110**(3): p. 333-46.
56. McMurdo, K., et al., *Normal and occluded mediastinal veins: MR imaging.* Radiology, 1986. **159**(1): p. 33-38.
57. Salik, E., A. Daftary, and M.G. Tal, *Three-dimensional anatomy of the left central veins: implications for dialysis catheter placement.* Journal of Vascular and Interventional Radiology, 2007. **18**(3): p. 361-364.
58. AbuRahma, A., *Noninvasive Vascular Diagnosis: A Practical Textbook for Clinicians*, ed. F. Edition. 2017: Springer Science & Business Media.
59. SCI. *Scientific Computing and Imaging Institute - Arterial System Lecture Block 10 Bioengineering 6000 CV Physiology*. 2019 2 January 2019]; Available from: http://www.sci.utah.edu/~macleod/bioen/be6000/notes/L10-arteries-veins.pdf.
60. Huang, T.-Y. and N. Baba, *Cardiac pathology of transvenous pacemakers.* American heart journal, 1972. **83**(4): p. 469-474.
61. Robboy, S.J., et al., *Autopsy findings with permanent pervenous pacemakers.* Circulation, 1969. **39**(4): p. 495-501.
62. Esposito, M., et al., *Morphologic and immunohistochemical observations of tissues surrounding retrieved transvenous pacemaker leads.* J Biomed Mater Res, 2002. **63**(5): p. 548-58.

63. Fromageau, J., et al., *Estimation of polyvinyl alcohol cryogel mechanical properties with four ultrasound elastography methods and comparison with gold standard testings.* IEEE transactions on ultrasonics, ferroelectrics, and frequency control, 2007. **54**(3).
64. Surry, K., et al., *Poly (vinyl alcohol) cryogel phantoms for use in ultrasound and MR imaging.* Physics in Medicine & Biology, 2004. **49**(24): p. 5529.
65. Nadkarni, S.K., et al., *A pulsating coronary vessel phantom for two-and three-dimensional intravascular ultrasound studies.* Ultrasound in medicine & biology, 2003. **29**(4): p. 621-628.
66. Wan, W., et al., *Optimizing the tensile properties of polyvinyl alcohol hydrogel for the construction of a bioprosthetic heart valve stent.* Journal of Biomedical Materials Research: An Official Journal of The Society for Biomaterials, The Japanese Society for Biomaterials, and The Australian Society for Biomaterials and the Korean Society for Biomaterials, 2002. **63**(6): p. 854-861.
67. Chu, K.C. and B.K. Rutt, *Polyvinyl alcohol cryogel: An ideal phantom material for MR studies of arterial flow and elasticity.* Magnetic Resonance in Medicine, 1997. **37**(2): p. 314-319.
68. Li, W., B. Belmont, and A. Shih, *Design and manufacture of polyvinyl chloride (PVC) tissue mimicking material for needle insertion.* Procedia Manufacturing, 2015. **1**: p. 866-878.
69. Ceh, D., T.M. Peters, and E.C. Chen. *Acoustic characterization of polyvinyl chloride and self-healing silicone as phantom materials*. in *Medical Imaging 2015: Physics of Medical Imaging*. 2015. International Society for Optics and Photonics.
70. Sekisui. *Solution preparation guidelines - Selvol polyvinyl alcohol*. 2018 4 December 2018]; Available from: https://www.sekisui-sc.com/wp-content/uploads/SelvolPVOH_SolutionPreparationGuidelines_EN.pdf.
71. de Jong, T.L., et al., *PVA matches human liver in needle-tissue interaction.* J Mech Behav Biomed Mater, 2017. **69**: p. 223-228.
72. Yusof, N.S.M., et al., *Ultrasound imaging characterization on tissue mimicking materials for cardiac tissue phantom: Texture analysis perspective.* Malaysian Journal of Fundamental and Applied Sciences, 2017. **13**(4-2): p. 501-508.
73. Tan, Z., et al., *Cryogenic 3D Printing of Super Soft Hydrogels.* Sci Rep, 2017. **7**(1): p. 16293.
74. CIRS. *Blood Mimicking Fluid*. 2019 2 January 2019]; Available from: http://www.cirsinc.com/file/Products/046/046%20DS%20100313(1).pdf.
75. Hebbard, P.D., *Artifactual mirrored subclavian artery on ultrasound imaging for supraclavicular block.* Canadian Journal of Anesthesia/Journal canadien d'anesthésie, 2009. **56**(7): p. 537-540.
76. Kirk Shung, K., et al., *Ultrasonic characterization of blood during coagulation.* Journal of clinical ultrasound, 1984. **12**(3): p. 147-153.
77. Huang, C.-C., S.-H. Wang, and P.-H. Tsui, *Detection of blood coagulation and clot formation using quantitative ultrasonic parameters.* Ultrasound in medicine & biology, 2005. **31**(11): p. 1567-1573.
78. Huang, C.-C. and S.-H. Wang, *Characterization of blood properties from coagulating blood of different hematocrits using ultrasonic backscatter and attenuation.* Japanese journal of applied physics, 2006. **45**(9R): p. 7191.
79. Huang, C.-C., et al., *High frequency ultrasonic characterization of human vocal fold tissue.* The Journal of the Acoustical Society of America, 2007. **122**(3): p. 1827-1832.
80. Yuan, Y. and K. Shung, *The effect of focusing on ultrasonic backscatter measurements.* Ultrasonic imaging, 1986. **8**(2): p. 121-130.
81. Huang, C.-C., et al., *Study of the blood coagulation by ultrasound.* J. Med. Biol. Eng., 2011. **31**(2): p. 79-86.
82. Lelovas, P.P., N.G. Kostomitsopoulos, and T.T. Xanthos, *A comparative anatomic and physiologic overview of the porcine heart.* Journal of the American Association for Laboratory Animal Science, 2014. **53**(5): p. 432-438.

83. Capper, S., et al., *Transoesophageal echocardiography for the detection and quantification of pleural fluid in cardiac surgical patients.* British journal of anaesthesia, 2007. **98**(4): p. 442-446.
84. Orihashi, K., et al., *New applications of two-dimensional transesophageal echocardiography in cardiac surgery.* Journal of cardiothoracic and vascular anesthesia, 1991. **5**(1): p. 33-39.
85. Alboliras, E.T. and Z.M. Hijazi, *Comparison of costs of intracardiac echocardiography and transesophageal echocardiography in monitoring percutaneous device closure of atrial septal defect in children and adults.* The American journal of cardiology, 2004. **94**(5): p. 690-692.
86. Bartel, T. and S. Muller, *Device closure of interatrial communications: peri-interventional echocardiographic assessment.* Eur Heart J Cardiovasc Imaging, 2013. **14**(7): p. 618-24.
87. Wilkoff, B.L., et al., *Transvenous lead extraction: Heart Rhythm Society expert consensus on facilities, training, indications, and patient management: this document was endorsed by the American Heart Association (AHA).* Heart Rhythm, 2009. **6**(7): p. 1085-104.
88. Maytin, M., T.P. Daily, and R.G. Carillo, *Virtual reality lead extraction as a method for training new physicians: a pilot study.* Pacing Clin Electrophysiol, 2015. **38**(3): p. 319-25.
89. Johnson, T., et al., *Dual energy CT in clinical practice*. 2011: Springer Science & Business Media.
90. Bickle, I.M., M.A. *Anisotropy*. 2019 14 January 2019]; Available from: https://radiopaedia.org/articles/anisotropy?lang=us.
91. Topaz, O., *Lasers in cardiovascular interventions*. Springer. 2015.
92. Chamis, A.L., Peterson, G. E., Cabell, C. H., Corey, G. R., Sorrentino, R. A., Greenfield, R. A., ... & Fowler, V. G. , *Staphylococcus aureus bacteremia in patients with permanent pacemakers or implantable cardioverter-defibrillators.* Circulation, 2001. **104(9), 1029-1033**.
93. Rodriguez, Y., J. Garisto, and R.G. Carrillo, *Management of cardiac device-related infections: a review of protocol-driven care.* Int J Cardiol, 2013. **166**(1): p. 55-60.
94. Health, U.S.D. *Pacemaker and ICD Lead Extraction*. 2018 23 April 2018]; Available from: https://www.youtube.com/watch?v=mpHKfCwphoc.
95. Brunner, M.P., et al., *Clinical predictors of adverse patient outcomes in an experience of more than 5000 chronic endovascular pacemaker and defibrillator lead extractions.* Heart Rhythm, 2014. **11**(5): p. 799-805.
96. Spectranetics, *GlideLight Laser Sheath - Instructions for use.* 2016.
97. Bongiorni, M.G., *Transvenous Lead Extraction: From Simple Traction to Internal Transjugular Approach*. Springer Science & Business Media. 2011.
98. Bongiorni, M.G. *Preparing and performing lead extraction*. in *ESC Congress 2012*. 2012. Munich Germany 25-29 August
99. Timischl, F., *The contrast-to-noise ratio for image quality evaluation in scanning electron microscopy.* Scanning, 2015. **37**(1): p. 54-62.
100. Bloomington, I.U. *Contrast to Noise Ratio - Lab Manual: 5 Modifications for P551 Fall 2013 Medical Physics Laboratory*. 2018 1 November 2018]; Available from: http://physics.indiana.edu/~courses/p551/f13/Experiments_files/Modus_DeskCAT_LM5_P551.pdf.

APPENDICES

APPENDIX A: PROCEDURE PROTOCOL TLE

This procedure protocol describes the steps necessary to perform a Transvenous Lead Extraction. It is adopted from a previous conducted literature study [14]. For the sake of clarity, the protocol is divided into a pre-procedural and intra-procedural step. Also, notice that within this protocol a powered laser catheter is used as extraction tool. This can be alternated, either by mechanical or other powered catheters. A comprehensive illustration of the clinical workflow is shown in Figure 44.

PRE-PROCEDURE

Pre-procedural evaluation and planning are an essential part for performing a TLE. Within this step a comprehensive assessment is made in which the risks and benefits of the procedure are considered per patient [91]. Three factors are included:

1. Indications for extraction

The first decision point is to determine the urgency of the operation, herein the cause of lead extraction important. When the indication includes infection, treatment should be expedited and all hardware should be extracted (since a delay in treatment with removal of all components is associated with an increased mortality rate [92]) whereas in non-infectious indications, extraction of all components is not specifically necessary and the lead may even be abandoned [19, 93-95].

Indications for lead extraction include:

- Infection at the site of the lead/device (account for two-thirds of all extractions)
- Lead malfunction
- The lead requires more energy to function than the device is able to deliver
- Blockage of the vein by clot or scar tissue
- Lead interference with blood flow back to the heart
- Lead interference with other/new leads

Subsequently, the physician can decide to perform an:

- Interventional extraction
- Open heart extraction, or to:
- Abandon the lead
- Refer the patient to a specialized site

2. The medical condition of the patient

The condition of the patient is assessed through consideration of patient history and the presence of other diseases. Examples of comorbidities are renal or heart failure, history of body radiation and Body Mass Index (BMI). Furthermore, considerations are done regarding medications and social history (e.g. smoking, drugs).

3. Device and lead history

Besides the cardiovascular history of the patient, this part also considers the history of cardiac, vascular, thoracic or other major surgeries. Furthermore, it is determined whether the patient is pacemaker dependent and if reimplantation is needed during intervention.

Within the risk assessment, various aspects of a lead are considered such as the:

- Type of lead i.e. ICD or pacing
- Fixation mechanism i.e. active/passive (with or without a mechanism that attaches the lead to the heart muscle respectively)
- Material e.g. silicone, polyurethane
- Lead diameter
- Number of leads [91]
- Period of implantation
  – low risk: less than 2 years of oldest lead implantation
  – medium risk: between 2 and 5 years of oldest lead implantation
  – high risk: between 6 and 20 years of oldest lead implantation
  – severe risk: greater than 20 years of oldest lead implantation

- To verify the intracardiac position of the lead, a 2D posteroanterior/lateral chest X-ray and/or 3D chest CT scan can be used although not necessary. The physician can also decide to perform the extraction without imaging information

At the start of the procedure, general steps should be taken regarding laser preparation and safety. Furthermore, packages of red blood cells should be available.

INTRA-PROCEDURE

- The procedure requires a well-trained laser extraction team including a cardiologist, cardiothoracic surgeon (on call/in room) and nurses (scrubbed and non-scrubbed). When necessary there can be anaesthesiologist, pacemaker representative and laser representative

Note: According a survey from the USA, electrophysiologists seem to perform approximately 89% of the lead extractions, cardiac surgeons 6% and cardiologists 5% [25].

Decisions

- The procedure should be performed under general anaesthesia or local anaesthesia
- Disinfection can be done of the entire chest or only of the pocket area
- The vascular point of entry i.e. often in the intraclavicular area, should be established
- Cardiac function can be monitored with the aid of TEE which requires preparation
- Placement of the pacing and defibrillating pads should be done on the skin of the patient

Preparation of equipment

- The pocket should be opened after which the generator and lead(s) can be liberated. Subsequently, perform a gentle traction under X-ray to assess if there is adherence to vascular structures and cut the leads
- When this is done, the sheath can be introduced into the subclavian vein (alternatives are the femoral and jugular veins)
- The procedure should be performed under 2D fluoroscopic guidance, this is the common standard
- In order to wash the blood or contrast medium away, the inner lumen of the laser sheath requires flushing with 10 cm^3 of saline infusion. For the outer sheath another 10 cm^3 of saline should be used [96]
- Since simple traction is most often ineffective due to multiple binding sites along the lead (and usually results in coil lengthening and lead damage [97]) preparation of the leads takes place by means of al locking stylet or lead locking device which minimizes the risk of losing access to the inner lumen of the lead. This should be inserted and locked into the lead as distal as possible and subsequently the locking mechanism should be deployed [96]
- Make sure that the laser catheter is positioned in the same axis as the lead to avoid vascular injury (Figure 41). Similar to a guidewire, the lead should be used as a guiding tool to lead the laser catheter into the endovenous space

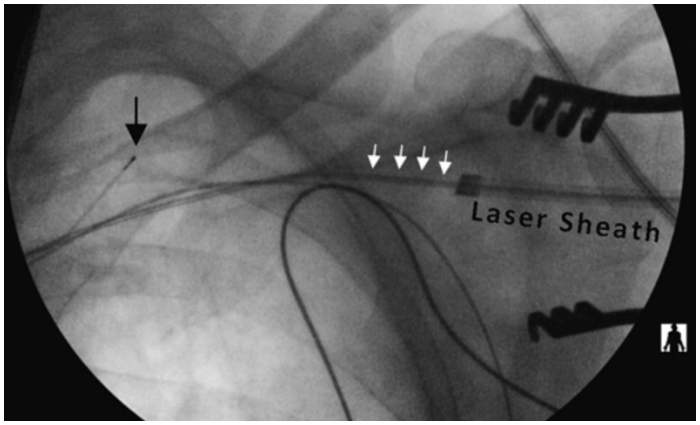

Figure 41. Angiography of the laser sheath [91]

Note that the laser is parallelly aligned with the lead, indicated with the white arrows. The black arrow shows a guidewire that is inserted via the femoral vein.

Extraction of the lead

- To ablate the scar tissue that surrounds the lead, first apply counterpressure, as shown in Figure 42 (simultaneous forward pressure on the sheath and traction to the lead/push and pull) and advance with the laser catheter as presented in Figure 43 [98]

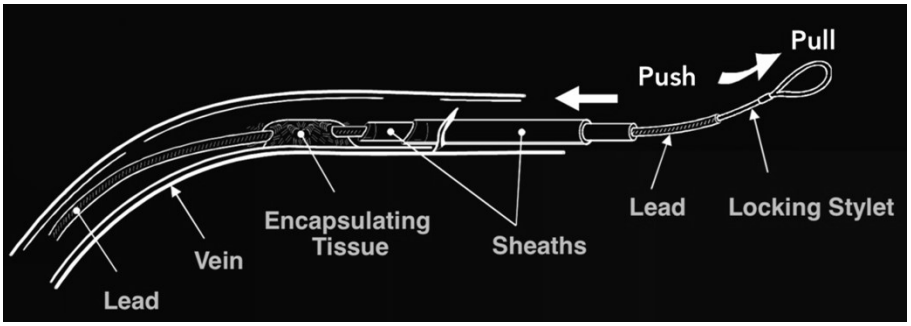

Figure 42. Performing counterpressure [98]

- Overcome the binding sites of the fibrous tissue between the lead and the vessel by applying a forward pressure. Simultaneously, allow the sheath to follow the lead by applying traction to the lead
- Identify the following areas while advancing the laser:

    1. Subclavian-Innominate vein
    2. Superior Vena Cava
    3. Right atrium and Tricuspid valve
    4. Myocardial interface

Note: Adhesions in the upper superior vena cava are considered as one of the most complex parts during the procedure since the leads may take a posterior turn within this area. 2D fluoroscopy guidance may lack in the ability to visualize this properly. Therefore, navigation with multiplanar fluoroscopic views could be useful.

- When approaching the right atrium, reduce the traction force to avoid any damage to the tricuspid valve and right ventricular cavity. Excessive force could result in hypotension, thus proper communication between the operator and anesthesiologist is necessary to prevent unnecessary use of vasoactive drugs
- When approaching the tip of the lead, stop the laser ablation a few millimeters before
- In order to detach the lead from the myocardial interface, perform countertraction (i.e. a gentle tug) to minimize the risk of myocardial tear
- Advance the catheter over the lead tip to minimize shearing forces on the right ventricular wall [91]
- When lead extraction is successfully completed, reimplant the generator and leads and subsequently take swabs for culture in case of vegetation (to determine antibiotics treatment)
- Wrap-up and closure

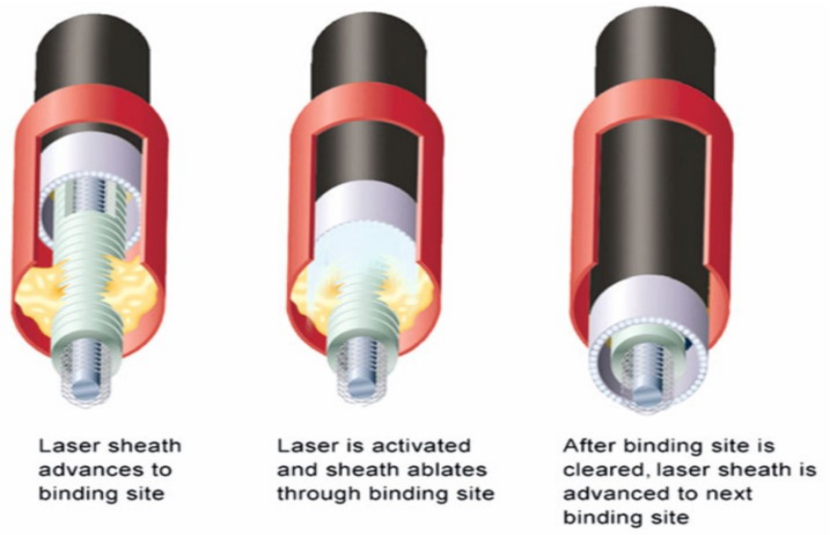

Figure 43. Lead extraction with a laser sheath to overcome binding sites [97]

Table 11. Predictors of difficult lead extractions and complications [18]

Risk factors
ICD lead
Presence of SVC coil[1]
Lead implantation > 5 years
Multiple leads
Prior extraction attempt
Tined lead fixation mechanism
Active fixation coronary sinus lead
Non-isodiametric lead design
Non-back filled ICD coils[2]
Female gender
BMI < 25
Low operator experience

[1]Dual coils have a second defibrillator (shock) coil, which is often positioned in the SVC. However, this latter is a high-risk area, particularly due to the presence of endovascular scar tissue. [2]Non-back filled ICD coils do not combat fibrous ingrowth into their coil.

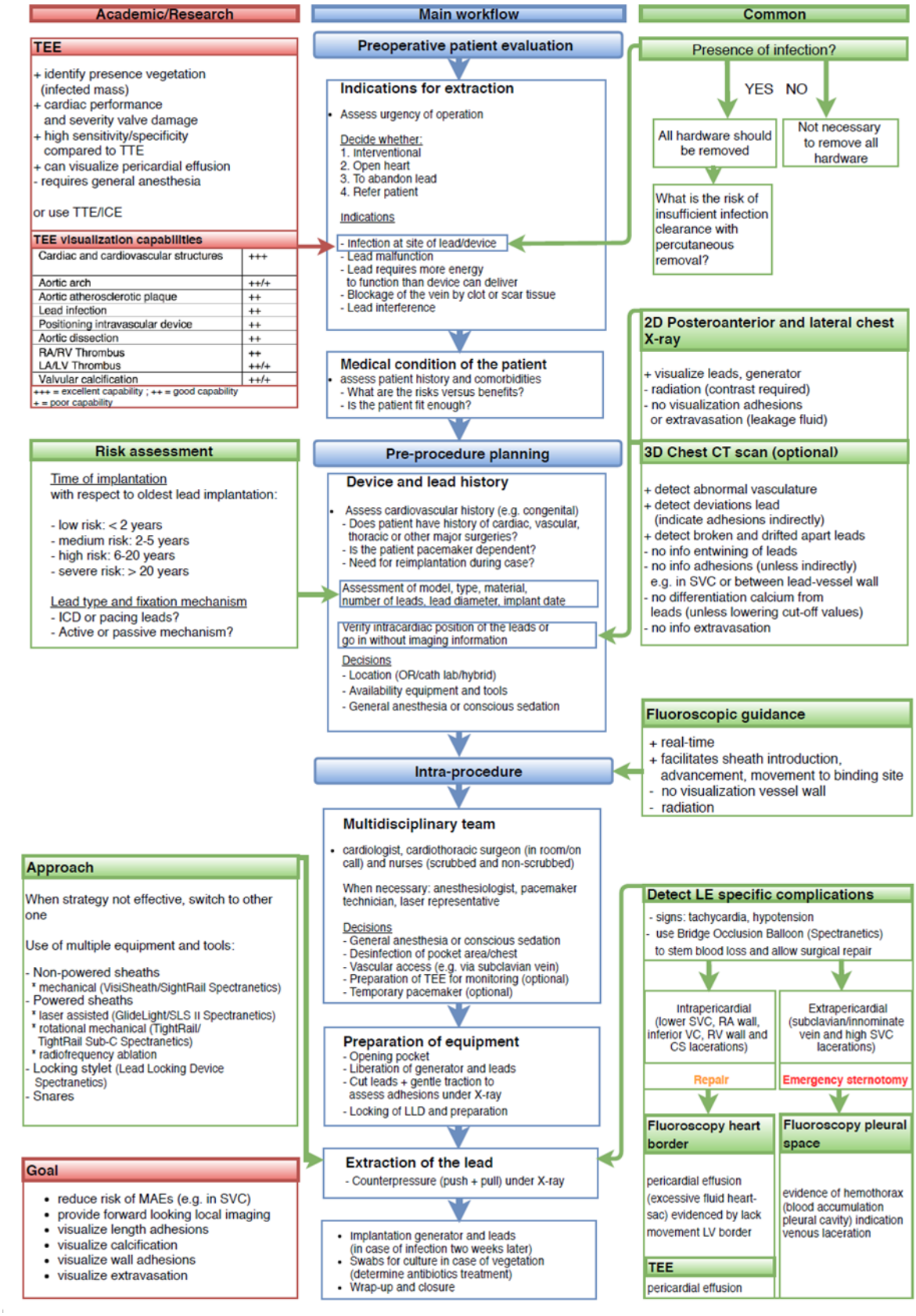

Figure 44. Comprehensive description of a TLE clinical workflow

CS = Coronary Sinus; ICE = Intracardiac Echocardiography; MAE = Major Adverse Event; LLD = Lead Locking Device; LV = Left Ventricle; OR = Operating Room; RA = Right Atrium; RV = Right Ventricle; SVC = Superior Vena Cava; TEE = Transesophageal Echocardiography; TTE = Transthoracic Echocardiography; VC = Vena Cava.

APPENDIX B: PHANTOM CONSTRUCTION

Table 12. Print settings Ultimaker 2 Extended +

Print settings	Ultimaker 2 Extended +
Material	PLA
Nozzle	0.4 mm
Quality	
Layer height	0.15 mm
Shell	
Wall thickness	0.7 mm
Wall line count	2
Top/bottom thickness	0.75 mm
Top/bottom layers	5
Infill	
Infill density	18%
Infill pattern	grid
Speed	
Print speed	60 mm/s

Table 13. Product specifications of Selvol PVA 165 [70]

Specifications Selvol Polyvinyl Alcohol 165	Limits
Hydrolysis (mole %)	99.65 ± 0.35
4% Solution Viscosity (cP)[1]	67 ± 5.00
Total Volatiles (wt %)[2]	5.00
Total Organic Volatiles (wt %)	1.00
Methanol (wt %)	0.90
Ash – ISE (wt %)	1.20
4% Solution pH	6.50 ± 1.00

[1]4% aqueous solution, 20°C; [2]Total Volatiles including water [3]As % Na20, corrected volatiles [4]4% aqueous solution.

APPENDIX C: PREPARATION PROTOCOL PVA

This protocol gives a step-by-step procedure to prepare tissue-mimicking phantoms made of Polyvinyl Alcohol (PVA) and suitable for US and MRI Imaging

1. MATERIALS

Basic Ingredients phantom

- Polyvinyl Alcohol (Selvol PVOH 165, Sekisui Chemical Group NJ, USA)
- Ultrasound scatterers (Silica gel 60, KGaA, Darmstadt, Germany)
- Calciumcarbonate (500 g Calciumcarbonat, Original Rügener Schlämmkreide, Germany)

Items

- Glass beaker
- Weighing scale
- Hot plate magnetic stirrer with temperature controller (IKA RET Control-Visc S1 Digital Hot Plate Magnetic Stirrer, IKA labor technik, Germany)
- Magnetc stir bar
- Stir bar retriever
- Temperature controllable freezer
- A mold to create the phantom of interest

2. BASIC PROCEDURE

The type of PVA used in this protocol (Selvol PVOH 165, Sekisui Chemical Group NJ, USA) has a maximum of 5 wt% volatiles (i.e. the tendency to evaporate) that needs to be taken into account when determining the amount of PVA in a sample.

To determine the desired amount of PVA addition, the following general formula can be applied [70]:

$$PVA\ addition\ (dry\ wt) = \frac{X * Y}{100\% - \%\ Total\ Volatiles}$$

Where X is the desired weight percentage of PVA and Y is the net weight of the final solution

Example: For a desired 100 grams of a 7% PVA solution, the amount of PVA to be added is:

$$PVA\ addition\ (dry\ wt) = \frac{\left(\frac{7}{100}\right) * 100\ grams}{(100\% - 5\%/100)} = 7.37\ grams$$

For the sake of clarity, the following preparation steps will be explained by means of two examples that comprise:

- *Example 1:* Preparation of a 100 grams of a 7.5 wt% solution (7 wt% of PVA and 0.5 wt% of scatterer)
- *Example 2:* Preparation of a 100 grams of a 12.5 wt% solution (7 wt% of PVA, 0.5 wt% of scatterer and 5 wt% of CaCO3)

2.1. Example 1: Preparation of a 100 grams of a 7.5 wt% solution

1	Place a glass beaker on a weighing scale and set to zero
2	Add 0.5 g of scatterers to the beaker and subsequently add 7.37 g of PVA, which gives a total of 7.87 g
3	Carefully add H_20 to a total of 100 g *Optional:* Even better is to add an amount of H_20 in a separate glass beaker (which is 100 g – 7.87 g = 92.13 g) and subsequently to add the PVA-scatterer mixture (slowly!*) to the H_20 *The aim is to dissolve PVA completely; this can be done through proper dispersion of the PVA particles in water. To avoid swelling and clumping of the particles, it is important to add the particles slowly to cool water
4	Once the particles are well dispersed, place the glass beaker on a hot plate magnetic stirrer. Before turning on the hot plate, put a magnetic stir bar into the beaker
5	Turn the hot plate on, hang the thermometer of the temperature controller in the mixture and set the temperature at 93°C *Optional:* To faster get the desired temperature of 93°C, put a plastic lid (with a small hole for the thermometer) on the beaker (in Figure 45 the set-up is illustrated)
6	Initial speed can be set around 400 rpm (observe quick spinning of the stir bar) When noticing a higher viscosity of the mixture, reduce the speed to 300-350 rpm
7	Leave the mixture to dissolve until it has reached the desired temperature of 93°C and hold this for 30 minutes
8	Then, remove the beaker from the hotplate and allow it to cool down to room temperature. Remove the stir bar from the beaker by using a stir bar retriever
9	Use the PVA gel directly (for best results) or either store it at room temperature (useable for a few days) or at 4°C (useable for about 2 weeks). Over time, the gel will tend to thicken, which makes pouring into small size moulds more difficult. Before using, bring it to room temperature

2.2. Example 2: Preparation of a 100 grams of a 12.5 wt% solution

1	Place a glass beaker on a weighing scale and set to zero
2	Add 0.5 g of scatterers to the beaker and subsequently add 7.37 g of PVA
3	Then, add 5 g of $CaCO_3$ to a total of 12.87 g
4	Carefully add H_20 to a total of 100 g *Optional:* Even better is to add an amount of H_20 in a separate glass beaker (which is 100 g – 12.87 g = 87.13 g) and subsequently to add the mixture (slowly!) to the H_20
5	Follow steps 4-9 as described in Example 1

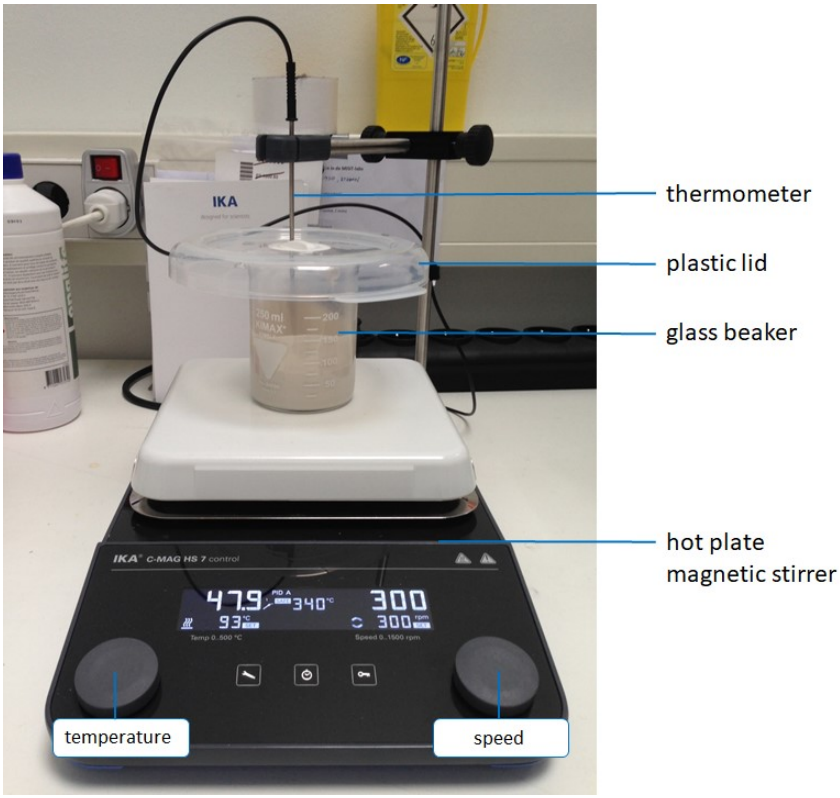

Figure 45. Set-up to create a PVA solution

3. RECOMMENDATIONS

- The aforementioned type of PVA has a maximum recommended soluble concentration of 7 wt% PVA to water.

- PVA without scatterer for US imaging is sometimes already sufficient to obtain a proper signal on an US image. However, to enhance the signal, addition of a scatterer concentration between 0.05-0.5 wt% is recommended.

APPENDIX D: PROTOCOL PVA POURING – TIPS AND TRICKS

This protocol could be adopted following preparation of PVA.

1 Let the PVA solution cool down to room temperature

Tip: It is not necessary to let the solution completely cool down to room temperature. However, consider the material of the mould you are using. When using a mould made of PLA, the glass transition temperature is between 60-65°C. ABS has a temperature of ± 105°C

2 After waiting about half an hour, a skin layer will form on the surface of the cooled solution. Remove this layer

3 Before pouring the PVA into the mould, consider the following important notes:

- PVA in general does not stick to plastic or metal. Therefore, using a mould made of the aforementioned materials is not expected to give extraction problems

  Tips and tricks
  - *In case of using a material other than plastic/metal, it is recommended to grease the inner side of the mould with Vaseline to prevent any difficulties during extraction of the phantom*
  - *Even with a mould made of plastic/metal, complex mould structures may induce difficulties. Therefore, using Vaseline for the inner side may facilitate the extraction process*

- When the mould consists of multiple parts and the edges are not carefully closed in advance, PVA pouring into the mould will result in fluid leakage at the edges of the mould

  Tips and tricks
  - *Use Vaseline to seal the edges of the mould before and after pouring*
  - *Use a rubber matt, cut in the right shape, to seal the sites where the parts of the mould attach each other (i.e. between the parts)*

- A reusable mould that already has undergone multiple FT cycles, may be affected by previous temperature changes (with resulting shrinkage/expansion of the material and shape). This means that PVA pouring may result in leakage of the mould in its entirety

  Tips and tricks
  - *Print the mould with higher quality settings and better layer adhesions. This will go at the expense of time but will result in a more robust printing, better able to resist temperature changes*
  - *Use another material than PLA to print the mould. For instance, ABS includes a acetone vapour polish which will better seal the outer layers of the mould*
  - *Use a coat painting (e.g. can be bought from http://www.formx.nl/) to create a solid shell, covering the mould after a few coats*

4 After accomplishing the preparation steps mentioned in nr. 3, pour the PVA solution into the mould

Tips and tricks

- *When the opening in which the PVA should be poured is quite small, use a syringe or funnel to perform precise pouring without spilling too much PVA*
- *When the PVA fluid flows too slowly to the bottom of the mould, use a vibration plate to facilitate and accelerate the process*

5 Wait for the air bubbles to disappear

Tips and tricks

- *Store the mould vertically at room temperature and wait for a couple of hours to allow the air bubbles to rise out*
- *Apply vacuum degassing by placing the mould including PVA solution for a few minutes in a vacuum chamber. As a result, the air will be sucked out of the solution causing the bubbles to rise out and subsequently collapse*

6 Put the mould including PVA solution in a temperature controllable freezer (± -19°C) with a recommended FT cycle of 16 hours of freezing followed by 8 hours of thawing at room temperature

Tip: The time duration required for one FT cycle depends on the mass of both the mould and phantom. This time cycle should be experimentally investigated. Furthermore, the number of FT cycles should be adjusted to the mechanical strength of interest

7 Remove the PVA phantom from the mould

- Keep the phantom from dehydration and bacterial growth

Tips and tricks

- *Store the PVA phantom in water or a fully humidified environment*
- *PVA cryogel can be used for months or even longer, provided that it is treated properly. To prevent any bacterial growth on it, keep it in clean/sterilized water and attempt to minimize contact with human skin*
- *When there is still any form of bacterial growth, use a concentrated salt solution (recommend 18 wt% salt solution) for a couple of minutes to kill the bacteria.*

APPENDIX E: PHANTOM 3 & 4: VASCULAR TREE

PHANTOM 3: DESIGN

Prior to this step, a straight vessel phantom was created that was equivalent to a human SVC in terms of geometry. Within this step, it was examined whether the SVC could be extended with two approximate innominate veins. Therefore, a vascular tree was designed that consisted of three parts, with each part representing one type of vein (Figure 46A). The parts could be easily connected and disconnected from each other (Figure 46B). This was done to facilitate the phantom extraction process from the mould. Next to the vascular tree, an outer mould was designed that consisted of a lower and upper part (Figure 46C and Figure 46E). Between the vascular tree and outer mould an open space of 2 mm distance was left (Figure 46D), allowing to be filled with PVA to create a 2 mm thick vessel wall. PVA could be poured through the opening at the upper part of the outer mould.

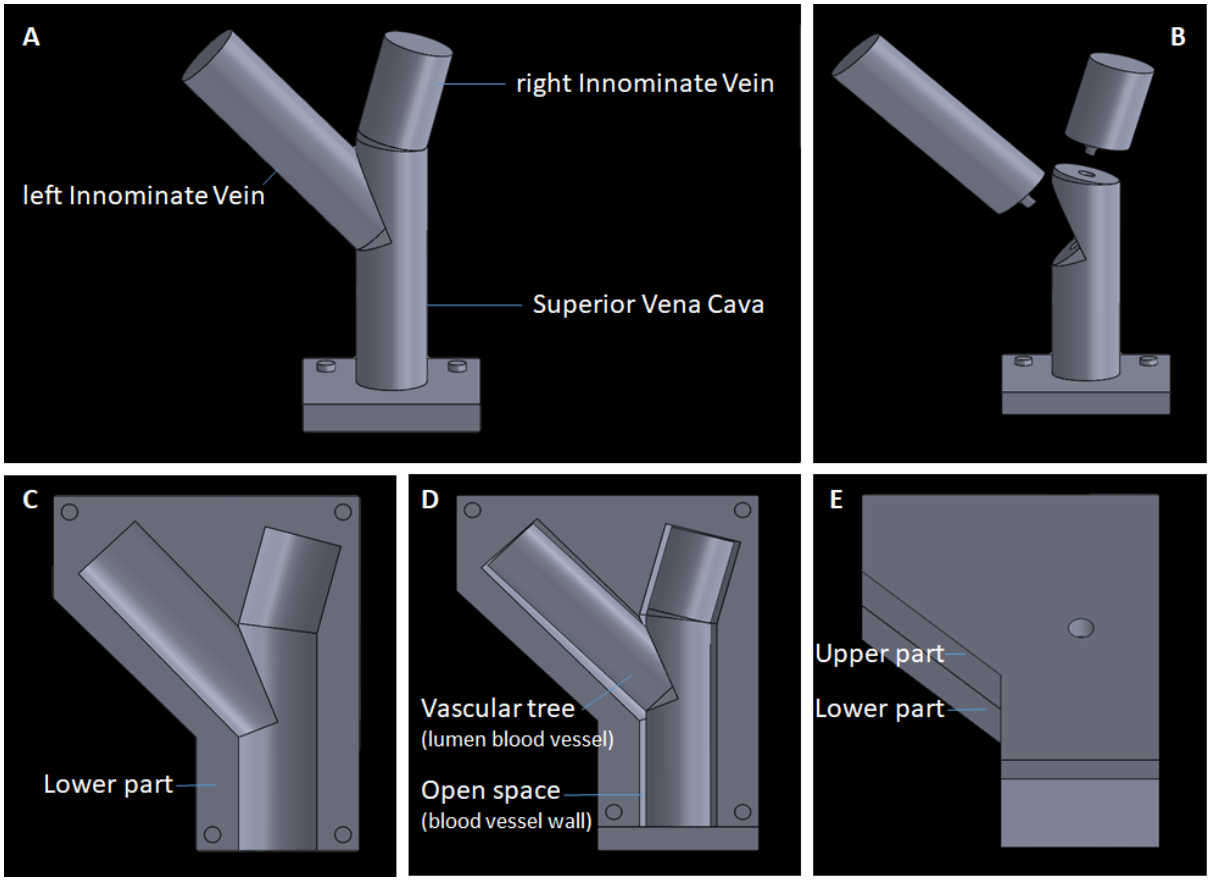

Figure 46. Design of a vascular tree mould

A: Vascular tree with corresponding veins. B: Disconnection of the parts. C: Lower part of the outer mould. D: Lower part attached to the vascular tree E: The outer mould including its upper and lower part.

PHANTOM 3: CONSTRUCTION

Figure 47A and Figure 47B present the outer mould including vascular tree after 3D printing. Already at the start of the pouring process, it could be observed that this mould could not be sufficiently sealed at the edges, and particularly between the upper and lower part. Consequently, at these sites there was a lot of PVA leakage during pouring even despite some precautionary measures were taken (e.g. use of Vaseline, rubber matt – see Appendix D: Protocol PVA pouring – tips and tricks). Due to this constraint, solely one half of the vascular phantom could be constructed as shown in Figure 47C.

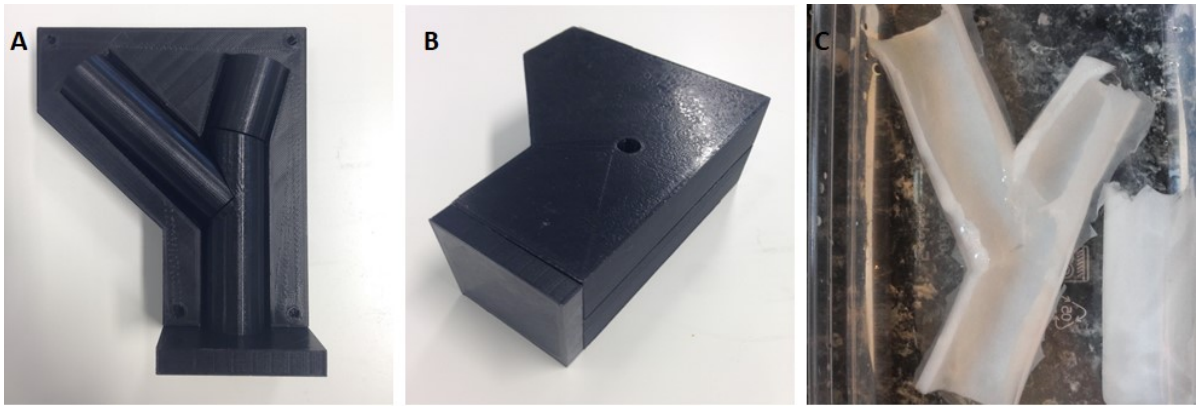

Figure 47. Construction of a vascular tree mould and phantom

A: Lower part of the outer mould with inside the vascular tree. B: Outer mould including its upper and lower part. C: Constructed vascular phantom. As can be observed from C, only one half of the phantom could be constructed.

PHANTOM 4: DESIGN

In order to overcome the major problem (i.e. leakage at the edges) encountered in mould design 3, the lower part of mould design 4 was extended upwards to minimize edges as far as possible (Figure 48A). Similar to the previous mould it contained a three parts vascular tree, separated by the lower part of the mould with a distance of 2 mm, intended to create the vessel wall (Figure 48B). Furthermore, it consisted of an upper part (Figure 48C) with similar geometry as the vascular tree at the bottom side, to close the mould. The wye shape opening at the top allowed for pouring. Figure 48D illustrates the optimized mould in its entirety.

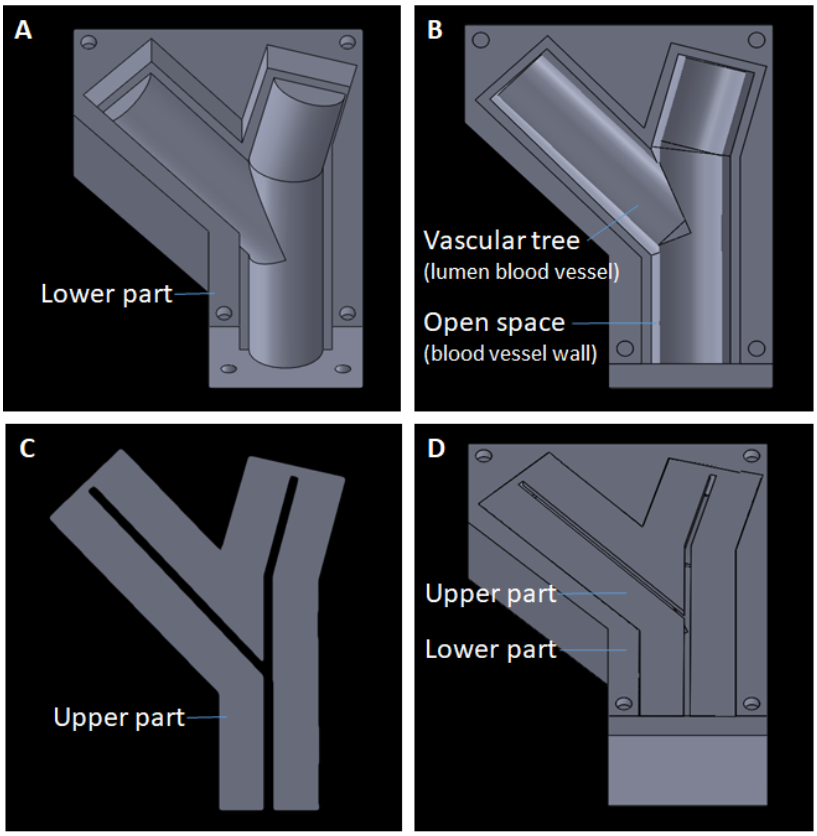

Figure 48. Optimized version of a vascular tree mould

A: Lower part of the mould. B: Lower part of the mould attached to the vascular tree. C: Upper part of the mould. D: The mould in its entirety.

PHANTOM 4: CONSTRUCTION

In figure Figure 49A and Figure 49B the optimized vascular tree mould is presented after 3D printing. As can be observed from Figure 49C and Figure 49D, the phantom could be constructed completely (i.e. both sides of the phantom), however, it encounters the problem of containing two large gaps at the left innominate vein (Figure 49C). This was due to the presence of air bubbles in the PVA solution but could not be observed at time of pouring because of the small wye shape opening at the upper part. Although this problem could be solved relatively easy by means of vacuum degassing, a few other problems were encountered which could only be solved through design optimization:

- Difficulty of PVA pouring due to the small wye shape opening
- Difficulty of removing the upper part from the lower part of the mould without rupturing the phantom
- Construction of a thin edge on top due to the wye shape opening of the upper part (Figure 49C)
- Unequal distribution of the vessel wall due to inward pushing of the upper part against the outer wall of the vascular tree at several sites
- Small amount of PVA leakage at the site were the vascular tree is attached to the lower part of the mould

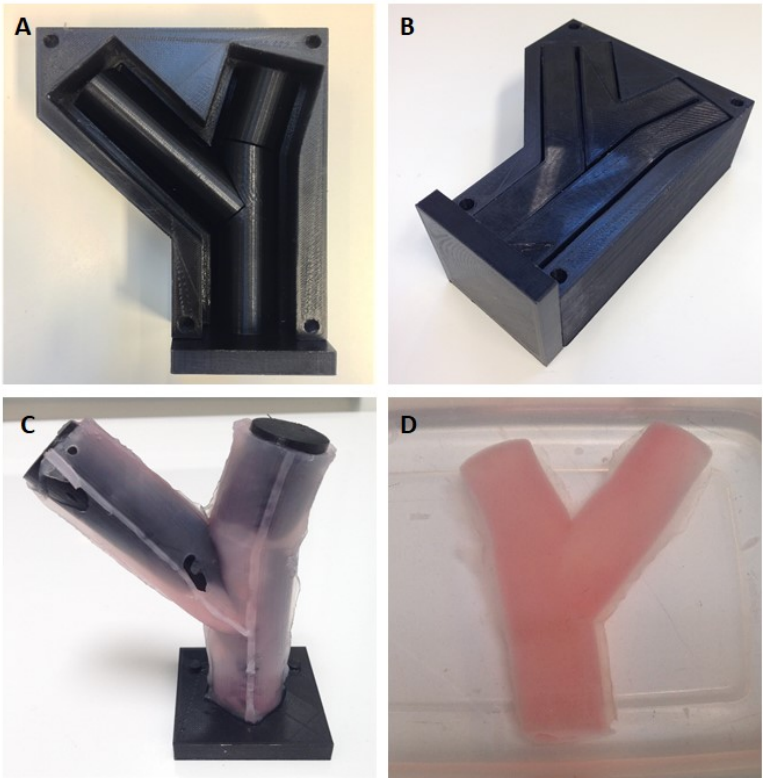

Figure 49. Construction of an optimized vascular tree mould and phantom

A: Lower part of the mould with inside the vascular tree. B: The optimized mould in its entirety (lower and upper part). C: Vascular tree phantom with two large gaps at the left innominate vein and a thin edge on top. D: The vascular tree phantom at the reverse side.

APPENDIX F: VALIDATION EXPERIMENT

Contrast-to-Noise Ratio

CNR is a metric used to specify image quality. It is expressed in the following formula

$$CNR = \frac{|\mu_{\mathrm{A}} - \mu_B|}{\sigma_0} = \frac{\Delta\mu}{\sigma_0}$$

where μ_{A} is the mean signal intensity of a structure in the region of interest (i.e. the phantom), μ_{B} the mean signal intensity of the image background that surrounds this structure (i.e. the medium) and σ_0 is the pure background noise in terms of standard deviation of the pixel values outside the region of interest [99, 100].

Table 14. Specimen specifications

Characteristics of the SVC phantoms used in the validation experiment	
Composition	
Weight percentage of PVA	7 wt %
Weight percentage of acoustic scatterer	0.1, 0.2, 0,3 wt %
Number of FT cycles	2
Dimensions	
Wall thickness	1 mm
Lumen diameter	20 mm
Length	70 mm
Characteristics of the porcine SVC used in the validation experiment	
Dimensions	
Wall thickness	± 1 mm
Lumen diameter	± 20 mm
Length	55 mm

Table 15. US settings

Ultrasound settings validation experiment	
Frequency	117 Hz
Penetration depth	5 cm
Frequency range	Resolution
Gain	46

Table 16. Specifications of water, BMF and human blood [74]

Material	Density ρ [kg m^{-3}]	Speed c [m s^{-1}]	Viscosity η [mPa s]	Attenuation μ [dB cm^{-1} MHz]
Water	1000	1484	1	0.0022
Blood mimicking fluid (CIRS, model 046)	1010-1090	1570 ± 30	4.0 ± 0.5	< 0.1
Human blood (37°C)	1060	1583	3	0.15